U.PORTO

FEUP FACULDADE DE ENGENHARIA
UNIVERSIDADE DO PORTO

CATIONIC NANO-SYSTEMS FOR DNA TRANSFECTION

BY

Diana Patrícia Soares de Paiva

THESIS SUBMITTED TO THE UNIVERSITY OF PORTO FOR A DOCTOR OF PHILOSOPHY IN CHEMICAL AND BIOLOGICAL ENGINEERING

SUPERVISION

MARIA DO CARMO DA SILVA PEREIRA

SANDRA CRISTINA PINTO DA ROCHA

PORTO, 2013

GOVERNO DE PORTUGAL

Lepae Laboratory for Process, Environmental and Energy Engineering

UNIÃO EUROPEIA
Fundo Social Europeu

FCT Fundação para a Ciência e a Tecnologia
MINISTÉRIO DA EDUCAÇÃO E CIÊNCIA

COMPETE
PROGRAMA OPERACIONAL FACTORES DE COMPETITIVIDADE

POPH
PROGRAMA OPERACIONAL POTENCIAL HUMANO

QREN QUADRO DE REFERÊNCIA ESTRATÉGICO NACIONAL
PORTUGAL 2007.2013

To my family ...

"Some people succeed
because they are destined to!
But most people succeed
because they are determined to!"
Henry Ford, 1863-1947

Acknowledgments

This thesis and, therefore, all the work done in the last 5 years was not possible without the valuable contribution of some people that I am very grateful.

I thank to Professor Maria do Carmo Pereira for accepting me as her PhD student in the Faculty of Engineering of the University of Porto (FEUP, Porto, Portugal) and for believe on my capabilities. Her guidance, support, suggestions and scientific discussions were always essential.

I would like to give my deepest appreciation to Doctor Sandra Rocha for her help and contribution for this PhD. She has always friendly and hopeful, and made easier to overcome the difficulties and frustrations of this work.

Also, I express my gratitude to the members of our investigation group, particularly, to Professor Manuel Coelho, for the group scientific discussions and brain storming. To LEPAE members and staff a special thank for their help and contribution.

Some fundamental studies where performed at Max Planck Institute of Colloids and Interface (Golm, Germany), so I want to thank to Professor Helmuth Möhwald for the opportunity and for his hospitality. Professor Gerald Brezesinski deserves may deeply gratitude for all the guidance and helpful discussions on Langmuir monolayers studies and for being such a good

and welcome friend. My stay in Germany was really pleasant and I would like to thank all the friends I made there, especially, Professor Gerald's group for the fantastic working atmosphere and my roommates for being such a good friends.

Many thanks to the co-workers that contributed for this research work. To Doctor Isabel Cardoso and the members of Molecular Neurobiology group from Instituto de Biologia Molecular e Celular (Porto, Portugal), my appreciation for the help on cellular transfection studies. To Doctor Galya Ivanova from Centro de Materiais da Universidade do Porto (Porto, Portugal) for her help on NMR work. To Doctor Alberto Martín Molina and his group from Facultad de Ciencias, Universidad de Granada (Granada, Spain), for their help on the liposome complexation theory.

To all my friends at Department of Chemical Engineering (FEUP, Porto, Portugal) and Tuna Feminina de Engenharia (TUNAFE, Porto, Portugal) for the support, encouragement and good times over the years. Thank you all for constant presence and friendship.

To my family, I offer all my gratitude, for being there and supporting my choices, encouraging me to pursue my dreams and go further. To my husband Joaquim Freitas a special thanks for being there all the time and helping me on the most challenging problems. To my baby, Gabriel, thank you for colouring my life and make me smile.

I am thankful to Fundação para a Ciência e Tecnologia (FCT) for a PhD fellowship (SFRH/BD/45384/2008). The research work was supported by FCT research projects: Nano-NMed–SD/0156/2007 and PTDC/QUI-BIQ/102827/2008.

Resumo

Este trabalho de investigação visou a preparação e caracterização de sistemas para o transporte e entrega de ADN. Esses sistemas são catiónicos e não virais e são constituídos por lípidos e polímeros.

As monocamadas de Langmuir foram utilizadas para prever as interações entre o lípido catiónico DOTAP (Cloreto de trimetil(2,3-dioleoilpropil)amónio) e o colesterol (CHOL) ou o seu derivado colesterol fluorado (heptafluorocolesterol, F7-CHOL). A mistura do DOTAP com cada um dos esteróis (rácio 1:1) origina monocamadas na fase líquida expandida, idênticas às do DOTAP. Verificou-se que a área por molécula das misturas é mais pequena que a esperada de acordo com a regra da adição aplicável no caso de ambos os compostos serem completamente miscíveis ou imiscíveis na monocamada. A adsorção de ADN na monocamada é similar para ambos os sistemas, o que sustenta a possibilidade da utilização de colesterol fluorado como lípido auxiliar na formulação de vetores para transfeção de ADN.

A compactação de ADN e respetiva transfeção foram testadas para lipossomas constituídos pelo DOTAP e pelo colesterol fluorado (rácio molar 1:1). Os resultados confirmaram que mais lipossomas do sistema DOTAP:F7-CHOL são necessários para compactar a mesma quantidade de ADN quando comparado com o sistema DOTAP:CHOL e que a ligação lipossoma-ADN é mais forte no caso do sistema DOTAP:F7-CHOL/ADN. A estabilidade de ambos

os sistemas na presença de ADN é idêntica, bem como a eficiência de transfeção.

Os vetores baseados em bola-anfifílicos foram produzidos por dois métodos distintos. Primeiro utilizou-se a metodologia de deposição de camadas. Após a adição de algumas camadas de polímeros para promover a estabilização do núcleo das micropartículas, camadas alternadas de ADN e bola-anfifílico (BA) foram depositadas. A presença quer do ADN quer do BA à superfície das micropartículas foi confirmada, visualmente, por microscopia confocal. A outra metodologia utilizada foi a formação de vesículas lipídicas preparadas com diferentes rácios molares de BA e DOTAP. O rácio molar que evidenciou melhor comportamento foi o de BA:DOTAP 1:5. As vesículas foram posteriormente complexadas com ADN (rácio mássico lípido:ADN 10:1). Os estudos de transfeção revelaram que o sistema BA:DOTAP possui um melhor potencial de transfeção com menos impacto na viabilidade das células do que o sistema de DOTAP.

Copolímeros de quitosano e maltodextrina foram sintetizados por aminação redutiva, partindo de quitosano de baixo peso molecular. O grau de substituição, quantificado por espectroscopia de ressonância magnética nuclear, foi superior a 70% para rácios molares de 1:1 e 1:5 entre as unidades de glucosaminas do quitosano e uma molécula de maltodextrina. O elevado grau de substituição obtido gerou um composto solúvel em água a pH de 7.4. Adicionalmente, o copolímero forma, espontaneamente, nanopartículas esféricas com diâmetros de cerca de 300 nm. As moléculas de ADN interagem eficientemente com as nanopartículas do copolímero, evidenciando potencial para a aplicação deste sistema como transportador de ADN.

Este estudo apresenta diferentes sistemas com possíveis aplicações na terapia génica. Estes sistemas exibem boas características como vetores de transfeção de ADN.

Abstract

This doctoral thesis had as objectives the preparation and characterisation of cationic non-viral DNA delivery systems based on lipids and polymers.

Langmuir monolayers were used to predict the interactions between the cationic lipid DOTAP (1,2-dioleoyl-3-trimethylammonium-propane, chloride salt) and cholesterol or its derivative heptafluorocholesterol (fluorinated cholesterol). The mixture of DOTAP with each of the sterols at 1:1 molar ratios leads to monolayers in a liquid expanded state, similarly to that of DOTAP alone. The area per molecule of the mixtures was smaller than that expected according to the additivity rule applicable if the two components are either completely miscible or immiscible within the monolayer. The adsorption of DNA to the monolayer is similar for both systems, supporting the use of fluorinated cholesterol as helper lipid in DNA transfection vectors.

Liposomes of the cationic lipid DOTAP and the fluorinated cholesterol (F7-CHOL) were tested at the molar ratios of 1:1 for DNA compaction and transfection. The results confirmed that more DOTAP:F7-CHOL liposomes are needed to compact the same amount of DNA as DOTAP:CHOL and that the liposome-DNA binding is stronger in the case of DOTAP:F7-CHOL/DNA system. The stability rates of both liposomes in the presence of DNA were similar as well as the transfection efficiencies.

Bolaamphiphile based vectors were prepared using two distinct methods: layer-by-layer (LbL) deposition method and hydration lipid film technique. Microparticles were coated with few polymer layers by LbL for stabilization, followed by deposition of DNA and bolaamphiphile (BA) layers, alternately. The amount of DNA present on the layers was 0.035 ± 0.005 mg/mL as estimated by ethidium bromide assays. The presence of both DNA and BA molecules at the surface of the microparticles was confirmed by confocal laser scanning microscopy. Vesicles of the bolamphiphile and DOTAP were also prepared using different molar ratios of each molecule. The ratio that exhibited better behaviour was BA:DOTAP 1:5. The vesicles were then successfully complexed with DNA at the lipid:DNA ratio of 10:1 (w:w). Transfection studies revealed that the BA:DOTAP mixed system has a higher transfection potential with less impact on cell viability than DOTAP system.

Graft copolymers of chitosan and maltodextrin were synthesised by reductive amination of a low molecular weight chitosan. The degree of substitution is 70% or above, as quantified by nuclear magnetic resonance spectroscopy, at molar ratios of chitosan glucosamine units and maltodextrin of 1:1 and 1:5. The high substitution degree generates a water-soluble compound at pH 7.4. In addition, the copolymer self-assembles into spherical nanoparticles with diameters of about 300 nm. DNA molecules interact efficiently with the copolymer nanoparticles indicating a potential application of the system for DNA delivery.

The current study presents different systems with possible applications in gene therapy. These systems exhibit good characteristics as DNA transfection vectors.

Contents

Preface

According to the Law n° 216/92 of 13th October and to the Doctoral Regulations of the University of Porto, we clarify that all the experiments, interpretation and discussion presented on this thesis are our own, except if stated otherwise. In this dissertation, results were presented from the following publications:

Paiva, D., Martin-Molina, A., Cardoso, I., Quesada-Perez, M., Pereira, M. C., Rocha, S. (**2013**). "The effect of a fluorinated cholesterol derivative on the stability and physical properties of cationic DNA vectors", *Soft Matter*, *9*, 401.

Paiva, D., Brezesinski, G., Pereira, M. C., Rocha, S. (**2013**). "Langmuir monolayers of monocationic lipid mixed with cholesterol or fluorocholesterol: DNA adsorption studies", *Langmuir*, *29*, 1920.

Paiva, D., Rocha, S., Ivanova, G., Pereira, M. C. "Synthesis and characterization of chitosan-maltodextrin graft copolymers: Novel nanoparticles for drug delivery", *Physical Chemistry* Chemical Physics, DOI: 10.1039/C3CP51215K.

Chapter 1

Introduction

The gene therapy concept states that a human disease might be treated if the correct genetic material is supplied to the targeted cell. The new genetic material can correct or supplement the defective genes responsible for the disease progression (Mansouri, 2004). Different gene therapeutics to treat diseases such as cancer, AIDS and neurological disorders are currently in clinical trials (Biffi, 2006; Ginn, 2013; Li, 2005; Strayer, 2005).

In gene therapy, the development and study of DNA vectors with high transfection efficiency and low toxicity is extremely important. Ideally, a DNA delivery system with therapeutic purposes should have high transfection efficiency and high specificity to the target cell to reduce the side effects. The system should in addition be small, stable, biodegradable, easy to prepare and should allow the DNA release and expression (Mansouri, 2004; Patil, 2005). Nanoparticles and nanocapsules offer many advantages in gene therapy due to their versatile chemical structures, surface functionalities and the ability to obtain controlled sizes.

The focus of this PhD research work is to prepare and characterise non-viral DNA delivery systems based on lipids and polymers. These systems avoid some of the problems associated to viral vectors such as high toxicity

and the generation of a strong immune response. Other advantages of non-viral vectors are easy formulation and assembly (Patil, 2005).

Non-viral vectors are typically positively charged such as cationic liposomes prepared with 1,2-dioleoyl-3-trimethylammonium-propane, chloride salt (DOTAP) or cationic nanoparticles made of chitosan. These systems compact efficiently the DNA through electrostatic interactions leading to the formation of complexes (Morille, 2008). In this thesis the preparation of three different non-viral systems is described.

One system is based on fluorinated compounds (fluorinated modified cholesterol) mixed with the cationic lipid DOTAP. Fluorinated cationic liposomes have shown a higher transfection potential in *in vitro* and *in vivo* studies when compared to their analogues (Krafft, 2001). Also, these compounds exhibit good properties regarding the transport and protection of active principles in the blood stream (Riess, 2002). The use of fluorinated cholesterol in cationic liposomes for DNA delivery is described in the point of view of the helper lipid effect. Cholesterol is normally added to lipid-based DNA vectors to help the fusion of the liposome with the membrane, but also to increase the stability and decrease the toxicity of the system. The use of fluorinated cholesterol might increase further the stability of the system due to its high hydrophobic character and protect DNA molecules from degradation in the blood stream, increasing the half-life of the system (Boulanger, 2004).

A second carrier was prepared with bolaamphiphiles, which are molecules with two hydrophilic end groups connected by a hydrophobic tail. Bolaamphiphiles are described to self-assemble in water and form packed monolayer lipid membranes (Forbes, 2006). A bolaamphiphile molecule with a hydrophobic chain of 22 carbon atoms, trimethylamine-quaternized at one end and with a hydroxyl group at the other end was synthesised. The carriers

containing this molecule were prepared by two different approaches. One strategy was to use the layer-by-layer technique to assemble bolaamphiphile and DNA layers on a microparticle core that could eventually be removed to originate micro- or nanocapsules (Sukhorukov, 2007). A different approach was to incorporate the bolaamphiphile in vesicles composed of the cationic lipid DOTAP. This mixture is expected to form stable vesicles with small sizes even in dry state due the two polar heads and the long carbon chain present in the bolaamphiphile (Jain, 2010).

A DNA vector system based on chitosan conjugates is also proposed. Chitosan is a non-toxic and natural biodegradable cationic polymer with low immunogenicity and high biocompatibility (Jayakumar, 2010). These properties made chitosan one of the more used polymers for gene therapies. However, this molecule shows some problems, like solubility at physiological pH and side effects as hypocholesterolemia if applied in high doses, limiting its application. To overcome these complications and to improve its ability to transfect genetic material, this cationic polymer was modified by grafting a neutral polymer. Maltodextrin was chosen because it is a non-ionic excipient that enhances gene expression and has low toxicity (Huang, 2002).

This thesis is organised into seven chapters. This chapter, *introduction*, covers the objectives and scope of the proposed work. Chapter 2, *nano-systems for gene delivery*, contains an overview of the non-viral vectors concerning their applications in gene therapy and their advantages and disadvantages. Chapter 3, *interaction of DNA with lipid monolayers*, covers the use of Langmuir lipid monolayers to predict the interactions between the fluorinated cholesterol and DOTAP and to study the interaction of DNA molecules with the monolayer. Chapter 4, *compaction process of DNA by fluorinated liposomes*, is dedicated to the characterisation of DOTAP liposomes mixed with fluorinated cholesterol and the comparison of this

system with the well-known DOTAP:cholesterol liposomes. In chapter 5, *bolaamphiphile-based vectors*, the potential application of a new synthesised bolaamphiphile in DNA carriers is discussed and in chapter 6, *chitosan-N-maltodextrin conjugates*, the synthesis of chitosan-graft-maltodextrin copolymers, their assembly into nanoparticles and their interaction with DNA are described. Finally, chapter 7, *concluding remarks*, summarises the main findings of this thesis.

References

Biffi, A.; Capotondo, A.; Fasano, S.; Carro, U.d.; Marchesini, S.; Azuma, H.; Malaguti, M.C.; Amadio, S.; Brambilla, R.; Grompe, M.; Bordignon, C.; Quattrini, A.; Naldini, L. (**2006**). Gene therapy of metachromatic leukodystrophy reverses neurological damage and deficits in mice, *The Journal of Clinical Investigation, 116*, 3070.

Boulanger, C.; Di Giorgio, C.; Gaucheron, J.; Vierling, P. (**2004**). Transfection with fluorinated lipoplexes based on new fluorinated cationic lipids and in the presence of a bile salt surfactant, *Bioconjugate Chemistry, 15*, 901.

Forbes, C.C.; DiVittorio, K.M.; Smith, B.D. (**2006**). Bolaamphiphiles Promote Phospholipid Translocation Across Vesicle Membranes, *Journal of the American Chemical Society, 128*, 9211.

Ginn, S.L.; Alexander, I.E.; Edelstein, M.L.; Abedi, M.R.; Wixon, J. (**2013**). Gene therapy clinical trials worldwide to 2012 – an update, *The Journal of Gene Medicine, 15*, 65.

Huang, C.-Y.; Ma, S.S.; Lee, S.; Radhakrishnan, R.; Braun, C.S.; Choosakoonkriang, S.; Wiethoff, C.M.; Lobo, B.A.; Middaugh, C.R. (**2002**). Enhancements in gene expression by the choice of plasmid

DNA formulations containing neutral polymeric excipients, *Journal of Pharmaceutical Sciences, 91*, 1371.

Jain, N.; Arntz, Y.; Goldschmidt, V.r.; Duportail, G.; Mély, Y.; Klymchenko, A.S. (**2010**). New Unsymmetrical Bolaamphiphiles: Synthesis, Assembly with DNA, and Application for Gene Delivery, *Bioconjugate Chemistry, 21*, 2110.

Jayakumar, R.; Chennazhi, K.P.; Muzzarelli, R.A.A.; Tamura, H.; Nair, S.V.; Selvamurugan, N. (**2010**). Chitosan conjugated DNA nanoparticles in gene therapy, *Carbohydrate Polymers, 79*, 1.

Krafft, M.P. (**2001**). Fluorocarbons and fluorinated amphiphiles in drug delivery and biomedical research, *Advanced Drug Delivery Reviews, 47*, 209.

Li, C.; Bowles, D.E.; van Dyke, T.; Samulski, R.J. (**2005**). Adeno-associated virus vectors: potential applications for cancer gene therapy, *Cancer Gene Therapy, 12*, 913.

Mansouri, S.; Lavigne, P.; Corsi, K.; Benderdour, M.; Beaumont, E.; Fernandes, J.C. (**2004**). Chitosan-DNA nanoparticles as non-viral vectors in gene therapy: strategies to improve transfection efficacy, *European Journal of Pharmaceutics and Biopharmaceutics, 57*, 1.

Morille, M.; Passirani, C.; Vonarbourg, A.; Clavreul, A.; Benoit, J.P. (**2008**). Progress in developing cationic vectors for non-viral systemic gene therapy against cancer, *Biomaterials, 29*, 3477.

Patil, S.; Rhodes, D.; Burgess, D. (**2005**). DNA-based therapeutics and DNA delivery systems: A comprehensive review, *The AAPS Journal, 7*, E61.

Riess, J.G. (**2002**). Blood substitutes and other potential biomedical applications of fluorinated colloids, *Journal of Fluorine Chemistry, 114*, 119.

Strayer, D.S.; Akkina, R.; Bunnell, B.A.; Dropulic, B.; Planelles, V.; Pomerantz, R.J.; Rossi, J.J.; Zaia, J.A. (**2005**). Current status of gene therapy strategies to treat HIV/AIDS, *Molecular Therapy, 11*, 823.

Sukhorukov, G.B.; Möhwald, H. (**2007**). Multifunctional cargo systems for biotechnology, *Trends in Biotechnology, 25*, 93.

Chapter 2

Nano-systems for gene delivery

Human diseases might be treated by the transfer of genetic material into specific cells in order to correct or supplement defective genes (Alderuccio, 2009; Buckley, 2011; Fischer, 2010). Gene therapy is been studied in clinical trials for different type of diseases such as cancer (Brannon-Peppas, 2004; Li, 2005; Ramesh, 2001), HIV/AIDS (Kiem, 2012; Strayer, 2005), diabetes (Callejas, 2013; Jean, 2011), cystic fibrosis (Mitomo, 2010; Pringle, 2009) and neurological disorders (Biffi, 2006; Kim, 2009; Manfredsson, 2010).

There are many processes to perform gene therapy treatments such as gene addition, gene correction/alteration and gene knockdown that could be used individually or in combination (Kay, 2011). Gene knockdown acts by introducing siRNA (short interfering RNA) or miRNA (mediated gene regulation circuits of RNA) to block or cleave a gene transcript, by selecting the sequences that should be replicated, eliminating the defective sequences (Summerton, 2007). Gene correction/alteration is not a common technique, however it is acquiring some interest by using artificially engineered nucleases

to cut the genome at a specific location, driving the cell endogenous mechanisms to repair the introduced break through natural processes (Urnov, 2010).

Gene addition is one of the more commonly used techniques and basically introduces a new sequence of DNA without removal of the endogenous mutated gene. The therapeutic gene needs to reach the interior of the cell and it will be treated by the subsequent cell processes. For this route of gene therapy, the limitation step is the carrier used to transport the genetic information through the human body and the ability to cross the cell membrane. It is known that DNA sequences and free oligonucleotides are rapidly degraded by serum nucleases in the blood when injected intravenously (Miguel, 2003). Thus, a vehicle is necessary to compact and protect the genetic material. The process is called DNA transfection (Figure 2.1).

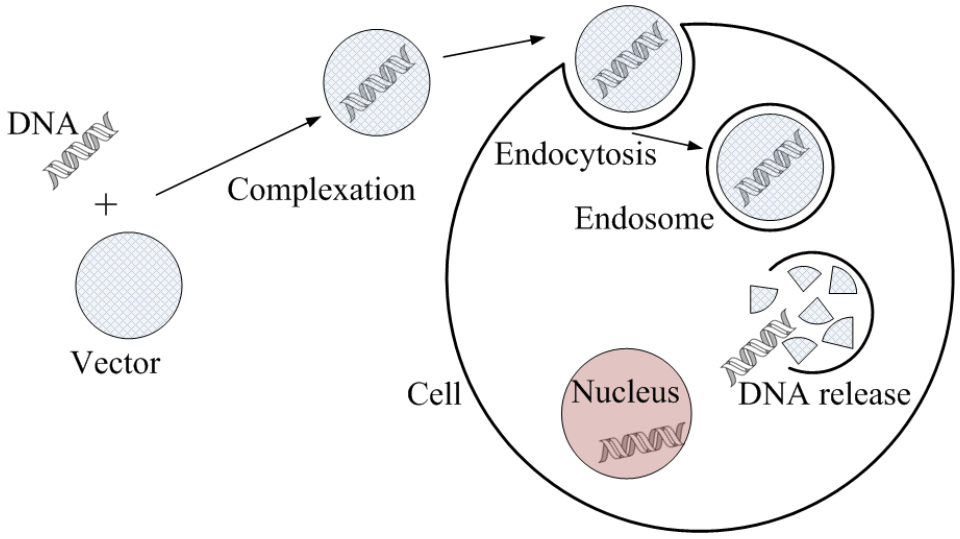

Figure 2.1. Schematic representation of the DNA transfection process (Patil, 2005a).

An ideal DNA delivery system should have high transfection efficiency with high specificity to the target cell, as well as low toxicity and immunogenicity. The system should be small, stable, biodegradable, simple and allow the release, delivery and expression of the DNA (Mansouri, 2004; Patil, 2005a). The development of novel nano-systems as DNA vectors with these properties is extremely important.

Gene delivery vehicles can be divided into two main categories, viral and non-viral particles that can be complexed with DNA molecules.

2.1. Viral Vectors

The main advantage of using viral vectors is that they are highly efficient in delivering genetic material through the cell membrane (Atkinson, 2010). The viral life cycle can be divided into two phases: infection and replication. The infection is the penetration of the viral genome into the cell, after which the expression occurs, releasing viral regulatory products used for viral replication. Viral–based gene therapy vectors encapsulate a modified genome that after expression transduce therapeutic genetic material (Kay, 2001).

Engineering genetically a virus DNA sequence is neither simple nor easy and it raises concerns about their safety. Misguided preparations can influence not only the efficacy of the system but also its toxicity and immunogenicity. These reasons and the high cost of preparation represent the major disadvantages of viral systems, because it is necessary to introduce a new disease to prevent or cure the genetic disorder and re-administration of the vector will be inefficient due to the immune response against the virus (Nayak, 2010). One of the more common viruses used in gene therapy are retrovirus and lentivirus, adenovirus and adeno-associated viruses and Herpes simplex virus (Saraswat, 2009).

Retrovirus and lentivirus can be modified to infect mammalian cells. When the virus is modified, it loses the ability of replicate and therefore it only affects one cell. Once it is in the cell it will integrate the chromosome of the host genome and provide a stable long expression of the transgene. However this integration has the negative effect of an inherent risk of insertional mutagenesis on future cells originated from the dividing process. Lentivirus suppressed this step, since it only transfects non-dividing cells and therefore will not be harmful to other cells (Atkinson, 2010; Mitomo, 2010).

Adenovirus vectors are appropriated to carry large sequences of DNA. However a severe immune response of the host leads to a limited action of the adenoviral DNA on the targeted cell, resulting in a transient expression of the therapeutic gene that is lost over time (Walther, 2000). The viral sequence is kept as an episome instead of a chromosome. The episome is constituted by closed circular DNA that can be replicated by the nucleus but it is lost during cell division. Nevertheless, after an appropriate modification the genetic information can be maintained active at least during the life of the host cell. Yet, the immune response will attack also the host cell probably in few weeks. Repeated doses of this virus will also be destroyed (Atkinson, 2010). High dosages of a first dose can induce severe toxicity. These problems affect the efficacy of this vector and are its bigger disadvantage (Kay, 2011).

Adeno-associated viral vectors represent an alternative to adeno virus. This is a non-pathogenic single stranded DNA virus that lacks of viral coding sequences and is not associated with any disease, so it does not have problems concerning toxicity or inflammatory responses (Walther, 2000). They have the ability to infect both dividing and non-dividing cells and can transduce on a broad range of *in vivo* tissues. Although the biggest disadvantage of these systems is the limitation on the size of the therapeutic gene, which cannot be higher than 5 kb (Li, 2005).

Herpes simplex virus (HSV) has a large capacity to encode therapeutic genes and can infect a large number of cell types. Due to its ability to persist in a latent state after the first infection, this virus provides the potential for a long term expression of the therapeutic gene (Kay, 2001). However, the lack of experience with recombinant herpes virus in patients and the difficulties on target specific cells as well as toxicity revealed to be limitations for this system (Saraswat, 2009).

Recombination of different types of virus or the combination of viral vectors with non-viral delivery systems could be the solution to optimise these carriers in order to obtain efficient vehicles with promising properties for gene therapies. Recently a new generation of non-viral vehicles with some of viral properties has risen. Virosomes combine the therapeutic gene with fusogenic viral envelope proteins (Bomsel, 2011; Moser, 2011; Sharma, 2010).

In conclusion, viral vectors have superior transfection efficiencies, but their use is dramatically limited by their severe side effects. However and despite their disadvantages, viral vectors represent more than 50% of the vectors used currently in clinical trials for gene therapeutics (Ginn, 2013; Lonez, 2008; Ramesh, 2001).

2.2. Non-viral vectors

Non-viral vehicles exhibit low transfection efficiency but properties like biocompatibility and potential for a large scale production make these systems very attractive for gene therapy. There are numerous non-viral systems that have reached clinical trials in the last few years (Ginn, 2013; Mintzer, 2009; Seow, 2009).

Naked DNA injections in live tissue are a non-viral method to transfect DNA into cells. This method consists in the injection of oligonucleotides or small interfering RNA (siRNA) directly to the targeted sites. The *in vivo*

expression for this therapy is effective for intravascular delivery into liver and muscle tissues. However the efficiency of transfection on skeletal or cardiac muscle is relatively low and variable (Herweijer, 2003; Luo, 2000). The use of mechanical and electrical procedures to deliver DNA into specific locations is limited. Electroporation, an electrical method, is used to facilitate the DNA transfection, by applying high voltage electrical current. As a result, high cell mortality is verified, making this strategy inadequate for clinical use. Mechanical strategies by means of applied pressure and particles bombardment are limited to external tissues, like muscle, mucosal and skin, because to reach internal organs an invasive procedure (through surgery) is needed, which will carry risks for the patient. Despite its difficulty to standardise, this methodology has reached clinical trials and, currently, represents 18% of trials for gene therapies (Ginn, 2013; Gu, 2011; Morishita, 2011).

The complexation of DNA with lipids (lipoplexes), polymers (polyplexes) and other non-viral vectors appear as an alternative methodology to classical vectors based on viruses (Morille, 2008; Zhu, 2010). One of the best properties of positively charged molecules is that they interact efficiently with negatively charged groups of DNA, mainly by electrostatic interactions, with DNA loadings close to 100%. This becomes a fast and easy method to prepare delivery systems that do not require an encapsulation step. However, the size of the complex can depend significantly on the type of cationic structure used and the preparation conditions including DNA concentration, pH, buffer, presence of salts and the N/P (nitrogen/phosphate) charge ratio (Kamimura, 2011; Leal, 2007; Sennato, 2008). Studies revealed that the optimal mean diameter of the vehicles for gene transfer is 50-60 nm (Gao, 2005; Laouini, 2013; Rodríguez-Pulido, 2009). Nevertheless, the positive overall charge of the generated DNA complex will interact with the negative

charged cell membrane and can promote forced endocytosis of larger vectors, increasing its uptake by cells and, consequently, improving DNA delivery (Lonez, 2008; Mansouri, 2004; Zelphati, 1996).

2.2.1. Lipid–based systems

Lipids are amphiphilic molecules that have the ability to self-form, in the presence of aqueous solutions, stable structures named liposomes. A lipid molecule is constituted by a head group (hydrophilic) and a hydrophobic tail composed mainly by a hydrocarbon chain. Due to the hydrophobic tail, when in contact with aqueous solutions they rearrange themselves to form a bilayer, where the lipid tails are oriented to the interior of the bilayer and the hydrophilic group is in contact with the water molecules. The size of the formed structures is easily controlled (50- 200 nm) applying methods such as freeze-thaw cycles, sonication and membrane extrusion (Dua, 2012; Honda, 2013; Jesorka, 2008).

Liposomes have several advantages over the viral systems. The low immunogenicity is one of the main advantages of liposomes. Also they are synthetic, relatively cheap to produce and do not induce cell contamination. Liposomal systems are stable and protect the DNA from nuclease degradation during transport. Additionally, liposomes can be prepared to target a specific group of cells. The principal disadvantages of these systems are the low transfection efficiency and some risk of inflammatory toxicity (Kamimura, 2011; Seow, 2009)

Liposomes can be used to transport and delivery DNA and drugs. Anionic liposomes, like DMPG (1,2-dimyristoyl-sn-glycero-3-[phospho-rac-(1-glycerol)]) can interact efficiently with positively charged drugs (Drulis-Kawa, 2010; Rodrigues, 2001; Shimanouchi, 2012). Studies with DNA molecules show that these vectors have limitations due to the inefficient entrapment.

Both liposomes and DNA possess negative charges, leading to a poor association. Therefore not many studies have been developed with this system for DNA delivery. However, it has been reported in the literature that DOPG (1,2-dioleoyl-sn-glycero-3-[phospho-rac-(1-glycerol)]) mixed with DOPE (1,2-dioleoyl-sn-glycero-3-phosphoethanolamine) can be complexed with DNA in the presence of calcium ions (Ca^{2+}) and transfect effectively the DNA (Patil, 2004; Patil, 2005b).

On the other hand, cationic liposomes interact efficiently with DNA molecules due to the opposite charges. Cationic liposomes are known to have more affinity to the cell surface or endothelial glycoproteins facilitating the crossover of the system through the membrane (Rao, 2010).

There are numerous type of cationic lipids used for gene delivery (Geusens, 2011). DOTMA (1,2-di-O-octadecenyl-3-trimethylammonium propane) was the first cationic lipid to be used. Currently, it is used in several studies and it is part of the Lipofectin® formulations, the first commercial formulation used as a standard to evaluate the effectiveness of the new transfection reagents, despite its toxicity (Tarahovsky, 2009). DOTAP (1,2-dioleoyl-3-trimethylammonium-propane, chloride salt) is a monovalent cationic aliphatic lipid first synthesised by Leventis and Silvius (Leventis, 1990). It has a high potential for transfection studies combined with its low toxicity, becoming one of the more used cationic lipids in gene therapy studies (Caracciolo, 2012). Other cationic lipids also used are DC-Chol (3β-[N-(N',N'-dimethylaminoethane)-carbamoyl]cholesterol hydrochloride) (Caracciolo, 2005; Muñoz-Úbeda, 2010); multivalent aliphatic lipids such as DOGS (dioctadecylaminoglycylspermine) and DOSPA (2,3 Dioleyloxy-N-[2(sperminecarboxaminino)ethyl]-N,N-dimethyl-1-propanaminium trifluroacetate). DOSPA is one of the lipids present in Lipofectamine®, one of

the more used commercial formulations available as reagent to assess transfection in cell experiments (Pedroso de Lima, 2003).

The transfection efficiency of cationic liposomes is dependent on the lipid molecule, the presence of helper lipids, the lipid/DNA ratio and which cells are targeted. Helper lipids, like cholesterol or DOPE (dioleoyl phosphoethanolamine), are normally neutral in charge and are used to improve the system stability, reduce the toxicity of cationic lipids and increase the half-life of liposomes and their transfection efficiency in *in vivo* studies (Crook, 1998; Hui, 1996; Miguel, 2003; Xu, 2008; Zhang, 2004). To improve the formulations based on cationic lipids, a new generation of lipids modified with fluorine atoms has emerged.

Fluorine is the most electronegative of the elements and it has a high ionisation potential and a very low polarizability (Kissa, 1994). Thereby, liquid fluorocarbons present low van der Waals interactions and low cohesive energy densities (Riess, 1994a). Consequently these fluorocarbons show very low surface tensions, excellent spreading properties, high fluidity, low dielectric constant and high compressibility (Krafft, 1998). The larger surface exhibited by these fluorinated chains combined with the low polarizability results on enhanced hydrophobicity. They show both hydrophobic and lipophobic properties at the same time (Krafft, 2001; Riess, 2009).

Many fluorocarbons are biocompatible, even at large doses they appear to be innocuous and physiologically inactive. No toxicity, carcinogenic, mutagenic effects or immunological reactions have been described for pure fluorocarbons with a molecular weight ranging from 460 to 520 g/mol. A phase I clinical trial revealed that perfluorooctyl bromide emulsion at a dosage of 1.2 or 1.8 g of fluorocarbon/kg do not present side effects in healthy humans (Krafft, 2001; Leese, 2000; Riess, 1984).

Fluorinated amphiphiles have increased tendency to self-assemble in water when compared to their hydrogenated analogues due to the strong hydrophobic character of the fluorinated chains (Krafft, 2003). They also have a lower critical micellar concentration than the hydrogenated analogues (Shinoda, 1972). Fluorinated lipids have been synthesised and tested as the main cationic lipid of DNA vectors (analogues of cationic DOSPA) as well as the helper lipid (analogues of DOPE) (Gaucheron, 2000; Gaucheron, 2001a; Gaucheron, 2001b; Gaucheron, 2002; Klein, 2010; Otmane Boussif, 2001). They have shown advantages over their hydrogenated analogues and cationic polymers (polyethylenimine) regarding the transfection potential (Huh, 1996). Due to the strong tendency to self-assemble, fluorinated lipids prevent the interaction of DNA with lipophilic or hydrophilic molecules responsible for lipofection inhibition, and protect DNA from degradation in the bloodstream since hemolytic activity is strongly suppressed (Boulanger, 2004; Riess, 1991; Riess, 1994b).

Bolaamphiphile lipids differ from conventional lipids because they have two hydrophilic heads in opposite sides of the molecule instead of one. These head groups are connected through a hydrocarbon chain (Fuhrhop, 1986). The more known natural bolaamphiphile is the monolayered membrane of thermophilic and acidophilic archaebacteria, as *Sulfolobus solfataricus* or *Sulfolobus acidocaldarius* species (Baek, 2010; Rosa, 1986). These molecules exhibit promising applications in gene therapy (Dakwar, 2012; Nuraje, 2012). They have enhanced physical stability due to the presence of the two polar groups. These molecules can be symmetrical or asymmetrical with respect to the charge present on the head groups. It is possible to synthesise a molecule with the same head group at both ends or with a positively charged group at one end and a neutral group at the other. According to the charges, the molecules will rearrange to form stable vesicles

that could be used to encapsulate, transport and deliver an active principle (Brunelle, 2009; Grinberg, 2010; Kaufman, 2013).

The self-assembly of bolaamphiphiles into structures can be very different, depending on its characteristics. If the bolaamphiphile has symmetrical head groups, it will have a tendency to generate monolayered vesicles. However if the head groups are asymmetrical, the rearrangement could be very different. Usually, they form monolayer lipid membranes when the head groups are smaller or about of the same size of the hydrophobic core. For bigger head groups, the molecules could form bilayered structures that are more rigid and can have crystal shapes. In crystal assemblies, three types of arrangements can occur. Considering *a* and *b* the head groups of an asymmetrical bolaamphiphile, the bilayer could be assembled in a parallel way, where the *a* head group is oriented to the inner space and the *b* head groups to the outer space or vice-versa with respect to the head groups (Figure 2.2.a/b). This orientation will depend on the forces present on the head groups and in the solution bulk or surface. These bolaamphiphiles can also organise themselves in an antiparallel way, where the *a* head group is oriented to a *b* head group, forming in the inner space a sequence of *a*-*b*-*a* in one layer to the corresponding sequence *b*-*a*-*b* on the other (Figure 2.2.c) (Fuhrhop, 2004).

Despite the influence of the head groups on the assembly of these structures, the hydrophobic part of the molecule also plays an important role on the way that these molecules self-assemble. Long carbon chains usually lead to monolayered lipid membranes, similar to liposomes, while short hydrocarbon chains generate vesicles like micelles (Jain, 2010; Jain, 2012; Popov, 2010). The presence of double bonds between carbons or other groups in the hydrophobic chain confers rigidity to the molecule and could lead to a U-shaped orientation of the molecule in which the hydrophilic

groups are aligned on the same side and the U bend is in the opposite side, generating a bilayered vesicle (Meister, 2007; Yan, 2009).

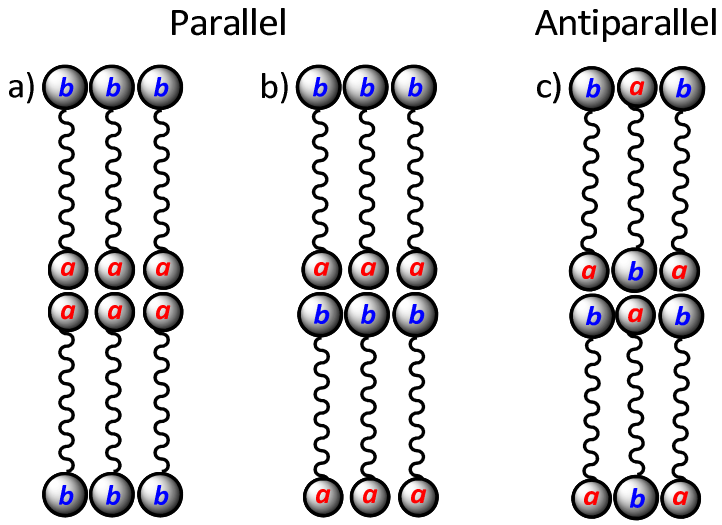

Figure 2.2. Schematic representation of possible arrangements of asymmetrical bolamphiphiles in crystals: a) parallel *a*,*a*; b) parallel *a*,*b*; c) antiparallel *a*,*b* and *b*,a (Fuhrhop, 2004).

Mixtures of bolaamphiphile with lipids are used to improve the properties of the transport vector (Caschera, 2011). The lipids present assembled according a bilayer vesicle and the bolaamphiphile can be intercalated if the size of its hydrophobic part is close to twice of the size of the hydrophobic part of the lipid molecule (Halter, 2004). Bolaamphiphile molecules can also acquire the U-shape to better blend within the bilayer (Gu, 2003; Hutter, 2012; Moss, 1991).

2.2.2. Polymeric carriers

Polymeric gene vectors are prepared by complexation of cationic polymers with anionic DNA molecules generating nanospheres with diameters ranging from 50 to 700 nm (Pannier, 2004). Polyplexes or polymer-DNA complexes are internalised by cells through endocytosis or membrane fusion, due to the overall positive charge of the complex, and the DNA release happens upon endosomal escape by proton-sponge mechanism (Boussif, 1995; Jewell, 2008). These vectors are more stable and less toxic than liposome systems and condense more DNA (Mansouri, 2004). Other advantages of these systems include low immunogenicity, versatility of physicochemical properties and easy manufacture (Merdan, 2002). Cationic polymers typically interact with DNA in a stronger way, through electrostatic interactions, leading to the formation of complexes with multiple DNA molecules. Therefore the size of the particles is related mostly with the polymer physical properties than the DNA molecule size (Mintzer, 2009). However, biocompatibility and, principally, transfection efficiency still have to be improved.

Polymer vectors strongly depend on the nature of the polymer and their molecular weight and on the ionic strength of the solutions. Modifications on the polymer structure confer specific physiological and physicochemical properties that help with the DNA uptake and the tissue targeting (Merdan, 2002).

Polyethylenimine (PEI) is one of the more used polymers in gene therapeutics. It can be synthesised in different lengths, be branched or linear and can be functionalised for better compatibility. Regarding polymer vectors, PEI presents good results when it comes to transfection efficiency (Pun, 2004). It condenses DNA efficiently forming homogeneous spherical nanoparticles.

Branched PEI has a higher molecular weight being more cytotoxic, but also condenses more DNA since it possesses more available positive charges, forming smaller nanoparticles. Linear PEI with low molecular weight shows higher transfection efficiency values and lower cytotoxicity when compared to branched PEI (Park, 2006). Despite its valuable characteristics, PEI showed high toxicity in *in vivo* trials, mostly due to the high amount of positive charges and the non-biodegradability of the compound. In order to reduce its toxicity, studies were performed to graft other polymers like polyethylene glycol (PEG), a non-ionic hydrophilic polymer (Petersen, 2002) or β-cyclodextrin (β-CD), a sugar polymer with low toxicity (Pun, 2004).

Poly(L-lysine) (PLL) is a homopolypeptide that combined with its biodegradable nature make it an ideal polymer for DNA transfection. PLL with a molecular weight above 3 kDa can effectively bind DNA molecules to form stable complexes. However, at physiological pH, all primary amine groups of PLL are protonated, which hampers the release of DNA by the endosomes and, therefore, has a weak transfection efficiency. In addition, PLL complexes exhibit a high cytotoxicity (Morille, 2008). To overcome these problems, a numerous of biodegradable PLL conjugates have been synthesised. Poly(lactic-*co*-glycolic acid)(PLGA)-grafted-PLL conjugates showed reduced toxicity and enhancements on the transfection efficiency (Jeong, 2002). Ester-linked PLL-PEG multiblock copolymers combined with various ratios of histidine residues promote gene transfer and reduce the cytotoxicity when compared to the non-derivatised PLL (Bikram, 2004). Polylysine has non-specific cell targeting. Derivatisation of PLL molecules with targeting moieties is one of the recurrent solutions for this problem. Hepatic cell targeting uses galactose (Han, 2000) or lactose (Choi, 1998) moieties. Tumor tissue targeting was achieved by conjugating PLL to folate (Cho, 2005) or transferrin (Wagner, 1991) molecules.

In order to target leukaemia T-cells a specific JL1 antigen was coupled to polylysine (Suh, 2001).

Natural polysaccharides or carbohydrates are used in gene therapy due to their properties such as biodegradability, reduced toxicity, long half-life in the blood stream and the ability to target cells of the liver, spleen, lung and spinal-cord (Liu, 2008). Numerous saccharides are used in gene delivery such as dextran (Bisht, 2009), amylose (Kaneko, 2007) and cyclodextrin (Teijeiro-Osorio, 2009).

Nanoparticles of chitosan and its derivatives are studied in the pharmaceutical field as drug carriers and DNA delivery systems (Pannier, 2004; Patel, 2012). Chitosan is a linear polymer of β-(1-4)-linked-D-glucosamine monomers with randomly distributed N-acetyl-D-glucosamine units obtained by partial deacetylation of chitin, a natural polysaccharide found principally in crustacean shells such as shrimps and crabs (Jayakumar, 2010b). It is a non-toxic and natural biodegradable cationic polymer with low immunogenicity and high biocompatibility. Other advantages of this macromolecule include stability, versatility of physicochemical properties and the possibility of modification by attaching cell compatible ligands (Jayakumar, 2010a). However, problems related to chitosan delivery systems have been reported: the pH dependence (chitosan is insoluble at neutral pH); the control of particle size, shape and polydispersity due to the variability of chitosan molecular weight; the limitation of chitosan application in humans due to hypocholesterolemia caused by high doses of chitosan; the *in vitro* transfection rate of DNA-chitosan nanoparticles is very much dependent on the cell type (Masotti, 2009; Patil, 2005a; Sato, 2001).

The systems are typically prepared either by complexation of the cationic polymer with anionic DNA or by encapsulation/entrapment of the active principle in the chitosan matrix. Chitosan colloidal systems have

normally a size ranging from a few nanometres to 500 nm (Agnihotri, 2004; Felt, 1998; Liu, 2008; Nguyen, 2009). They have been used in non-conventional drug delivery for nasal, ocular and peroral administration in order to prolong the contact time and protect DNA from nuclease degradation (Mansouri, 2004; Saranya, 2011).

There are many factors influencing the gene expression or drug delivery using chitosan systems (Kim, 2007; Mao, 2010). Kiang *et al.* tested chitosan molecules with different molecular weight and degree of deacetylation and determined that these properties play a key role in the optimisation of the formulations for DNA transfection (Kiang, 2004). An alternative approach to improve chitosan properties is to chemically modify its structure by grafting other molecules (Dünnhaupt, 2012; Gao, 2008; Kaneko, 2007; Zhou, 2011). Mathew *et al.* conjugated folic acid with carboxymethyl chitosan to produce nanoparticles capable of targeting and controlling the release of 5-fluorouracil, an anticancer drug used in chemotherapy (Mathew, 2010). Park *et al.* suggested grafting dextran to galactosylated chitosan for targeting genes to hepatocytes (Park, 2001). Unmodified chitosan was also grafted to dextran molecules of different molecular weights, resulting in compounds with different degrees of substitution and water solubility at different pH (Janciauskaite, 2008).

Dendrimers are spherical, highly branched polymers. They consist of a central core molecule, where highly branched arms grow to form a tree-like structure (Chen, 2000). The ramification happens in a well-ordered and symmetrical way with the repetition of the same sequence of reactions, producing monodisperse nanoparticles. Dendrimers are classified by the number of generations, which corresponds to the number of repeated branching sequences that are performed during the synthesis. High generation dendrimers (10) have superior transfection efficiencies when

compared to low generation dendrimers (2) (Zhu, 2010). Polyamidoamine (PAMAM) is one of the more popular dendrimers. It is safe, non-immunogenic and has a high capacity regarding transfection efficiency, due the presence of primary and tertiary amines (Vaidya, 2011). The primary amine groups play an important role on the DNA binding, producing compact nanoparticles and promoting the cellular uptake. The tertiary amines favour the release of DNA into the cytoplasm by disabling the endosomes (Vaidya, 2011).

2.2.3. Inorganic based nanoparticles

Apart from liposomal and polymeric vectors, some new DNA vehicles have gained attention in the last few years. Inorganic nanoparticles allies optical, magnetic and other physical properties to the inertness, stability and ease of functionalization, making them an attractive alternative to organic vehicles (Huang, 2011).

Metal based nanoparticles hold a high potential for applications in both diagnostic imaging and targeted drug delivery. Normally, these nanoparticles are delivered in colloidal formulations with increased circulatory half-life and carry large amounts of drug due to its extremely small sizes with large surface areas (Naahidi, 2013). Gold nanoparticles (AuNPs) are one of the more studied metals as delivery system. They are easy to synthesise with different sizes, and the process is simple, cheap and reliable. Studies have shown that these nanoparticles are biocompatible, non-toxic and that their negative charged surface can be easily functionalised with diverse macromolecules (Li, 2009; Parveen, 2012). Bhattarai *et al.* modified the surface of gold nanoparticles with chitosan. This formulation formed complexes with plasmid DNA and exhibited higher transfection efficiency in the stomach and intestine after oral delivery, when compared with Lipofectin® formulation (Bhattarai, 2008). Li *et al.* coated gold nanoparticles

with DDAB (didodecyldimethylammonium bromide, a cationic lipid). These nanoparticles can complex to lipoplexes in order to condense more DNA molecules. This combined system had higher transfection efficiency when compared to the lipoplexes alone (Li, 2010).

Quantum dots (QDs) are nanoparticles with broad applications in imaging detection and targeting. Quantum dot refers to a specific kind of nanoparticles with crystalline structure and composed by a semiconducting material, such as cadmium sulphite or cadmium selenide. These materials possess unique optical properties, which associated with its small size (2-10 nm) and the flexible surface chemistry make them ideal systems for gene therapy (Vengala, 2012). QDs nanoparticles are known to induce toxicity. To overcome this problem, surface functionality with polymers or peptides has been done and the systems showed reduced cytotoxicity and enhanced uptake *in vitro* and *in vivo* (Clarke, 2010; Daou, 2009; Tan, 2010). Zhang *et al.* proposed water-soluble QDs modified with aminoethanethiol hydrochloride and sodium thioglycolate, which interact with plasmid DNA through electrostatic interactions. This system revealed to have high transfection efficiencies and lower cellular toxicity when compared to Lipofectamine 2000® formulation (Zhang, 2012).

Magnetic nanoparticles (MNPs) have been widely used for biotechnological and biomedical applications. These nanoparticles have the ability to target a specific site and thereby reduce the systemic distribution of the cytotoxic compounds *in vivo*. The MNPs are dispersed in organic or inorganic liquid carriers that will be injected into the vascular system and driven to the targeted site by application of a magnetic field. The genetic material is released by changing the physiological conditions, for example (Veiseh, 2010). Super paramagnetic iron oxide nanoparticles (SPIONs) are one of the more used MNPs in biomedical applications. Based normally on

magnetite (Fe_3O_4) or maghemite (γ-Fe_2O_3), they are biocompatible and biodegradable nanoparticles with small sizes up to 500 nm in diameter. SPIONs are hydrophobic particles with large surface area to volume ratio. Coating these MNPs with synthetic or natural polymers, such as PEI, chitosan, dextran, PEG and PLL generates biostable and non-toxic carriers (Kami, 2011). Fouriki et al. used MNPs composed by iron oxide cores coated with PEI derivatives. Plasmid DNA was coupled to the MNPs and the system showed higher transfection potential and lower toxicity when compared with the commercial formulation Lipofectamine 2000® (Fouriki, 2012).

2.3. References

Agnihotri, S.A.; Mallikarjuna, N.N.; Aminabhavi, T.M. (**2004**). Recent advances on chitosan-based micro- and nanoparticles in drug delivery, *Journal of Controlled Release, 100*, 5.

Alderuccio, F.; Chan, J.; Scott, D.W.; Toh, B.-H. (**2009**). Gene therapy and bone marrow stem-cell transfer to treat autoimmune disease, *Trends in Molecular Medicine, 15*, 344.

Atkinson, H.; Chalmers, R. (**2010**). Delivering the goods: viral and non-viral gene therapy systems and the inherent limits on cargo DNA and internal sequences, *Genetica, 138*, 485.

Baek, K.; Kim, Y.; Kim, H.; Yoon, M.; Hwang, I.; Ko, Y.H.; Kim, K. (**2010**). Unconventional U-shaped conformation of a bolaamphiphile embedded in a synthetic host, *Chemical Communications, 46*, 4091.

Bhattarai, S.R.; K.C, R.B.; Aryal, S.; Bhattarai, N.; Kim, S.Y.; Yi, H.K.; Hwang, P.H.; Kim, H.Y. (**2008**). Hydrophobically modified chitosan/gold nanoparticles for DNA delivery, *Journal of Nanoparticle Research, 10*, 151.

Biffi, A.; Capotondo, A.; Fasano, S.; Carro, U.d.; Marchesini, S.; Azuma, H.; Malaguti, M.C.; Amadio, S.; Brambilla, R.; Grompe, M.; Bordignon, C.; Quattrini, A.; Naldini, L. (**2006**). Gene therapy of metachromatic leukodystrophy reverses neurological damage and deficits in mice, *The Journal of Clinical Investigation, 116*, 3070.

Bikram, M.; Ahn, C.-H.; Chae, S.Y.; Lee, M.; Yockman, J.W.; Kim, S.W. (**2004**). Biodegradable Poly(ethylene glycol)-co-poly(l-lysine)-g-histidine Multiblock Copolymers for Nonviral Gene Delivery, *Macromolecules, 37*, 1903.

Bisht, S.; Maitra, A. (**2009**). Dextran–doxorubicin/chitosan nanoparticles for solid tumor therapy, *Wiley Interdisciplinary Reviews: Nanomedicine and Nanobiotechnology, 1*, 415.

Bomsel, M.; Tudor, D.; Drillet, A.-S.; Alfsen, A.; Ganor, Y.; Roger, M.-G.; Mouz, N.; Amacker, M.; Chalifour, A.; Diomede, L.; Devillier, G.; Cong, Z.; Wei, Q.; Gao, H.; Qin, C.; Yang, G.-B.; Zurbriggen, R.; Lopalco, L.; Fleury, S. (**2011**). Immunization with HIV-1 gp41 Subunit Virosomes Induces Mucosal Antibodies Protecting Nonhuman Primates against Vaginal SHIV Challenges, *Immunity, 34*, 269.

Boulanger, C.; Di Giorgio, C.; Gaucheron, J.; Vierling, P. (**2004**). Transfection with fluorinated lipoplexes based on new fluorinated cationic lipids and in the presence of a bile salt surfactant, *Bioconjugate Chemistry, 15*, 901.

Boussif, O.; Lezoualc'h, F.; Zanta, M.A.; Mergny, M.D.; Scherman, D.; Demeneix, B.; Behr, J.P. (**1995**). A versatile vector for gene and oligonucleotide transfer into cells in culture and in vivo: polyethylenimine, *Proceedings of the National Academy of Sciences, 92*, 7297.

Brannon-Peppas, L.; Blanchette, J.O. (**2004**). Nanoparticle and targeted systems for cancer therapy, *Advanced Drug Delivery Reviews, 56*, 1649.

Brunelle, M.; Polidori, A.; Denoyelle, S.; Fabiano, A.S.; Vuillaume, P.Y.; Laurent-Lewandowski, S.; Pucci, B. (**2009**). A structure-activity investigation of hemifluorinated bifunctional bolaamphiphiles designed for gene delivery, *Comptes Rendus Chimie, 12*, 188.

Buckley, S.M.K.; Rahim, A.A.; Chan, J.K.Y.; David, A.L.; Peebles, D.M.; Coutelle, C.; Waddington, S.N. (**2011**). Recent advances in fetal gene therapy, *Therapeutic Delivery, 2*, 461.

Callejas, D.; Mann, C.J.; Ayuso, E.; Lage, R.; Grifoll, I.; Roca, C.; Andaluz, A.; Ruiz-de Gopegui, R.; Montane, J.; Muńoz, S.; Ferre, T.; Haurigot, V.; Zhou, S.; Ruberte, J.; Mingozzi, F.; High, K.; Garcia, F.; Bosch, F. (**2013**). Treatment of Diabetes and Long-term Survival Following Insulin and Glucokinase Gene Therapy, *Diabetes, DOI:* 10.2337/db12-1113.

Caracciolo, G.; Caminiti, R. (**2005**). Do DC-Chol/DOPE-DNA complexes really form an inverted hexagonal phase?, *Chemical Physics Letters, 411*, 327.

Caracciolo, G.; Amenitsch, H. (**2012**). Cationic liposome/DNA complexes: from structure to interactions with cellular membranes, *European Biophysics Journal, 41*, 815.

Caschera, F.; de la Serna, J.B.; Löffler, P.M.G.; Rasmussen, T.E.; Hanczyc, M.M.; Bagatolli, L.A.; Monnard, P.A. (**2011**). Stable Vesicles Composed of Monocarboxylic or Dicarboxylic Fatty Acids and Trimethylammonium Amphiphiles, *Langmuir, 27*, 14078.

Chen, W.; Turro, N.J.; Tomalia, D.A. (**2000**). Using ethidium bromide to probe the interactions between DNA and dendrimers, *Langmuir, 16*, 15.

Cho, K.C.; Kim, S.H.; Jeong, J.H.; Park, T.G. (**2005**). Folate Receptor-Mediated Gene Delivery Using Folate-Poly(ethylene glycol)-Poly(L-lysine) Conjugate, *Macromolecular Bioscience, 5*, 512.

Choi, Y.H.; Liu, F.; Park, J.S.; Kim, S.W. (**1998**). Lactose-Poly(ethylene Glycol)-Grafted Poly-l-Lysine as Hepatoma Cell-Targeted Gene Carrier, *Bioconjugate Chemistry, 9*, 708.

Clarke, S.; Pinaud, F.; Beutel, O.; You, C.; Piehler, J.; Dahan, M. (**2010**). Covalent Monofunctionalization of Peptide-Coated Quantum Dots for Single-Molecule Assays, *Nano Letters, 10*, 2147.

Crook, K.; Stevenson, B.J.; Dubouchet, M.; Porteous, D.J. (**1998**). Inclusion of cholesterol in DOTAP transfection complexes increases the delivery of DNA to cells in vitro in the presence of serum, *Gene Therapy, 5*, 137.

Dakwar, G.R.; Hammad, I.A.; Popov, M.; Linder, C.; Grinberg, S.; Heldman, E.; Stepensky, D. (**2012**). Delivery of proteins to the brain by bolaamphiphilic nano-sized vesicles, *Journal of Controlled Release, 160*, 315.

Daou, T.J.; Li, L.; Reiss, P.; Josserand, V.r.; Texier, I. (**2009**). Effect of Poly(ethylene glycol) Length on the in Vivo Behavior of Coated Quantum Dots, *Langmuir, 25*, 3040.

Drulis-Kawa, Z.; Dorotkiewicz-Jach, A. (**2010**). Liposomes as delivery systems for antibiotics, *International Journal of Pharmaceutics, 387*, 187.

Dua, J.S.; Rana, A.C.; Bhandari, A.K. (**2012**). Liposome: methods of preparation and applications, *International Journal of Pharmaceutical Studies and Research, 3*, 14.

Dünnhaupt, S.; Barthelmes, J.; Iqbal, J.; Perera, G.; Thurner, C.C.; Friedl, H.; Bernkop-Schnürch, A. (**2012**). In vivo evaluation of an oral drug

delivery system for peptides based on S-protected thiolated chitosan, *Journal of Controlled Release, 160*, 477.

Felt, O.; Buri, P.; Gurny, R. (**1998**). Chitosan: A unique polysaccharide for drug delivery, *Drug Development and Industrial Pharmacy, 24*, 979.

Fischer, A.; Hacein-Bey-Abina, S.; Cavazzana-Calvo, M. (**2010**). 20 years of gene therapy for SCID, *Nature Immunology, 11*, 457.

Fouriki, A.; Clements, M.A.; Farrow, N.; Dobson, J. (**2012**). Efficient transfection of MG-63 osteoblasts using magnetic nanoparticles and oscillating magnetic fields, *Journal of Tissue Engineering and Regenerative Medicine,* 10.1002/term.1508.n/a.

Fuhrhop, J.-H.; Wang, T. (**2004**). Bolaamphiphiles, *Chemical Reviews, 104*, 2901.

Fuhrhop, J.H.; Fritsch, D. (**1986**). Bolaamphiphiles form ultrathin, porous and unsymmetric monolayer lipid membranes, *Accounts of Chemical Research, 19*, 130.

Gao, H.; Shi, W.; Freund, L.B. (**2005**). Mechanics of receptor-mediated endocytosis, *Proceedings of the National Academy of Sciences of the United States of America, 102*, 9469.

Gao, Y.; Xu, Z.; Chen, S.; Gu, W.; Chen, L.; Li, Y. (**2008**). Arginine-chitosan/DNA self-assemble nanoparticles for gene delivery: In vitro characteristics and transfection efficiency, *International Journal of Pharmaceutics, 359*, 241.

Gaucheron, J.; Santaella, C.; Vierling, P. (**2000**). Highly Fluorinated Lipospermines for Gene Transfer: Synthesis and Evaluation of Their in Vitro Transfection Efficiency, *Bioconjugate Chemistry, 12*, 114.

Gaucheron, J.; Boulanger, C.; Santaella, C.; Sbirrazzuoli, N.; Boussif, O.; Vierling, P. (**2001a**). In Vitro Cationic Lipid-Mediated Gene Delivery

with Fluorinated Glycerophosphoethanolamine Helper Lipids, *Bioconjugate Chemistry, 12*, 949.

Gaucheron, J.; Santaella, C.; Vierling, P. (**2001b**). Improved in vitro gene transfer mediated by fluorinated lipoplexes in the presence of a bile salt surfactant, *The Journal of Gene Medicine, 3*, 338.

Gaucheron, J.; Santaella, C.; Vierling, P. (**2002**). Transfection with fluorinated lipoplexes based on fluorinated analogues of DOTMA, DMRIE and DPPES, *Biochimica et Biophysica Acta (BBA) - Biomembranes, 1564*, 349.

Geusens, B.; Strobbe, T.; Bracke, S.; Dynoodt, P.; Sanders, N.; Gele, M.V.; Lambert, J. (**2011**). Lipid-mediated gene delivery to the skin, *European Journal of Pharmaceutical Sciences, 43*, 199.

Ginn, S.L.; Alexander, I.E.; Edelstein, M.L.; Abedi, M.R.; Wixon, J. (**2013**). Gene therapy clinical trials worldwide to 2012 – an update, *The Journal of Gene Medicine, 15*, 65.

Grinberg, S.; Kipnis, N.; Linder, C.; Kolot, V.; Heldman, E. (**2010**). Asymmetric bolaamphiphiles from vernonia oil designed for drug delivery, *European Journal of Lipid Science and Technology, 112*, 137.

Gu, Q.; Zou, A.; Yuan, C.; Guo, R. (**2003**). Effects of a bolaamphiphile on the structure of phosphatidylcholine liposomes, *Journal of Colloid and Interface Science, 266*, 442.

Gu, Y.; Zhang, J.; Guo, L.; Cui, S.; Li, X.; Ding, D.; Kim, J.-M.; Ho, S.-H.; Hahn, W.; Kim, S. (**2011**). A phase I clinical study of naked DNA expressing two isoforms of hepatocyte growth factor to treat patients with critical limb ischemia, *The Journal of Gene Medicine, 13*, 602.

Halter, M.; Nogata, Y.; Dannenberger, O.; Sasaki, T.; Vogel, V. (**2004**). Engineered Lipids That Cross-Link the Inner and Outer Leaflets of Lipid Bilayers, *Langmuir, 20*, 2416.

Han, J.; Il Yeom, Y. (**2000**). Specific gene transfer mediated by galactosylated poly-l-lysine into hepatoma cells, *International Journal of Pharmaceutics, 202*, 151.

Herweijer, H.; Wolff, J.A. (**2003**). Progress and prospects: naked DNA gene transfer and therapy, *Gene Therapy, 10*, 453.

Honda, M.; Asai, T.; Oku, N.; Araki, Y.; Tanaka, M.; Ebihara, N. (**2013**). Liposomes and nanotechnology in drug development: Focus on ocular targets, *International Journal of Nanomedicine, 8*, 495.

Huang, H.-C.; Barua, S.; Sharma, G.; Dey, S.K.; Rege, K. (**2011**). Inorganic nanoparticles for cancer imaging and therapy, *Journal of Controlled Release, 155*, 344.

Huh, N.W.; Porter, N.A.; McIntosh, T.J.; Simon, S.A. (**1996**). The interaction of polyphenols with bilayers: Conditions for increasing bilayer adhesion, *Biophysical Journal, 71*, 3261.

Hui, S.W.; Langner, M.; Zhao, Y.L.; Ross, P.; Hurley, E.; Chan, K. (**1996**). The role of helper lipids in cationic liposome-mediated gene transfer, *Biophysical Journal, 71*, 590.

Hutter, T.; Linder, C.; Heldman, E.; Grinberg, S. (**2012**). Interfacial and self-assembly properties of bolaamphiphilic compounds derived from a multifunctional oil, *Journal of Colloid and Interface Science, 365*, 53.

Jain, N.; Arntz, Y.; Goldschmidt, V.r.; Duportail, G.; Mély, Y.; Klymchenko, A.S. (**2010**). New Unsymmetrical Bolaamphiphiles: Synthesis, Assembly with DNA, and Application for Gene Delivery, *Bioconjugate Chemistry, 21*, 2110.

Jain, N.; Goldschmidt, V.; Oncul, S.; Arntz, Y.; Duportail, G.; Mély, Y.; Klymchenko, A.S. (**2012**). Lactose-ornithine bolaamphiphiles for efficient gene delivery in vitro, *International Journal of Pharmaceutics, 423*, 392.

Janciauskaite, U.; Rakutyte, V.; Miskinis, J.; Makuska, R. (**2008**). Synthesis and properties of chitosan-N-dextran graft copolymers, *Reactive and Functional Polymers, 68*, 787.

Jayakumar, R.; Chennazhi, K.P.; Muzzarelli, R.A.A.; Tamura, H.; Nair, S.V.; Selvamurugan, N. (**2010a**). Chitosan conjugated DNA nanoparticles in gene therapy, *Carbohydrate Polymers, 79*, 1.

Jayakumar, R.; Prabaharan, M.; Nair, S.V.; Tokura, S.; Tamura, H.; Selvamurugan, N. (**2010b**). Novel carboxymethyl derivatives of chitin and chitosan materials and their biomedical applications, *Progress in Materials Science, 55*, 675.

Jean, M.; Alameh, M.; Buschmann, M.D.; Merzouki, A. (**2011**). Effective and safe gene-based delivery of GLP-1 using chitosan/plasmid-DNA therapeutic nanocomplexes in an animal model of type 2 diabetes, *Gene Therapy, 18*, 807.

Jeong, J.H.; Park, T.G. (**2002**). Poly(l-lysine)-g-poly(d,l-lactic-co-glycolic acid) micelles for low cytotoxic biodegradable gene delivery carriers, *Journal of Controlled Release, 82*, 159.

Jesorka, A.; Orwar, O. (**2008**). Liposomes: Technologies and Analytical Applications, *Annual Review of Analytical Chemistry, 1*, 801.

Jewell, C.M.; Lynn, D.M. (**2008**). Surface-mediated delivery of DNA: Cationic polymers take charge, *Current Opinion in Colloid & Interface Science, 13*, 395.

Kami, D.; Takeda, S.; Itakura, Y.; Gojo, S.; Watanabe, M.; Toyoda, M. (**2011**). Application of Magnetic Nanoparticles to Gene Delivery, *International Journal of Molecular Sciences, 12*, 3705.

Kamimura, K.; Suda, T.; Guisheng, Z.; Dexi, L. (**2011**). Advances in Gene Delivery Systems, *Pharmaceutical Medicine - New Zealand, 25*, 293.

Kaneko, Y.; Matsuda, S.I.; Kadokawa, J.I. (**2007**). Chemoenzymatic synthesis of amylose-grafted chitin and chitosan, *Biomacromolecules, 8*, 3959.

Kaufman, Y.; Grinberg, S.; Linder, C.; Heldman, E.; Gilron, J.; Freger, V. (**2013**). Fusion of bolaamphiphile micelles: A method to prepare stable supported biomimetic membranes, *Langmuir, 29*, 1152.

Kay, M.A.; Glorioso, J.C.; Naldini, L. (**2001**). Viral vectors for gene therapy: the art of turning infectious agents into vehicles of therapeutics, *Nature Medicine, 7*, 33.

Kay, M.A. (**2011**). State-of-the-art gene-based therapies: The road ahead, *Nature Reviews Genetics, 12*, 316.

Kiang, T.; Wen, J.; Lim, H.W.; Leong, K.W.K.W. (**2004**). The effect of the degree of chitosan deacetylation on the efficiency of gene transfection, *Biomaterials, 25*, 5293.

Kiem, H.-P.; Jerome, Keith R.; Deeks, Steven G.; McCune, Joseph M. (**2012**). Hematopoietic-Stem-Cell-Based Gene Therapy for HIV Disease, *Cell Stem Cell, 10*, 137.

Kim, S.U.; de Vellis, J. (**2009**). Stem cell-based cell therapy in neurological diseases: A review, *Journal of Neuroscience Research, 87*, 2183.

Kim, T.-H.; Jiang, H.-L.; Jere, D.; Park, I.-K.; Cho, M.-H.; Nah, J.-W.; Choi, Y.-J.; Akaike, T.; Cho, C.-S. (**2007**). Chemical modification of chitosan as a gene carrier in vitro and in vivo, *Progress in Polymer Science, 32*, 726.

Kissa, E.; *Fluorinated Surfactants: Synthesis, Properties, Applications,* Vol. 50, Marcel Dekker, United States of America, **1994**.

Klein, E.; Ciobanu, M.; Klein, J.; MacHi, V.; Leborgne, C.; Vandamme, T.; Frisch, B.; Pons, F.; Kichler, A.; Zuber, G.; Lebeau, L. (**2010**). "HFP" fluorinated cationic lipids for enhanced lipoplex stability and gene delivery, *Bioconjugate Chemistry, 21*, 360.

Krafft, M.P.; Riess, J.G. (**1998**). Highly fluorinated amphiphiles and colloidal systems, and their applications in the biomedical field. A contribution, *Biochimie, 80*, 489.

Krafft, M.P. (**2001**). Fluorocarbons and fluorinated amphiphiles in drug delivery and biomedical research, *Advanced Drug Delivery Reviews, 47*, 209.

Krafft, M.P.; Goldmann, M. (**2003**). Monolayers made from fluorinated amphiphiles, *Current Opinion in Colloid & Interface Science, 8*, 243.

Laouini, A.; Charcosset, C.; Fessi, H.; Holdich, R.G.; Vladisavljevic, G.T. (**2013**). Preparation of liposomes: a novel application of microengineered membranes - investigation of the process parameters and application to the encapsulation of vitamin E, *RSC Advances, 3*, 4985.

Leal, C.; Moniri, E.; Pegado, L.; Wennerstrom, H. (**2007**). Electrostatic attraction between DNA and a cationic surfactant aggregate. The screening effect of salt, *Journal of Physical Chemistry B, 111*, 5999.

Leese, P.T.; Noveck, R.J.; Shorr, J.S.; Woods, C.M.; Flaim, K.E.; Keipert, P.E. (**2000**). Randomized safety studies of intravenous perflubron emulsion. I. Effects on coagulation function in healthy volunteers, *Anesthesia and Analgesia, 91*, 804.

Leventis, R.; Silvius, J.R. (**1990**). Interactions of mammalian cells with lipid dispersions containing novel metabolizable cationic amphiphiles, *Biochimica et Biophysica Acta (BBA) - Biomembranes, 1023*, 124.

Li, C.; Bowles, D.E.; van Dyke, T.; Samulski, R.J. (**2005**). Adeno-associated virus vectors: potential applications for cancer gene therapy, *Cancer Gene Therapy, 12*, 913.

Li, D.; Li, P.; Li, G.; Wang, J.; Wang, E. (**2009**). The effect of nocodazole on the transfection efficiency of lipid-bilayer coated gold nanoparticles, *Biomaterials, 30*, 1382.

Li, D.; Li, G.; Li, P.; Zhang, L.; Liu, Z.; Wang, J.; Wang, E. (**2010**). The enhancement of transfection efficiency of cationic liposomes by didodecyldimethylammonium bromide coated gold nanoparticles, *Biomaterials, 31*, 1850.

Liu, Z.; Jiao, Y.; Wang, Y.; Zhou, C.; Zhang, Z. (**2008**). Polysaccharides-based nanoparticles as drug delivery systems, *Advanced Drug Delivery Reviews, 60*, 1650.

Lonez, C.; Vandenbranden, M.; Ruysschaert, J.-M. (**2008**). Cationic liposomal lipids: From gene carriers to cell signaling, *Progress in Lipid Research, 47*, 340.

Luo, D.; Saltzman, W.M. (**2000**). Synthetic DNA delivery systems, *Nature Biotechnology, 18*, 33.

Manfredsson, F.P.; Mandel, R.J. (**2010**). Development of gene therapy for neurological disorders, *Discovery medicine, 9*, 204.

Mansouri, S.; Lavigne, P.; Corsi, K.; Benderdour, M.; Beaumont, E.; Fernandes, J.C. (**2004**). Chitosan-DNA nanoparticles as non-viral vectors in gene therapy: strategies to improve transfection efficacy, *European Journal of Pharmaceutics and Biopharmaceutics, 57*, 1.

Mao, S.; Sun, W.; Kissel, T. (**2010**). Chitosan-based formulations for delivery of DNA and siRNA, *Advanced Drug Delivery Reviews, 62*, 12.

Masotti, A.; Ortaggi, G. (**2009**). Chitosan Micro- and Nanospheres: Fabrication and Applications for Drug and DNA Delivery, *Mini-Reviews in Medicinal Chemistry, 9*, 463.

Mathew, M.E.; Mohan, J.C.; Manzoor, K.; Nair, S.V.; Tamura, H.; Jayakumar, R. (**2010**). Folate conjugated carboxymethyl chitosan-manganese doped zinc sulphide nanoparticles for targeted drug delivery and imaging of cancer cells, *Carbohydrate Polymers, 80*, 442.

Meister, A.; Weygand, M.J.; Brezesinski, G.; Kerth, A.; Drescher, S.; Dobner, B.; Blume, A. (**2007**). Evidence for a Reverse U-Shaped Conformation of Single-Chain Bolaamphiphiles at the Air−Water Interface, *Langmuir, 23*, 6063.

Merdan, T.; Kopeček, J.; Kissel, T. (**2002**). Prospects for cationic polymers in gene and oligonucleotide therapy against cancer, *Advanced Drug Delivery Reviews, 54*, 715.

Miguel, M.G.; Pais, A.; Dias, R.S.; Leal, C.; Rosa, M.; Lindman, B. (**2003**). DNA-cationic amphiphile interactions, *Colloids and Surfaces A: Physicochemical and Engineering Aspects, 228*, 43.

Mintzer, M.A.; Simanek, E.E. (**2009**). Nonviral Vectors for Gene Delivery, *Chemical Reviews, 109*, 259.

Mitomo, K.; Griesenbach, U.; Inoue, M.; Somerton, L.; Meng, C.; Akiba, E.; Tabata, T.; Ueda, Y.; Frankel, G.M.; Farley, R.; Singh, C.; Chan, M.; Munkonge, F.; Brum, A.; Xenariou, S.; Escudero-Garcia, S.; Hasegawa, M.; Alton, E.W. (**2010**). Toward gene therapy for cystic fibrosis using a lentivirus pseudotyped with Sendai virus envelopes, *Molecular Therapy, 18*, 1173.

Morille, M.; Passirani, C.; Vonarbourg, A.; Clavreul, A.; Benoit, J.P. (**2008**). Progress in developing cationic vectors for non-viral systemic gene therapy against cancer, *Biomaterials, 29*, 3477.

Morishita, R.; Makino, H.; Aoki, M.; Hashiya, N.; Yamasaki, K.; Azuma, J.; Taniyama, Y.; Sawa, Y.; Kaneda, Y.; Ogihara, T. (**2011**). Phase I/IIa Clinical Trial of Therapeutic Angiogenesis Using Hepatocyte Growth Factor Gene Transfer to Treat Critical Limb Ischemia, *Arteriosclerosis, Thrombosis, and Vascular Biology, 31*, 713.

Moser, C.; Amacker, M.; Zurbriggen, R. (**2011**). Influenza virosomes as a vaccine adjuvant and carrier system, *Expert Review of Vaccines, 10*, 437.

Moss, R.A.; Fujita, T.; Okumura, Y. (**1991**). Dynamics of a bolaamphiphilic lipid in a bilayer liposome, *Langmuir, 7*, 2415.

Muñoz-Úbeda, M.; Rodríguez-Pulido, A.; Nogales, A.; Martín-Molina, A.; Aicart, E.; Junquera, E. (**2010**). Effect of lipid composition on the structure and theoretical phase diagrams of DC-Chol/DOPE-DNA lipoplexes, *Biomacromolecules, 11*, 3332.

Naahidi, S.; Jafari, M.; Edalat, F.; Raymond, K.; Khademhosseini, A.; Chen, P. (**2013**). Biocompatibility of engineered nanoparticles for drug delivery, *Journal of Controlled Release, 166*, 182.

Nayak, S.; Herzog, R.W. (**2010**). Progress and prospects: Immune responses to viral vectors, *Gene Therapy, 17*, 295.

Nguyen, D.N.; Green, J.J.; Chan, J.M.; Longer, R.; Anderson, D.G. (**2009**). Polymeric Materials for Gene Delivery and DNA Vaccination, *Advanced Materials, 21*, 847.

Nuraje, N.; Bai, H.; Su, K. (**2012**). Bolaamphiphilic molecules: Assembly and applications, *Progress in Polymer Science,*

Otmane Boussif; Jérôme Gaucheron; Caroline Boulanger; Catherine Santaella; Hanno V. J. Kolbe; Pierre Vierling (**2001**). Enhanced in vitro and in vivo cationic lipid-mediated gene delivery with a fluorinated glycerophosphoethanolamine helper lipid, *The Journal of Gene Medicine, 3*, 109.

Pannier, A.K.; Shea, L.D. (**2004**). Controlled release systems for DNA delivery, *Molecular Therapy, 10*, 19.

Park, I.K.; Park, Y.H.; Shin, B.A.; Choi, E.S.; Kim, Y.R.; Akaike, T.; Cho, C.S. (**2001**). Galactosylated chitosan-graft-dextran as hepatocyte-targeting DNA carrier, *Journal of Controlled Release, 75*, 433.

Park, T.G.; Jeong, J.H.; Kim, S.W. (**2006**). Current status of polymeric gene delivery systems, *Advanced Drug Delivery Reviews, 58*, 467.

Parveen, S.; Misra, R.; Sahoo, S.K. (**2012**). Nanoparticles: a boon to drug delivery, therapeutics, diagnostics and imaging, *Nanomedicine: Nanotechnology, Biology and Medicine, 8*, 147.

Patel, T.; Zhou, J.; Piepmeier, J.M.; Saltzman, W.M. (**2012**). Polymeric nanoparticles for drug delivery to the central nervous system, *Advanced Drug Delivery Reviews, 64*, 701.

Patil, S.; Rhodes, D.; Burgess, D. (**2004**). Anionic liposomal delivery system for DNA transfection, *The AAPS Journal, 6*, 13.

Patil, S.; Rhodes, D.; Burgess, D. (**2005a**). DNA-based therapeutics and DNA delivery systems: A comprehensive review, *The AAPS Journal, 7*, E61.

Patil, S.D.; Rhodes, D.G.; Burgess, D.J. (**2005b**). Biophysical characterization of anionic lipoplexes, *Biochimica et Biophysica Acta (BBA) - Biomembranes, 1711*, 1.

Pedroso de Lima, M.C.; Neves, S.; Filipe, A.; Düzgüneş, N.; Simões, S. (**2003**). Cationic liposomes for gene delivery: from biophysics to biological applications, *Current Medicinal Chemistry, 10*, 1221.

Petersen, H.; Fechner, P.M.; Fischer, D.; Kissel, T. (**2002**). Synthesis, Characterization, and Biocompatibility of Polyethylenimine-graft-poly(ethylene glycol) Block Copolymers, *Macromolecules, 35*, 6867.

Popov, M.; Linder, C.; Deckelbaum, R.J.; Grinberg, S.; Hansen, I.H.; Shaubi, E.; Waner, T.; Heldman, E. (**2010**). Cationic vesicles from novel bolaamphiphilic compounds, *Journal of Liposome Research, 20*, 147.

Pringle, I.; Hyde, S.; Gill, D. (**2009**). Non-viral vectors in cystic fibrosis gene therapy: recent developments and future prospects, *Expert Opinion on Biological Therapy, 9*, 991.

Pun, S.H.; Bellocq, N.C.; Liu, A.; Jensen, G.; Machemer, T.; Quijano, E.; Schluep, T.; Wen, S.; Engler, H.; Heidel, J.; Davis, M.E. (**2004**). Cyclodextrin-Modified Polyethylenimine Polymers for Gene Delivery, *Bioconjugate Chemistry, 15*, 831.

Ramesh, R.; Saeki, T.; Templeton, N.S.; Ji, L.; Stephens, L.C.; Ito, I.; Wilson, D.R.; Wu, Z.; Branch, C.D.; Minna, J.D.; Roth, J.A. (**2001**). Successful treatment of primary and disseminated human lung cancers by systemic delivery of tumor suppressor genes using an improved liposome vector, *Molecular Therapy, 3*, 337.

Rao, N.M. (**2010**). Cationic lipid-mediated nucleic acid delivery: beyond being cationic, *Chemistry and Physics of Lipids, 163*, 245.

Riess, J.G. (**1984**). Reassessment of Criteria for the Selection of Perfluorochemicals for Second-Generation Blood Substitutes: Analysis of Structure/Property Relationships, *Artificial Organs, 8*, 44.

Riess, J.G.; Pace, S.; Zarif, L. (**1991**). Highly effective surfactants with low hemolytic activity, *Advanced Materials, 3*, 249.

Riess, J.G. (**1994a**). Highly fluorinated systems for oxygen transport, diagnosis and drug delivery, *Colloids and Surfaces A: Physicochemical and Engineering Aspects, 84*, 33.

Riess, J.G. (**1994b**). Fluorinated Vesicles, *Journal of Drug Targeting, 2*, 455.

Riess, J.G. (**2009**). Highly fluorinated amphiphilic molecules and self-assemblies with biomedical potential, *Current Opinion in Colloid & Interface Science, 14*, 294.

Rodrigues, C.; Gameiro, P.; Reis, S.; Lima, J.L.; de Castro, B. (**2001**). Derivative spectrophotometry as a tool for the determination of drug partition

coefficients in water/dimyristoyl-L-alpha-phosphatidylglycerol (DMPG) liposomes, *Biophysical Chemistry, 94*, 97.

Rodríguez-Pulido, A.; Martín-Molina, A.; Rodríguez-Beas, C.s.; Llorca, O.; Aicart, E.; Junquera, E. (**2009**). A Theoretical and Experimental Approach to the Compaction Process of DNA by Dioctadecyldimethylammonium Bromide/Zwitterionic Mixed Liposomes, *The Journal of Physical Chemistry B, 113*, 15648.

Rosa, M.; Gambacorta, A.; Gliozzi, A. (**1986**). Structure, biosynthesis, and physicochemical properties of archaebacterial lipids, *Microbiological Reviews, 50*, 70.

Saranya, N.; Moorthi, A.; Saravanan, S.; Devi, M.P.; Selvamurugan, N. (**2011**). Chitosan and its derivatives for gene delivery, *International Journal of Biological Macromolecules, 48*, 234.

Saraswat, P.; Soni, R.R.; Bhandari, A.; Nagori, B.P. (**2009**). DNA as therapeutics; An update, *Indian Journal of Pharmaceutical Sciences, 71*, 488.

Sato, T.; Ishii, T.; Okahata, Y. (**2001**). In vitro gene delivery mediated by chitosan. Effect of pH, serum, and molecular mass of chitosan on the transfection efficiency, *Biomaterials, 22*, 2075.

Sennato, S.; Truzzolillo, D.; Bordi, F.; Cametti, C. (**2008**). Effect of Temperature on the Reentrant Condensation in Polyelectrolyte-Liposome Complexation, *Langmuir, 24*, 12181.

Seow, Y.; Wood, M.J. (**2009**). Biological gene delivery vehicles: beyond viral vectors, *Molecular Therapy, 17*, 767.

Sharma, R.; Yasir, M. (**2010**). Virosomes: A novel carrier for drug delivery, *International Journal of PharmTech Research, 2*, 2327.

Shimanouchi, T.; Shimauchi, N.; Ohnishi, R.; Kitaura, N.; Yagi, H.; Goto, Y.; Umakoshi, H.; Kuboi, R. (**2012**). Formation of spherulitic amyloid β

aggregate by anionic liposomes, *Biochemical and Biophysical Research Communications, 426*, 165.

Shinoda, K.; Hato, M.; Hayashi, T. (**1972**). Physicochemical properties of aqueous solutions of fluorinated surfactants, *The Journal of Physical Chemistry, 76*, 909.

Strayer, D.S.; Akkina, R.; Bunnell, B.A.; Dropulic, B.; Planelles, V.; Pomerantz, R.J.; Rossi, J.J.; Zaia, J.A. (**2005**). Current status of gene therapy strategies to treat HIV/AIDS, *Molecular Therapy, 11*, 823.

Suh, W.; Chung, J.-K.; Park, S.-H.; Kim, S.W. (**2001**). Anti-JL1 antibody-conjugated poly (l-lysine) for targeted gene delivery to leukemia T cells, *Journal of Controlled Release, 72*, 171.

Summerton, J.E. (**2007**). Morpholino, siRNA, and S-DNA compared: impact of structure and mechanism of action on off-target effects and sequence specificity, *Current Topics in Medicinal Chemistry*, 7, 651.

Tan, S.J.; Jana, N.R.; Gao, S.; Patra, P.K.; Ying, J.Y. (**2010**). Surface-Ligand-Dependent Cellular Interaction, Subcellular Localization, and Cytotoxicity of Polymer-Coated Quantum Dots, *Chemistry of Materials, 22*, 2239.

Tarahovsky, Y.S. (**2009**). Cell transfection by DNA-lipid complexes - lipoplexes, *Biochemistry. Biokhimiia, 74*, 1293.

Teijeiro-Osorio, D.; Remuñán-López, C.; Alonso, M.J. (**2009**). Chitosan/cyclodextrin nanoparticles can efficiently transfect the airway epithelium in vitro, *European Journal of Pharmaceutics and Biopharmaceutics, 71*, 257.

Urnov, F.D.; Rebar, E.J.; Holmes, M.C.; Zhang, H.S.; Gregory, P.D. (**2010**). Genome editing with engineered zinc finger nucleases, *Nature Reviews: Genetics, 11*, 636.

Vaidya, A.; Agarwal, A.; Jain, A.; Agrawal, R.K.; Jain, S.K. (**2011**). Bioconjugation of polymers: a novel platform for targeted drug delivery, *Current Pharmaceutical Design, 17*, 1108.

Veiseh, O.; Gunn, J.W.; Zhang, M. (**2010**). Design and fabrication of magnetic nanoparticles for targeted drug delivery and imaging, *Advanced Drug Delivery Reviews, 62*, 284.

Vengala, P.; Dasari, A.; Yeruva, N. (**2012**). Quantum dots for drug delivery and therapy, *International Journal of Pharmacy and Technology, 4*, 2055.

Wagner, E.; Cotten, M.; Mechtler, K.; Kirlappos, H.; Birnstiel, M.L. (**1991**). DNA-binding transferrin conjugates as functional gene-delivery agents: synthesis by linkage of polylysine or ethidium homodimer to the transferrin carbohydrate moiety, *Bioconjugate Chemistry, 2*, 226.

Walther, W.; Stein, U. (**2000**). Viral vectors for gene transfer: a review of their use in the treatment of human diseases, *Drugs, 60*, 249.

Xu, L.; Anchordoquy, T.J. (**2008**). Cholesterol domains in cationic lipid/DNA complexes improve transfection, *Biochimica et Biophysica Acta (BBA) - Biomembranes, 1778*, 2177.

Yan, Y.; Lu, T.; Huang, J. (**2009**). Recent advances in the mixed systems of bolaamphiphiles and oppositely charged conventional surfactants, *Journal of Colloid and Interface Science, 337*, 1.

Zelphati, O.; Szoka, F.C. (**1996**). Liposomes as a carrier for intracellular delivery of antisense oligonucleotides: a real or magic bullet?, *Journal of Controlled Release, 41*, 99.

Zhang, H.-L.; Zhang, M.-Z.; Li, X.-Y.; Wan, M.; Li, Y.-Q.; Zhang, R.-Y.; Zhao, Y.-D. (**2012**). A convenient method of preparing gene vector for real time monitoring transfection process based on the quantum dots, *Materials Research Bulletin, 47*, 3330.

Zhang, S.; Xu, Y.; Wang, B.; Qiao, W.; Liu, D.; Li, Z. (**2004**). Cationic compounds used in lipoplexes and polyplexes for gene delivery, *Journal of Controlled Release, 100*, 165.

Zhou, Y.; Chen, J.H.; Wang, H.; Wang, C.X.; Zhang, J.Y.; Tao, Y.W.; Zheng, G.; Xie, H.Y. (**2011**). Synthesis and characterization of folate-poly(ethylene glycol) chitosan graft-polyethylenimine as a non-viral carrier for tumor-targeted gene delivery, *African Journal of Biotechnology, 10*, 6120.

Zhu, L.; Mahato, R.I. (**2010**). Lipid and polymeric carrier-mediated nucleic acid delivery, *Expert Opinion on Drug Delivery, 7*, 1209.

Chapter 3

Interaction of DNA with lipid monolayers

Interfacial research investigates the thermodynamics of the adsorption layers at the liquid interface in order to better understand the equilibrium process at the surface of liquids or at the interface between two liquids (Fainerman, 1998). Mixed monolayers of insoluble lipids usually present deviations to the Langmuir adsorption isotherm and the equation of state for adsorption layers, due to different molar area values. Also the ability for reorientation and aggregation of some lipids interferes with the fluid state of the monolayers (Fainerman, 1998).

The application of emerging technology with high resolutions at the nanoscale level allows a deeper study of the thermodynamics involved in the interfacial equilibrium through Langmuir monolayers. Techniques as pressure-area isotherms, surface potential, Brewster angle microscopy (BAM) and infrared reflection-absorption spectroscopy (IRRAS) were used to study interactions in two-dimensional arrangements of amphiphilic molecules (Buschow, 2001; Butt, 2006; Maltseva, 2005). These methods allow a

considerable knowledge on interactions between different species, their molecular orientation and defects, the shape and texture of the domains and the two-dimensional lattice structure. These techniques are also used to mimic the binding of polyelectrolytes to the interface (peptides, proteins, DNA) and to simulate enzymatic reactions at the membrane surfaces (Brezesinski, 2003).

The study using Langmuir monolayers provided information about the lipid mixtures, DOTAP and cholesterol or fluorinated cholesterol that was useful for the studies with liposomes. A comparative study between cholesterol and fluorinated cholesterol as the helper lipids in DOTAP systems was performed using Langmuir monolayer studies (Gromelski, 2006; Symietz, 2004). Pressure-area isotherms, surface potential and Brewster angle microscopy measurements were carried out to gain information about molecular distribution and mixing behaviour of the lipids in the monolayer. The DNA adsorption process at the monolayer interface was studied by vibrational spectroscopy (Brezesinski, 2003). DNA is expected to adsorb from the subphase to the interface due to electrostatic forces and to induce changes in the density and composition of the interface layer, which is detected by infrared reflection absorption spectroscopy (Gromelski, 2006).

3.1. Lipid Monolayer experiments

3.1.1. Chemicals

DOTAP (1,2-dioleoyl-3-trimethylammonium-propane, chloride salt, MW 698.542), cholesterol (ovine wool, > 98%, MW 386.355) and F7-cholesterol (25,26,26,26,27,27,27-heptafluorocholesterol, MW 512.587) (Figure 3.1) were purchased from Avanti Polar Lipids, Inc. Salmon testes DNA

and PBS (phosphate buffered saline: 0.01 M phosphate buffer, 0.0027 M potassium chloride and 0.137 M sodium chloride, pH 7.4) were purchased from Sigma-Aldrich. The deionised water was purified with Milli-Q apparatus with the specific resistance of 18.2 MΩ·cm. Chloroform (Merck) was used to dissolve the lipids.

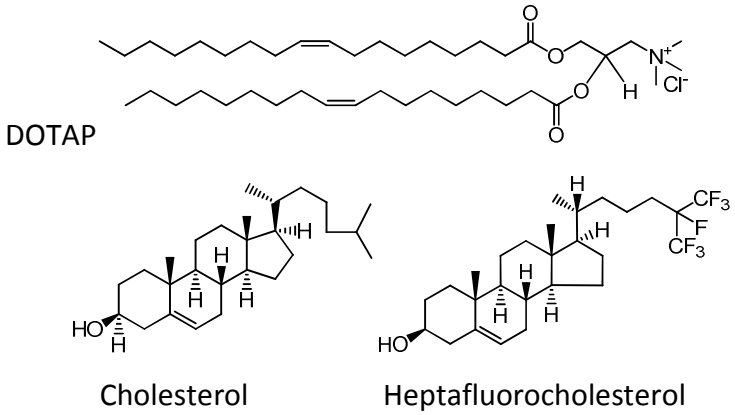

Figure 3.1. Chemical structures of DOTAP, CHOL (cholesterol) and F7-CHOL (heptafluorocholesterol).

3.1.2. Pressure/area Isotherms

The early research on Langmuir monolayers stated that different two-dimensional phases exist or co-exist. Monolayer phases are classified in gaseous (G), Liquid-expanded (LE), Liquid-condensed (LC) and solid (S), as visible in Figure 3.2. The monolayer compressibility varies according to the sequence G>LE>LC>S, and it is determined by measuring the surface pressure-

molecular area (π-A) isotherms under equilibrium conditions (Vollhardt, 2006).

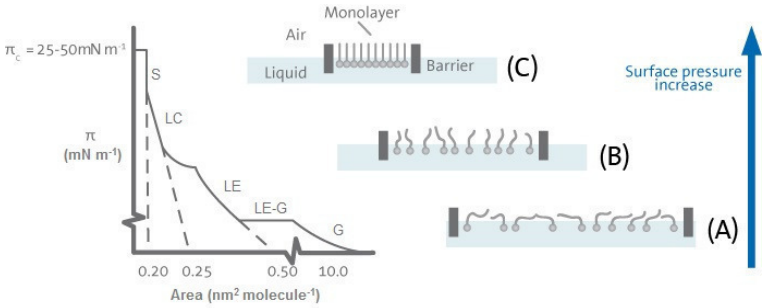

Figure 3.2. Representative phases of a surface pressure-area isotherm of a Langmuir monolayer.

The lateral surface pressure π of the monolayer is the difference between the surface tension (γ) of pure water (72.8 mN/m at 20°C) and water covered with monolayer (Gromelski, 2004; 2006):

$$\pi = \gamma_{solvent} - \gamma_{solution} \tag{3.1}$$

The surface pressure is a measurement of the cohesive energy present at the interface. The lipid molecules will interact with each other through attractive and repulsive forces (Freire, 2007). The air/water interface possesses an excess of free energy from the difference in environment between the surface molecules and those in the bulk. This interfacial free energy is responsible for the surface tension. The surface pressure-area isotherms were recorded using a PTFE Langmuir film balance system (Riegler & Kirstein, Potsdam, Germany), represented on Figure 3.3.

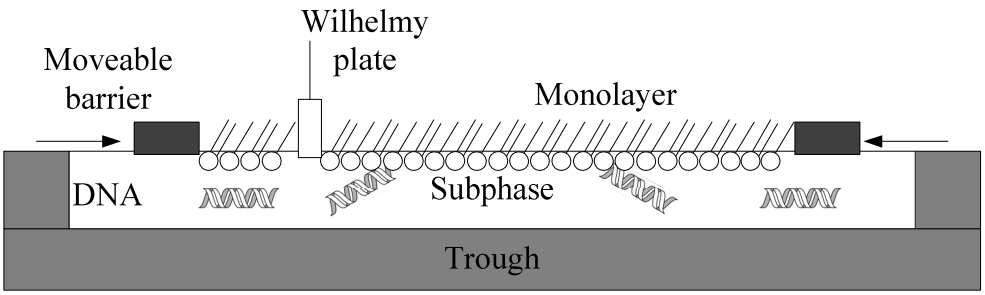

Figure 3.3. Langmuir film balance system.

Monolayers of DOTAP, cholesterol, F7-cholesterol or their mixtures were obtained by spreading the solution of lipids in chloroform at a concentration of 1 mM on the buffer surface (PBS buffer or PBS containing 0.1 mg/mL of DNA). The surface tension was determined with a continuous Wilhelmy-type pressure measuring system using a 10 mm wide filter paper as plate. The monolayers were compressed at a constant velocity of 5 $Å^2$/molecule/min and at a temperature of (20 ± 1)°C. The average area per molecule *A* of an ideal mixture was calculated by the additivity relationship considering the molar fraction *X* of each component,

$$A = X_1 A_1 + X_2 A_2 \tag{3.2}$$

3.1.3. Surface Potential

Cells need an electric field and concentration profiles of ions in the proximity of their membranes to exist. These parameters are described by the classical Gouy-Chapman (GC) model of electrical double layer (EDL). However

deviations from that rule happen in non-homogeneously charged surfaces, like the lipid water interface of many mixtures (Shapovalov, 2006).

Surface potential experiments provide additional information on the packing and orientation of the lipid molecules at the monolayer. The potential of the surface is read as a function of the area per molecule and depends on the monolayer phase. At larger areas per molecule the surface potential is close to zero. It remains constant till a critical area is reached on compression, increasing or decreasing depending on the charge of the lipids in study (Oliveira, 1997). These critical areas normally coincide with the increase of the surface pressure values on Langmuir isotherms, indicating that the monolayer become more structured than before, due the compression effect.

Surface potential measurements were recorded using a homemade device (V. L. Shapovalov, Institute of Chemical Physics, RAS, Moscow, Russia) that combines a Kelvin probe sensor and a Wilhelmy plate in order to record at the same time the surface potential and the surface pressure isotherm. Briefly, a 250 x 100 x 8 mm^3 Teflon trough with a single barrier (asymmetric compression) contains a gold-plated electrode of 10 mm diameter that vibrates at *ca.* 80 Hz. The reference electrode was made of Ag/AgCl (Shapovalov, 2006). Surface potential and surface pressure was set to zero before spreading the monolayer onto the subphase and the results are recorded at the same conditions described above. Final surface potential data were referenced to the surface potential of a subphase without the monolayer.

3.1.4. Brewster Angle Microscopy (BAM)

BAM technique was first developed to clarify the structural characteristics of amphiphilic substances at the air-water interface. It provides information on the morphology of the monolayers including the

inner structure of the formed domains as well as heterogeneities in thin films (Melzer, 1997). Inhomogeneities on the monolayer can be from lipid density variation at the water surface (Symietz, 2004).

A clean and perfect interface between two media with different refractive index has no reflection if it is illuminated by parallel (p)-polarised light under a unique angle of incidence, called Brewster angle (α). For the air/water interface, the Brewster angle is 53.1° (Henon, 1991; Kaercher, 1993). The formation of a thin film with a different refractive index changes the optical status that is now reflecting the light and producing an image of the monolayer (Rodríguez Patino, 1999). The occurrence of domains with higher molecular densities will reflect the light and be visible as brighter areas compared with the dark background of the water surface.

The system used is available commercially (BAM2, Nanofilm Technology Ltd., Germany; 20 mW laser, wavelength 514 nm, resolution 3 µm) and consists of a CCD camera that detects the p-polarised light of the diode laser reflected from the surface for film characterisation. The Brewster angle for air-water interface is 53.1°. The recorded images were analysed with the existing software and corrected for the perspective of observation under the Brewster angle with a spatial resolution of about 2 µm.

3.1.5. Infrared Reflection Absorption Spectroscopy (IRRAS)

Infrared reflection absorption spectroscopy of lipid monolayers at the air/water interface contributes with unique molecular structure and orientation information from the film compounds. Parameters as lipid chain conformation, tilt angle and presence of DNA molecules at the interface could

be determined with this technique via changes in vibrational frequencies (Brezesinski, 2003; Gromelski, 2004).

IRRAS is based on the observation that when mid-IR radiation reaches the aqueous monolayers, a fraction of the light is reflected from the molecular compounds of the thin film at the surface. Light in a well-defined polarisation state, either parallel (p-polarised) or perpendicular (s-polarised) to the plane of incidence, impinges onto the surface at a well-defined and controlled angle of incidence, which is reflected and detected at the same angle (Mendelsohn, 2010). Table 3.1 shows some of the more important Mid-IR group frequencies of phospholipids and DNA (Banyay, 2003; Blume, 1996; Gromelski, 2006).

Table 3.1. More common Mid-IR group frequencies of phospholipids and DNA (Banyay, 2003; Blume, 1996; Gromelski, 2006).

Wavenumber (cm^{-1})	**Symbol**	**Description**
DNA characteristic bands		
1720-1710	ν(C=O)	DNA base pairing
1225-1220	$\nu_{as}(PO_2^-)$	Asymmetric PO_2^- stretching (B form)
1090-1085	$\nu_s(PO_2^-)$	Symmetric PO_2^- stretching of backbone (A/B form)
1069-1044	ν(C-O)	C-O stretching of backbone
970	ν(C-C)	C-C stretching of backbone (B form)
Phospholipid characteristic bands		
3400-3700	ν(O-H)	H-O-H stretching
2925	$\nu_{as}(CH_2)$	Asymmetric CH_2 stretching (LE phase)
2918	$\nu_{as}(CH_2)$	Asymmetric CH_2 stretching (LC phase)
2855	$\nu_s(CH_2)$	Symmetric CH_2 stretching (LE phase)
2849	$\nu_s(CH_2)$	Symmetric CH_2 stretching (LC phase)
1740	ν(C=O)	C=O stretching

IRRAS spectra were recorded using an IFS 66 FTIR spectrometer (Bruker, Germany) equipped with a liquid nitrogen cooled MCT detector. The spectrometer was coupled to a Langmuir film balance, placed in a sealed container, to guarantee a constant water vapour atmosphere. The IR beam was focused on the water surface of the Langmuir trough at an angle of incidence equal to 40° and was polarised vertically (s) using a KRS-5 (thallium bromide and iodide mixed crystal) wire grid polariser. FTIR spectra were collected at 8 cm^{-1} resolution with 400 scans and subtracted from the spectrum of the reference trough (PBS buffer). The waiting time for DNA adsorption was the same in all experiments and was 1 hour (Gromelski, 2006).

3.2. Results and Discussion

3.2.1. DOTAP/F7-cholesterol monolayers

The surface pressure-area (π-A) isotherm of DOTAP on phosphate buffered saline (PBS) is characteristic of a liquid-expanded phase and has an initial pressure increase at 105 $Å^2$/molecule. The addition of cholesterol (CHOL) or F7-cholesterol (F7-CHOL) to DOTAP (chemical structures shown in Figure 3.1) at 1:1 ratio leads to the same overall liquid-expanded phase behaviour with a decrease in the area per molecule (Figure 3.4). The isotherms of the pure CHOL monolayer and the pure F7-CHOL monolayer on PBS buffer are identical and are characteristic of a condensed phase, showing small changes in average molecular area with increasing surface pressure. The initial increase is at 55 $Å^2$/molecule and their limiting area A_0 (extrapolation of the linear part of the isotherm to $\pi = 0$) is 40 $Å^2$/molecule. The lateral interactions between DOTAP and the sterols were analysed by calculating the

average area per molecule within the mixed monolayer as a function of lipid concentration at the surface pressures of 5 and 35 mN/m (Table 3.2). A negative deviation to the ideal mixing or complete demixing is observed experimentally, particularly at 5 mN/m, supporting the condensing effect of the sterols. BAM analysis of DOTAP/CHOL 1:1 shows domains at surface pressures below 15 mN/m, which disappear completely when the pressure reaches 20 mN/m (Figure 3.4).

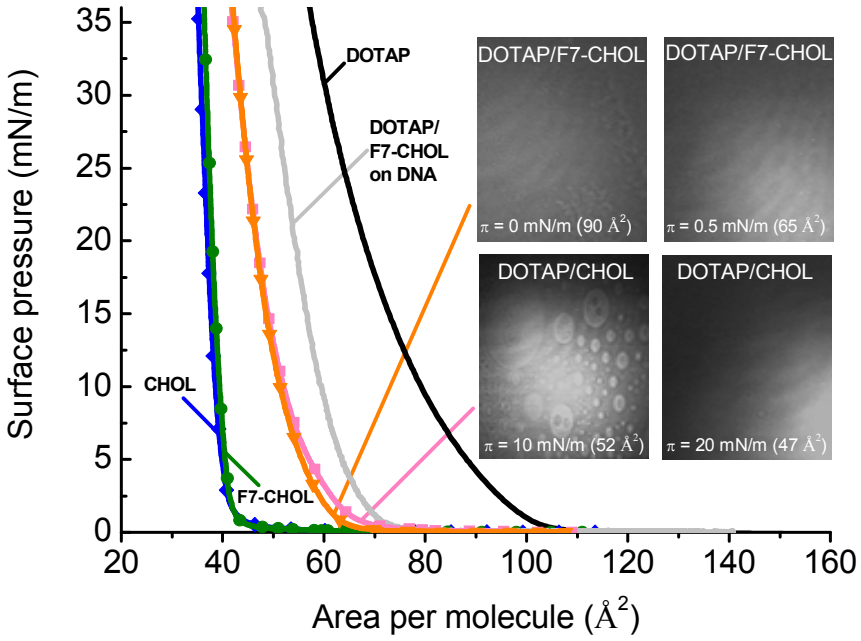

Figure 3.4. Pressure-area isotherms of monolayers of DOTAP, cholesterol (CHOL), F7-cholesterol (F7-CHOL), DOTAP/cholesterol 1:1 mixture (DOTAP/CHOL) and DOTAP/F7-cholesterol 1:1 mixture (DOTAP/F7-CHOL) on PBS buffer and of DOTAP/F7-cholesterol 1:1 mixture on 0.1 mg/mL of DNA dissolved in PBS. Brewster angle microscopy images of the mixtures of DOTAP and the sterols at different surface pressures are also shown.

Table 3.2. Average molecular area (A_m) and surface potential (ΔV) of the lipid monolayers at constant surface pressures.

Lipid Monolayer	*A_m ($Å^2$)*		*Calculated A_m ($Å^2$)*		*ΔV (mV)*
π =	5 mN/m	35 mN/m	5 mN/m	35 mN/m	35 mN/m
DOTAP	88.3	57.7	-	-	+ 560
CHOL	39.8	35.3	-	-	+ 430
DOTAP/CHOL 1:1	57.2	42.0	64.1	46.5	+ 540
F7-CHOL	40.5	36.4	-	-	− 620
DOTAP/F7-CHOL 1:1	55.6	42.3	64.4	47.1	+ 20

The domains have well-defined shapes. DOTAP/F7-CHOL mixture forms domains only at π = 0 mN/m, demonstrating that their miscibility is not complete, but the monolayer is homogeneous immediately when the surface pressure is increased (Figure 3.4). In the case of DOTAP/CHOL 1:1 monolayer a demixing is observed indicating a miscibility gap between two liquid phases: liquid-disordered with more DOTAP and liquid-ordered with more CHOL. The isotherms are not sensitive enough to distinguish between these two phases because the difference in the molecular area must be very small and will even decrease on increasing pressure because the upper critical miscibility point will be approached. This is a phase diagram very similar to the one observed for 1,2-dimyristoyl-*sn*-glycero-3-phosphocholine (DMPC)/CHOL system (Okonogi, 2004; Wagner, 2008). In the case of DOTAP/F7-CHOL there is only a liquid-ordered phase.

Coupling of DNA to DOTAP or mixtures of DOTAP and the sterols (1:1 ratio) leads to the expansion of the monolayers, indicating a partial penetration of the DNA (isotherm shown for the DOTAP/F7-CHOL case, Figure

3.4). The molecular areas in the monolayers are larger when DNA is in the subphase. This might be due to an expanding effect of adsorbed DNA. This shift to larger molecular areas is observed at all pressures studied showing that partially penetrated DNA is not squeezed-out by compression. As shown in a previous study, the amount of adsorbed DNA increases with increasing electrolyte concentration up to physiological values (Shapovalov, 2010). This has been explained by the fact that the ionic atmosphere around a macromolecule becomes more compact and stable with increasing ionic strength. For this reason, the reduction of the effective charge requires larger amounts of DNA for the compensation of the overall monolayer charge.

The surface potential (ΔV) of DOTAP monolayers on PBS buffer is positive and increases gradually with pressure as it is described for phospholipids in the fluid phase, which is attributed to an increase in molecular density (Figure 3.5) (Miller, 1987; Möhwald, 1995).

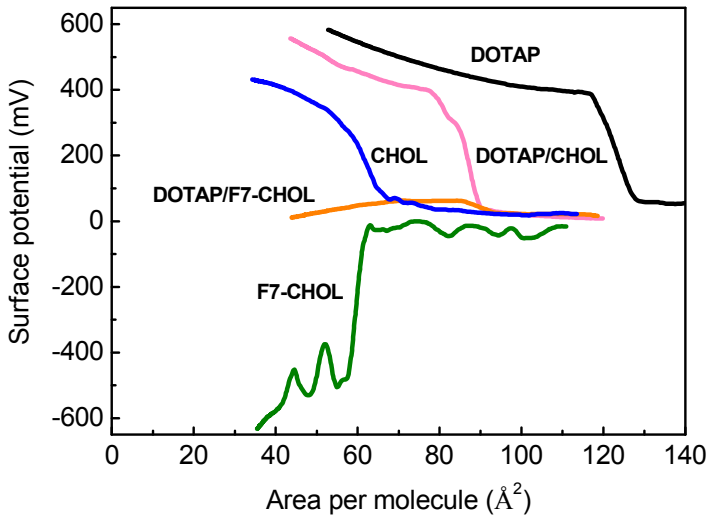

Figure 3.5. Surface potential isotherms of monolayers of DOTAP, cholesterol (CHOL), F7-cholesterol (F7-CHOL), DOTAP/cholesterol 1:1 (DOTAP/CHOL) and DOTAP/F7-cholesterol 1:1 (DOTAP:F7-CHOL) on PBS buffer.

Condensed CHOL monolayers show a positive *ΔV* whereas the potential of F7-CHOL monolayers for similar surface pressures is highly negative, comparably to that observed for amphiphiles with perfluorocarbon chain (Figure 3.5 and Table 3.2) (Andreeva, 2008; Shibata, 1996). The mixtures of DOTAP and the sterols show that the *ΔV* lies between the values of the pure lipid monolayers (Table 3.2). The *ΔV* of DOTAP/CHOL 1:1 monolayers is highly positive whereas that of DOTAP/F7-CHOL 1:1 is close to zero (Figure 3.5 and Table 3.2).

The sterols increase the structural order of the DOTAP hydrocarbon acyl chains by stabilising forces (hydrogen bonding and van der Waals attraction) and lead to an increase in the packing density of the monolayer. The condensing effect of CHOL on fluid monolayers has been known for a long time (Demel, 1967; Leathes, 1925; Stockton, 1976). Although the process by which CHOL induces this effect is not completely understood, it has recently been suggested that the molecule maximises the hydrocarbon contacts, minimising the contact of lipophilic groups with the aqueous phase and forms a contiguous hydrophilic surface (template model) (Daly, 2011). The fluorination of the CHOL tail does not induce significant changes on this condensing effect (Kauffman, 2000). This indicates that the attractive interaction between DOTAP and the fluorinated CHOL is not affected by the lipophobicity character of CF_3 groups (O'Hagan, 2008) and most likely depends on the head group and on the sterol ring. This relates also to the fact that the molecular areas of CHOL and F7-CHOL monolayers are comparable, which strongly suggests that they orient similarly in a vertical way at the interface throughout compression with the OH group towards the polar interface (Kauffman, 2000). The *ΔV* of a charged monolayer results from different contributions. The dipole moments of the lipid molecules, $\mu_{\perp,m}$(vertical component of the molecular dipole moment), the change in orientation of the

water molecules at the monolayer-subphase interface, the type of charges in the head groups and the counter charges in the subphase (diffuse layer potential):

$$\Delta V = \frac{\mu_{\perp,m}}{\varepsilon \cdot \varepsilon_0 \cdot A} + \psi \tag{3.9}$$

where ε_0 is the absolute permittivity of vacuum, ε is the relative permittivity of the monolayer considering the contributions of the hydrocarbon chains, polar heads and hydration water, A is the area per molecule, ψ is the diffuse double layer contribution (that can be calculated by the Gouy–Chapman–Stern theory) (Miller, 1987; Möhwald, 1995; Oliveira, 1997; Truzzolillo, 2008). The surface pressure values are given with respect to the free water (buffer) surface, hence the influence of water molecules can be excluded. Besides opposite signs, similar absolute potential values have been measured for the same hydrophilic group but different chains (fluorinated or hydrocarbon) excluding the predominance of the water structure on the potential (Miller, 1987). DOTAP is fully charged at pH 7.4 (Zuidam, 1997). The *ΔV* value of DOTAP monolayer is thus a result of the double-layer potential and the dipole moments of the molecules (Bordi, 2006; Truzzolillo, 2008). The polarisation of the carbonyl groups may largely contribute to the positive values of *ΔV (*inferred by studies with phospholipid monolayers, either non-ionic or negatively charged) considering the molecular arrangement in which the oxygen is deeper in the subphase than the carbon atom yielding to the correct polarity (orientation of the dipoles with negative ends toward the water) (Miller, 1987; Möhwald, 1995). In addition, a contribution from the methyl groups terminating the aliphatic tails has to be taken into account (Möhwald, 1995; Vogel, 1988). For uncharged monolayers, only the dipole moments contribute to the *ΔV* and for CHOL monolayers the positive values can be attributed to the dipole moment of the C-OH (C3) group (Kauffman, 2000).

The presence of CHOL in DOTAP monolayers only slightly decreases the *ΔV* value when compared to pure DOTAP (Table 3.2). The dipole potential varies inversely with molecular area and dielectric constant. CHOL decreases the molecular area of DOTAP monolayer and it is known to reduce the dielectric constant of the membrane interface (Haldar, 2012). On the other hand, the surface potential of the charged monolayer also depends directly on the diffuse layer potential, which is proportional to the charge density at the interface (Truzzolillo, 2008), which is lower in the case of DOTAP/CHOL monolayers. The highly negative dipole moment for F7-CHOL monolayers results from the polarisation of the fluorinated side chain (Kauffman, 2000). Fluorination of terminal methyl group or the upper part of hydrocarbon chains of lipids results in negative dipoles at the monolayer-air boundary, due to the preferred orientation of the hydrophobic CF_3 group toward air (Bernett, 1963; Fox, 1957; McIntosh, 1996; Vogel, 1988). The surface potential oscillations observed for F7-CHOL are probably due to the fact that in the coexistence region of a 2D-gas and a condensed monolayer, the monolayer is not homogeneous and the measured values strongly depend on particular experimental conditions (Shapovalov, 2006). The dipole moment of F7-CHOL most likely cancels partly that of DOTAP leading to an overall *ΔV* close to zero for the two-component monolayer (Table 3.2).

3.2.2. DNA interaction with DOTAP/F7-cholesterol monolayers

IRRA spectra of the monolayers of DOTAP and DOTAP mixed with sterols on 0.1 mg/mL of salmon testes DNA in PBS buffer also showed adsorption of DNA to the interface, indicated by the presence of the

characteristic band at 970 cm^{-1} (spectra shown for surface pressures of 35 mN/m, Figure 3.6.a).

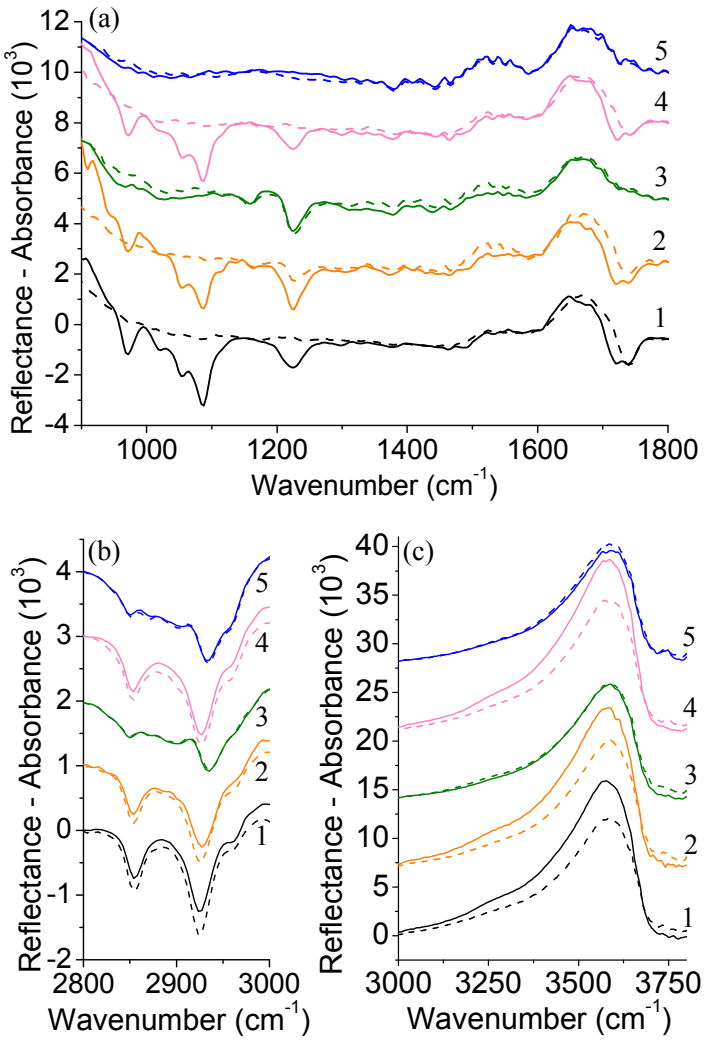

Figure 3.6. Different regions of the IRRAS spectra of monolayers of (1) DOTAP, (2) DOTAP/F7-cholesterol 1:1, (3) F7-cholesterol, (4) DOTAP/cholesterol 1:1 and (5) cholesterol on PBS buffer (dashed line) and on 0.1 mg/mL DNA dissolved in PBS buffer (solid line) subphases. Different regions of the IRRA spectra are presented in separate plots and the spectra are offset for clarity: DNA marker bands (a), CH_2 stretching vibrations (b), and OH stretching band (c). The surface pressure is in all cases 35 mN/m.

The region between 900 and 1800 cm^{-1} is rich in DNA marker bands (Dittrich, 2011). The band at 970 cm^{-1} is caused by 2´*endo* deoxyribose conformation of the DNA backbone. In the 1000-1250 cm^{-1} region, one can see the vibrations of phosphate groups. The band at 1223 cm^{-1} corresponds to the phosphate group asymmetric stretching, while the band at 1088 cm^{-1} is given by the symmetric stretching. For DOTAP/F7-CHOL mixtures the characteristic band of C-F stretching of pure F7-CHOL at 1223 cm^{-1} can interfere with the asymmetric band from the phosphate group of DNA, but the increase in that band is clearly evident when DNA is in the subphase. The region between 3000 and 3800 cm^{-1} gives information about surface layer thickness through the OH stretching vibration band (Dopico, 2007). The intensity of OH stretching vibration band increases in the presence of DNA, indicating an increase in surface layer thickness. The DOTAP head group is positively charged at pH 7.4, which enables the electrostatic interaction with DNA even in the presence of other salt ions. The symmetric and asymmetric CH_2-valence vibrations (bands between 2850 and 2920 cm^{-1}) provide qualitative information about hydrocarbon chain conformation (Macphail, 1984; Snyder, 1982). The monolayers of DOTAP and of its mixture with sterols exhibit a high amount of gauche conformers because CH_2 symmetric and asymmetric stretching bands are at 2854 and 2924 cm^{-1}, respectively (Figure 3.6.b). These values are in accordance with a liquid-expanded phase and do not change on compression (Table 3.3). The adsorption of DNA at the interface does not induce significant changes on the phase state of the monolayers.

Table 3.3. Symmetric CH_2 vibration band of the lipid monolayers obtained by IRRAS.

Lipid Monolayer on PBS or DNA/PBS	$\nu_s CH_2$ (cm^{-1})	
	π=5 mN/m	35 mN/m
DOTAP	2854	2854
CHOL	2850	2850
DOTAP/CHOL 1:1	2854	2854
F7-CHOL	2850	2850
DOTAP/F7-CHOL 1:1	2854	2854

CHOL has the CH_2 symmetric stretching band at 2850 cm^{-1}, indicating an all-trans conformation (condensed phase). The same is valid for F7-CHOL CH2 stretching bands. The CH_2 asymmetric stretching band is not considered in this case since it contains significant overlapping contributions from methyl groups (Lewis, 1998). In the case of pure CHOL and F7-CHOL monolayers, DNA is not detected at the interface. From direct observation of the intensity of the symmetric stretching band of the phosphate group (1088 cm^{-1}) of DNA it is possible to perform a comparison of the different systems. When the amount of positively charged lipids decreases, a decreasing in the amount of absorbed DNA is visible. This decrease of the band intensity is more noticeable for the mixture of DOTAP and F7-CHOL. The difference in OH-band intensities around 3600 cm^{-1} between DOTAP, DOTAP/CHOL and DOTAP/F7-CHOL also indicates a smaller amount of adsorbed DNA for the mixture with the fluorinated cholesterol.

3.3. Conclusions

The use of F7-CHOL as the helper lipid in cationic non-viral gene vectors is proposed. The effect of this neutral lipid on the structure of monolayers formed by the cationic lipid DOTAP was studied and compared with that of CHOL. Both isotherms and IRRAS results demonstrate that the mixtures of DOTAP and the sterols (1:1 molar ratio) are in the liquid expanded state. The mixtures appeared homogeneous at pressures between 30-35 mN/m, which is considered the lateral pressure in liposomes and will have implications for the ability of the lipoplexes formed by these lipids to condense DNA. F7-CHOL and CHOL induce a condensing effect on DOTAP monolayers but BAM showed that CHOL is less miscible with DOTAP than F7-CHOL. CHOL and F7-CHOL orient similarly in a vertical way at the interface throughout compression with the OH group towards the polar interface, as concluded from the surface potential measurements and molecular areas. From IRRAS results, it is possible to conclude that a smaller amount of DNA is adsorbed at DOTAP/F7-CHOL monolayers when compared with DOTAP/CHOL. Since the isotherms of the mixtures show very similar molecular areas, similar charge densities are expected in the mixed monolayers. The only possible explanation for the moment is a different miscibility behaviour between DOTAP and CHOL or F7-CHOL, respectively. If CHOL is less miscible with DOTAP, more patches containing different amounts of CHOL and therefore different charge densities are expected. This is in line with the BAM experiments showing a homogeneous DOTAP/F7-CHOL monolayer at any lateral pressure above zero. This leads to a homogeneous monolayer with a smaller charge density compared to that of the DOTAP/CHOL mixtures, which shows the coexistence of cholesterol-rich and cholesterol-poor domains up to 20 mN/m, indicating the coexistence of patches with higher or smaller charge

densities in the mixed monolayer. The patches with the higher charge density are responsible for the attraction of a larger amount of DNA. According to these results, F7-CHOL and DOTAP are completely miscible, and DNA adsorbs to this mixed monolayer even at ionic strength close to the physiological values, thus F7-CHOL is a promising candidate for the preparation of gene delivery vectors.

3.4. References

Andreeva, T.D.; Petrov, J.G.; Brezesinski, G.; Moehwald, H. (**2008**). Structure of the Langmuir monolayers with fluorinated ethyl amide and ethyl ester polar heads creating dipole potentials of opposite sign, *Langmuir, 24*, 8001.

Banyay, M.; Sarkar, M.; Gräslund, A. (**2003**). A library of IR bands of nucleic acids in solution, *Biophysical Chemistry, 104*, 477.

Bernett, M.K.; Zisman, W.A. (**1963**). Behavior of Monolayers of Progressively Fluorinated Fatty Acids Absorbed on Water, *Journal of Physical Chemistry, 67*, 1534.

Blume, A. (**1996**). Properties of lipid vesicles: FT-IR spectroscopy and fluorescence probe studies, *Current Opinion in Colloid & Interface Science, 1*, 64.

Bordi, F.; Cametti, C.; Sennato, S.; Paoli, B.; Marianecci, C. (**2006**). Charge renormalization in planar and spherical charged lipidic aqueous interfaces, *Journal of Physical Chemistry B, 110*, 4808.

Brezesinski, G.; Möhwald, H. (**2003**). Langmuir monolayers to study interactions at model membrane surfaces, *Advances in Colloid and Interface Science, 100-102*, 563.

Buschow, K.H.J.C., Robert W.; Flemings, Merton C.; Ilschner, Bernhard; Kramer, Edward J.; Mahajan, Subhash; *Encyclopedia of Materials* -

Science and Technology, Volume 1-11, 1st Edition, Elsevier, The Netherlands, **2001**.

Butt, H.-J.; Graf, K.; *Physics and chemistry of interfaces,* Wiley-VCH, Germany, **2006**.

Daly, T.A.; Wang, M.H.; Regen, S.L. (**2011**). The Origin of Cholesterol's Condensing Effect, *Langmuir, 27*, 2159.

Demel, R.A.; Vandeene.Ll; Pethica, B.A. (**1967**). Monolayer Interactions of Phospholipids and Cholesterol, *Biochimica Et Biophysica Acta, 135*, 11.

Dittrich, M.; Bottcher, M.; Oliveira, J.S.L.; Dobner, B.; Mohwald, H.; Brezesinski, G. (**2011**). Physical-chemical characterization of novel cationic transfection lipids and the binding of model DNA at the air-water interface, *Soft Matter, 7*, 10162.

Dopico, A.M.; *Methods in Membrane Lipids,* Volume 400, 16th Edition, Humana Press, United States of America, **2007**.

Fainerman, V.B.; Lucassen-Reynders, E.H.; Miller, R. (**1998**). Adsorption of surfactants and proteins at fluid interfaces, *Colloids and Surfaces A: Physicochemical and Engineering Aspects, 143*, 141.

Fox, H.W. (**1957**). Force-Area and Potential-Area Relations of Monolayers of Terminally Fluorinated Octadecylamine and Octadecanoic Acid, *Journal of Physical Chemistry, 61*, 1058.

Freire, M.G.; Carvalho, P.J.; Fernandes, A.M.; Marrucho, I.M.; Queimada, A.J.; Coutinho, J.A.P. (**2007**). Surface tensions of imidazolium based ionic liquids: Anion, cation, temperature and water effect, *Journal of Colloid and Interface Science, 314*, 621.

Gromelski, S.; Brezesinski, G. (**2004**). Adsorption of DNA to zwitterionic DMPE monolayers mediated by magnesium ions, *Physical Chemistry Chemical Physics, 6*, 5551.

Gromelski, S.; Brezesinski, G. (**2006**). DNA condensation and interaction with zwitterionic phospholipids mediated by divalent cations, *Langmuir, 22*, 6293.

Haldar, S.; Kanaparthi, R.K.; Samanta, A.; Chattopadhyay, A. (**2012**). Differential Effect of Cholesterol and Its Biosynthetic Precursors on Membrane Dipole Potential, *Biophysical Journal, 102*, 1561.

Henon, S.; Meunier, J. (**1991**). Microscope at the Brewster angle: Direct observation of first-order phase transitions in monolayers, *Review of Scientific Instruments, 62*, 936.

Kaercher, T.; Hönig, D.; Möbius, D. (**1993**). Brewster angle microscopy, *International Ophthalmology, 17*, 341.

Kauffman, J.M.; Westerman, P.W.; Carey, M.C. (**2000**). Fluorocholesterols, in contrast to hydroxycholesterols, exhibit interfacial properties similar to cholesterol, *Journal of Lipid Research, 41*, 991.

Leathes, J.B. (**1925**). Role of fats in vital phenomena., *Lancet, 1*, 853.

Lewis, R.N.A.H.; McElhaney, R.N. (**1998**). The structure and organization of phospholipid bilayers as revealed by infrared spectroscopy, *Chemistry and Physics of Lipids, 96*, 9.

Macphail, R.A.; Strauss, H.L.; Snyder, R.G.; Elliger, C.A. (**1984**). C-H Stretching Modes and the Structure of Normal-Alkyl Chains .2. Long, All-Trans Chains, *Journal of Physical Chemistry, 88*, 334.

Maltseva, E.; *Model membrane interactions with ions and peptides at the air/water interface,* Ph.D, Universität Potsdam, **2005**.

McIntosh, T.J.; Simon, S.A.; Vierling, P.; Santaella, C.; Ravily, V. (**1996**). Structure and interactive properties of highly fluorinated phospholipid bilayers, *Biophysical Journal, 71*, 1853.

Melzer, V.; Weidemann, G.; Vollhardt, D.; Brezesinski, G.; Wagner, R.; Struth, B.; Möhwald, H. (**1997**). Brewster Angle Microscopy and X-ray GID

Studies of Morphology and Crystal Structure in Monolayers of N-Tetradecyl-γ,δ-dihydroxypentanoic Acid Amide, *The Journal of Physical Chemistry B, 101*, 4752.

Mendelsohn, R.; Mao, G.; Flach, C.R. (**2010**). Infrared reflection–absorption spectroscopy: Principles and applications to lipid–protein interaction in Langmuir films, *Biochimica et Biophysica Acta (BBA) - Biomembranes, 1798*, 788.

Miller, A.; Helm, C.A.; Mohwald, H. (**1987**). The Colloidal Nature of Phospholipid Monolayers, *Journal De Physique, 48*, 693.

Möhwald, H., *Phospholipid Monolayers*, in *Handbook of Biological Physics* R.L.a.E. Sackmann, Editor. 1995, Elsevier Science The Netherlands. p. 161.

O'Hagan, D. (**2008**). Understanding organofluorine chemistry. An introduction to the C-F bond, *Chemical Society Reviews, 37*, 308.

Okonogi, T.M.; McConnell, H.M. (**2004**). Contrast inversion in the epifluorescence of cholesterol-phospholipid monolayers, *Biophysical Journal, 86*, 880.

Oliveira, O.N.; Bonardi, C. (**1997**). The surface potential of Langmuir monolayers revisited, *Langmuir, 13*, 5920.

Rodríguez Patino, J.M.; Sánchez, C.C.; Rodríguez Niño, M.R. (**1999**). Morphological and Structural Characteristics of Monoglyceride Monolayers at the Air−Water Interface Observed by Brewster Angle Microscopy, *Langmuir, 15*, 2484.

Shapovalov, V.L.; Brezesinski, G. (**2006**). Breakdown of the Gouy−Chapman Model for Highly Charged Langmuir Monolayers: Counterion Size Effect, *The Journal of Physical Chemistry B, 110*, 10032.

Shapovalov, V.L.; Dittrich, M.; Konovalov, O.V.; Brezesmski, G. (**2010**). Use of Total Reflection X-ray Fluorescence (TRXF) for the Quantification of

DNA Binding to Lipid Monolayers at the Air-Water Interface, *Langmuir, 26*, 14766.

Shibata, O.; Yamamoto, S.K.; Lee, S.; Sugihara, G. (**1996**). Mixed monolayer properties of tetradecanoic acid with n-perfluorocarboxylic acids with 10, 12, 14, 16, and 18 carbon atoms, *Journal of Colloid and Interface Science, 184*, 201.

Snyder, R.G.; Strauss, H.L.; Elliger, C.A. (**1982**). C-H Stretching Modes and the Structure of Normal-Alkyl Chains .1. Long, Disordered Chains, *Journal of Physical Chemistry, 86*, 5145.

Stockton, G.W.; Smith, I.C.P. (**1976**). Deuterium Nuclear Magnetic-Resonance Study of Condensing Effect of Cholesterol on Egg Phosphatidylcholine Bilayer Membranes .1. Perdeuterated Fatty-Acid Probes, *Chemistry and Physics of Lipids, 17*, 251.

Symietz, C.; Schneider, M.; Brezesinski, G.; Möhwald, H. (**2004**). DNA alignment at cationic lipid monolayers at the air/water interface, *Macromolecules, 37*, 3865.

Truzzolillo, D.; Bordi, F.; Cametti, C.; Sennato, S. (**2008**). Phenomenological surface characterization of cationic-lipid monolayers in the presence of oppositely charged polyions, *Colloids and Surfaces a-Physicochemical and Engineering Aspects, 319*, 51.

Vogel, V.; Mobius, D. (**1988**). Local Surface-Potentials and Electric-Dipole Moments of Lipid Monolayers - Contributions of the Water Lipid and the Lipid Air Interfaces, *Journal of Colloid and Interface Science, 126*, 408.

Vollhardt, D.; Fainerman, V.B. (**2006**). Progress in characterization of Langmuir monolayers by consideration of compressibility, *Advances in Colloid and Interface Science, 127*, 83.

Wagner, K.; Desbat, B.; Brezesinski, G. (**2008**). Liquid-liquid immiscibility in model membranes activates secretory phospholipase A2, *Biochimica Et Biophysica Acta, 1778*, 166.

Zuidam, N.J.; Barenholz, Y. (**1997**). Electrostatic parameters of cationic liposomes commonly used for gene delivery as determined by 4-heptadecyl-7-hydroxycoumarin, *Biochimica Et Biophysica Acta-Biomembranes, 1329*, 211.

Chapter 4

Compaction process of DNA by fluorinated liposomes

Numerous cationic lipids have been synthesised and tested for gene delivery in cell cultures, animal models and patients who take part in clinical trials (Morille, 2008; Zhu, 2010). Gene therapy uses plasmid DNA or cellular RNA interference machinery to turn off gene expression in cancer cells or other diseased cells (Aagaard, 2007; Morille, 2008). The use of naked nucleic acids is limited by the presence of serum nucleases and thus it is only valid for direct injection of the macromolecule on tissues that are easily accessible such as skin and muscle (Morille, 2008). These lipids are usually used for gene delivery in the form of liposomes that are complexed with DNA through electrostatic interactions. The toxicity of these complexes, named lipoplexes, is related to the charge ratio between the cationic liposomes and DNA plus the dose that is administered (Lv, 2006). Also, the toxicity of such systems in cell cultures is attributed to the free liposomes present in the mixture, as the separate components of the lipoplexes do not show any toxicity when injected in mice models (Xu, 1999). Thus the study of the interaction between

liposomes and nuclei acids as well as the physicochemical characterisation of such complexes is critical for the development of novel DNA vectors.

The use of fluorinated cholesterol as helper lipid in DOTAP liposomes is described and their colloidal properties are compared with that of DOTAP:cholesterol liposomes (Crook, 1998). When administered intravenously, cationic liposome–DNA complexes are rapidly cleared from the bloodstream (Audouy, 2002). Fluorinated liposomes have the advantage of long-term self-stability (Ravily, 1997). Their half-live time in the blood stream is similar to pegylated liposomes (Santaella, 1993). Although fluorinated systems seem to have high transfection potency, their use as gene vectors is still poorly explored (Boulanger, 2004; Gaucheron, 2001b; Gaucheron, 2002). In this work, liposomes of mixtures of DOTAP and heptafluorocholesterol were produced and used to form complexes with DNA, which were characterised experimentally by measurements of hydrodynamic diameter, electrophoretic mobility, fluorescence and turbidity. The compaction of DNA by fluorinated liposomes was also theoretically analysed by a phenomenological theory addressed by Nguyen and Shklovskii (Nguyen, 2001a; b). This theory provides phase diagrams of the systems including the charge inversion and re-entrant condensation processes among the lipoplexes. These phase diagrams contain information about the liposome and DNA concentration necessary to have either anionic or cationic isolated lipoplexes or clusters of lipoplexes. By predicting them, it is possible to know the optimum values of DNA and liposome concentrations for an efficient transfection from a physicochemical standpoint.

4.1. Experimental details

4.1.1. Chemicals

DOTAP (1,2-dioleoyl-3-trimethylammonium-propane, chloride salt, MW 698.542), cholesterol (ovine wool, > 98%, MW 386.355) and F7-cholesterol (25,26,26,26,27,27,27-heptafluorocholesterol, MW 512.587) (Figure 3.1) were purchased from Avanti Polar Lipids, Inc. DNA (Deoxyribonucleic acid sodium salt from calf thymus, type I), Hepes buffer (4-(2-Hydroxyethyl) piperazine-1-ethanesulfonic acid, ≥ 99.5%), Tris buffer (2-amino-2-(hydroxymethyl)-1,3-propanediol, ≥ 99.9%) and the probe ethidium bromide (EtBr, 3,8-Diamino-5-ethyl-6-phenylphenanthridinium bromide, ≥ 95.0%) were supplied by Sigma-Aldrich. The deionised water was purified with Milli-Q apparatus with the specific resistance of 18.2 MΩ·cm. Chloroform was from Merck.

4.1.2. Preparation of Liposomes, DNA solution and lipoplexes

Liposomes were prepared by the thin lipid film hydration method (Figure 4.1) (Palmerini, 2006; Sharma, 1997). Briefly, the appropriate lipid mixture (DOTAP:cholesterol or DOTAP:F7-cholesterol 1:1 molar ratio) was dissolved in chloroform, which was then evaporated under vacuum using a rotating apparatus.

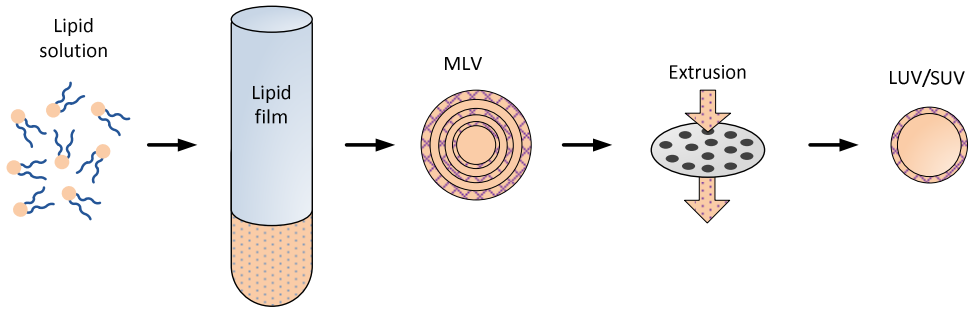

Figure 4.1. Lipid film hydration method.

The lipid film was hydrated with 10 mL of 10 mM Hepes buffer pH 7.4 (ionic strength 0.00325 M). The suspension was vortexed for 15 minutes and extruded through Whatman filters of decreasing sizes (up to 100 nm pore size membranes) using a pressure extruder apparatus. The total lipid concentration was 5 mM. DNA was dissolved in 10 mM Hepes buffer at a concentration of 1 mg/mL (stock solution), which was kept at 4°C under magnetic stirring for at least 1 day. Liposome-DNA complexes were prepared by adding equal volumes of DNA solution at a constant concentration (final concentration was 0.05 mg/mL) and liposome suspension at different concentrations (final concentrations ranging from 0.05 and 0.50 mg/mL). DNA solution was added drop wise to the liposomes and the mixture was kept under magnetic stirring for at least 15 minutes.

4.1.3. Dynamic light scattering

Light scattering effects are an optical phenomenon where the particles interact with light that strikes them and some of that light is deflected from its original direction. The intensity of the scattered light depends on many

factors, such as: wavelength of the incident light, shape and size of the scattering particles, optical properties of the scatters and the angle of observation. The light scattering can be classified as static or dynamic depending on how the intensity is measured. If the time-averaged total intensity is measured as a function of scattering angle, concentration or both it is called static light scattering. In dynamic light scattering what is measured is the temporal variation of the intensity, and it is represented as the intensity autocorrelation function. The variation of the intensity with time contains information on the random motion of the particles due to their kinetic energy and can be used to measure the diffusion coefficient of the particles. The hydrodynamic radius of the particle is calculated by means of the diffusion coefficient and the Stokes-Einstein equation (Hiemenz, 1997):

$$D = \frac{k_B T}{f} = \frac{k_B T}{6\pi\eta R_H} \tag{4.1}$$

In the first part of this equation, k_B is the Boltzmann constant, T is the absolute temperature of the dispersion and f is the Stokes coefficient that is equal to $6\pi\eta R_H$, where η is the viscosity and R_H is the hydrodynamic radius, which gives the particle size (Hiemenz, 1997).

The hydrodynamic diameter of liposomes and lipoplexes was measured at room temperature with a Malvern Zetasizer Nano instrument by dynamic light scattering (DLS) at 173°. The results were averaged from five measurements for each sample and were obtained for at least three independent procedure of sample preparation. The final concentration of liposomes varied from 0.05 to 0.50 mg/mL (0.1–1.0 mM) and the concentration of DNA was 0.05 mg/mL.

4.1.4. Electrophoretic mobility

The electrokinetic phenomena can be defined by a liquid that moves tangential to a charge surface, so it combines effects of motion and electrical phenomena, which are interpreted to yield a quantity known as the zeta potential (ζ). There are four phenomena related with the term electrokinetic: electrophoresis, electroosmosis, streaming potential and sedimentation potential. Electrophoresis refers to movement of a particle in a stationary liquid when an electric field is applied. So this method measures the velocity at which the particles move in a liquid induced by an electrical field (Butt, 2006; Hiemenz, 1997).

Around each particle there is an electrical double layer with a high concentration of opposite charged ions. That layer can be divided into two parts, an inner region, called stern layer, where opposite charged ions are strongly bond to the particle surface and an outer region or diffuse layer, where the ions are loosely bond to the particle. The zeta potential is the potential at the point where the bound Stern layer ends and the mobile diffuse layer begins (Butt, 2006; Hiemenz, 1997).

When an electric field is applied, the particles are attracted towards the electrode with opposite charge, but forces including viscosity tend to oppose this movement. When the equilibrium of forces is established, the particles move with a constant velocity. This velocity is normally called electrophoretic mobility (μ_e) and depends on the strength of the electric field or voltage gradient, the dielectric constant (e), the viscosity (η) and the zeta potential (ζ). Henry's equation gives the relationship between these four properties (Butt, 2006; Hiemenz, 1997):

$$\mu_e = \frac{2e\zeta f(ka)}{3\eta} \tag{4.2}$$

Zeta potential magnitude gives the indication of potential stability of the colloidal system. Generally a suspension is unstable if zeta potential is between -30 mV to 30 mV. So in this case the particles might flocculate. The stability is reduced at the isoelectric point (iep) where the zeta potential is zero at the hydrodynamic interface. This can be confused with the point of zero charge (pzc), where the surface charge (solid-liquid interface) is zero (Butt, 2006; Hiemenz, 1997).

The electrophoretic mobility μ_e of liposomes and lipoplexes was measured at room temperature with a Malvern Zetasizer Nano series instrument by laser Doppler velocimetry (LDV), where the light scattered at an angle of 17° is converted into a zeta potential distribution. The results were averaged from five measurements for each sample and were obtained for at least three independent procedure of sample preparation. The final concentration of liposomes varied from 0.05 to 0.50 mg/mL (0.1–1.0 mM) and the concentration of DNA was 0.05 mg/mL.

4.1.5. Fluorescence spectroscopy

Luminescence is the emission of light from any substance when excited at a specific wavelength. Depending on the nature of the excited state, luminescence can be classified as fluorescence (excited singlet states) or phosphorescence (excited triplet states). Briefly, a fluorophore is excited from the ground electronic state to a higher vibrational level of energy. Collisions with other molecules cause the excited molecule to lose its excess of vibrational energy until it reaches the lowest vibrational level of the excited electronic state. From this level the molecule can return to any of the vibrational levels of the ground state, emitting its energy in the form of fluorescence. Typically, the emission spectrum is collected at the wavelength

with maximum fluorescence intensity of the excitation spectrum and vice versa (Lakowicz, 2006).

Fluorescence measurements are commonly executed in steady-state but time-resolved measurements can also be done. Steady-state measurements are performed with constant illumination of the sample by a continuous beam of light and the emission spectrum is recorded due to the nanosecond scale of fluorescence (Lakowicz, 2006).

Steady-state fluorescence measurements were carried out using a Perkin-Elmer LS-50B luminescence spectrometer (REQUIMTE, Department of Chemistry, Faculty of Pharmacy, University of Porto). The DNA concentration was kept constant (0.025 mg/mL) and liposomes were added at liposome-DNA mass ratio (L/D) varying from 0 to 10, similarly to the other characterisation studies. Ethidium bromide (EtBr) was added to DNA solution at a DNA:EtBr mass ratio of 6:1. Fluorescence emission spectra were recorded between 560-700 nm at an excitation wavelength of 540 nm, emission and excitation band slits of 10 nm and scan rate of 400 nm/min. All spectra were subtracted to the spectra of blanks (buffer or buffer plus liposomes at the same concentrations that were used for the formation of lipoplexes).

4.1.6. Transmission Electron Microscopy

Transmission electron microscopy (TEM) gives real space images allowing a direct interpretation of the structure geometry (Buschow, 2001). In TEM technique, an electron beam is transmitted through the sample under observation and the applied intensity depends on the thickness of the sample and the concentration of atoms in that sample (Ebnesajjad, 2006; Hiemenz, 1997). The electrons have the same energy and wavelength as they are accelerated by the same voltage. TEM is not a surface-sensitive method because the electrons pass through the whole sample (Butt, 2006). The

produced image is a two-dimensional projection of the entire object, including the surface and the internal structures. Different contrast is obtained due to the thickness and composition of the material and the absorption of electrons in the material.

TEM (Jeol JEM-1400, JEOL) images allow a morphological analysis of the liposomes and its complexes. Liposomes were prepared as reported in section 4.1.2, but in this case the hydration solvent used was 5% sucrose solution in 10 mM HEPES buffer. Sucrose allows rigidity and consequent stability of the vesicles after the drying process. Each sample of vesicles (5 µL) was placed on copper grids (Formvar/carbon on 400 mesh – Agar) and let to adsorb for 5 minutes. The staining was performed with 2% (w/v) of filtered aqueous solution of uranyl acetate for 45 seconds. Dried grids were visualised at 80 kV and digital Images were collected at a magnification of 200 000 x.

4.1.7. Complexation theory

As in previous works (Barrán-Berdón, 2012; Muñoz-Úbeda, 2010; Muñoz-Úbeda, 2011; Rodriguez-Pulido, 2009), we have used the complexation theory of Nguyen and Shklovskii to study lipoplexes formed by cationic liposomes and DNA (Nguyen, 2001a; b). This phenomenological theory describes the complexation of a long flexible charged polyelectrolyte of contour length l, with oppositely charged spherical and rod-like particles. According to these authors, the free energy of the system formed by negative charged polyions and cationic liposomes $F(N,x)$, can be expressed as the sum of the free energy of a complex formed by a single liposome and N polyions, $F_c(N,x)$, the free energy of the aggregates $F_a(N,x)$, and the free energy of the remaining free polyion in the solution, $F_p(N,x)$. If we particularise for our case in which polyions are DNA molecules, the theory predicts that for a given concentration of DNA (P), the state of the system can be described in terms of

the DNA concentration in the limit of new negligible small liposome concentration (P_0). To this end, a minimising calculation of the function *F(N,x)* with respect to *N* and *x* is required. As a consequence, a phase diagram can be obtained to characterise the whole complexation process in which lipoplexes experience aggregation (*condensation*) and disaggregation (*reentrant condensation*) as a function of the liposome-DNA ratio. Namely, for a given concentration of DNA and growing concentration of liposomes (*S*), lipoplexes experience aggregation at some critical concentration, S_a, below the isoneutrality, and remain in this aggregated (or condensed) state up to another concentration, S_d, above the isoneutrality. For concentrations of liposomes higher than S_d, clusters of lipoplexes start to disaggregate as a consequence of a charge inversion process (Nguyen, 2001a; b). In order to build the corresponding phase diagram, the theory provides two equations that can be solved in terms of the phenomenological parameters P_0 and E_0. P_0 is related to the DNA concentration in the limit of negligible liposome concentrations whereas E_0 is related to the energy gained per complex by forming the aggregates (compared to a free neutral isolated liposome-DNA complex in solution):

$$S_a \frac{Q}{q}\left(1+\sqrt{\frac{2C_eE_0}{qQ}}\right) = P - P_0 exp\left(\sqrt{\frac{E_0 2qQ}{(k_BT)^2 C_e}}\right) \tag{4.3}$$

$$S_d \frac{Q}{q}\left(1-\sqrt{\frac{2C_eE_0}{qQ}}\right) = P - P_0 exp\left(-\sqrt{\frac{E_0 2qQ}{(k_BT)^2 C_e}}\right) \tag{4.4}$$

where q and Q are the total charge of DNA and liposomes respectively, k_BT is the thermal energy, C_e is the electrical capacitance. This last parameter can be calculated as $C_e = 4\pi\varepsilon_0\varepsilon a(1+\kappa_D a)$ if liposomes are assumed to be spherical particles of radius *a* immersed in an electrolytic solution characterised by the dielectric permittivity $\varepsilon_0\varepsilon$ and a reciprocal Debye length κ_D. Accordingly,

knowing the phenomenological parameters P_0 and E_0, this set of equations allows the calculation of the two boundary concentrations of liposomes S_a and S_d for each DNA concentration. Apart from this theory, there are other theoretical and computer simulation studies that contribute to a better understanding of DNA complexes. For instance, theoretical analysis of the physical properties of cationic and zwitterionic lipid-DNA complexes based on a coarse-grained molecular model implemented by Monte Carlo (MC) simulations (Farago, 2006; Farago, 2007). Coarse-grained and Molecular Dynamics Simulations have been applied to study charged dendrimers in the presence of multivalent salt solution as well as their complexation with linear polyelectrolyte (Tian, 2009; 2010a; b; 2011). Also, numerical calculations of the mean-field electrostatic free energy of a zwitterionic lipid monolayer and DNA support the experimental observations where DNA adsorbs onto a zwitterionic lipid monolayer in the presence of divalent cations (Bohinc, 2012; Mengistu, 2009).

4.1.8. Turbidity measurements

The turbidity of the equilibrium phase is related to the formation of a non-soluble phase that may precipitate or remain stable for short or long periods of time (Espinosa-Andrews, 2007). Turbidity measurements can be assessed by absorbance kinetic studies, since aggregation leads to an increase of the average size of the scattered particles. Then, a spectrophotometer working with a visible wavelength is capable of detect and analyse the aggregation kinetics of many colloidal systems (Peula-García, 2010).

Ultraviolet-visible spectroscopy (UV-Vis) refers to absorption spectroscopy in the UV-Vis spectral region. Molecules can absorb the energy in the form of ultraviolet or visible light to excite photons from the ground

state to an excited state. This technique is complementary to fluorescence spectroscopy, previously described (Lakowicz, 2006).

The stability studies of the liposome suspensions were performed by turbidity measurements as a function of DNA concentration at room temperature using a UV-1700 PharmaSpec Spectrometer (Kyoto, Japan). Absorbance kinetic data were obtained at 570 nm, during 180 seconds, with an interval of 2 seconds. The liposome concentration was 0.5 mM and DNA was added at concentrations ranging from 0.003 to 0.150 mg/mL. The reported data are the average of 4 independent measurements. The Fuchs stability ratio *W* (or stability factor) was determined from these data. This magnitude is a criterion for the stability of the colloidal system: $W = k_r / k_s$ where the rate constant k_r describes rapid coagulation and k_s is the rate constant for the slow coagulation regime. Thus, the inverse of the stability ratio provides a measure of the effectiveness of collisions leading to coagulation. Information on the kinetics-aggregation constants of dimer formation can be directly derived from the initial slopes of the absorbance vs. time curves (*dAbs/dt*) (Peula-García, 2010). Accordingly, plotting *W* as a function of the electrolyte concentration in a double-logarithmic scale becomes useful to estimate the critical coagulation concentration (CCC), which is generally defined as the minimum concentration of electrolyte required to induce coagulation ($W = 1$). The CCC value is therefore related to destabilisation processes (*i. e.* low CCC means low stability) and its value has been previously determined for the case of anionic liposomes in the presence of divalent cations (Martín-Molina, 2012). In the present study, however, DNA plays the role of the electrolyte so the CCC in this case would be the minimum concentration of DNA required to induce coagulation of liposomes. On the other hand, in some cases the stability curves can exhibit an increase of *W* for electrolyte concentrations larger than the CCC. This phenomenon is usually

called *colloidal restabilisation* and the minimum salt concentration at which the system begins to restabilise is defined as the critical stabilisation concentration (CSC). This restabilisation phenomenon at high salt concentrations is well known in hydrophilic colloidal systems and is governed by hydration forces (Peula-García, 2010). In our case, the CSC will be redefined as the minimum DNA concentration at which the system begins to restabilise and such procedure of restabilisation will be attributed to the formation of lipoplexes stabilised by the complexation of the DNA with the cationic liposomes.

4.1.9. Circular Dichroism

The DNA structure when bound to the liposomes can be predicted by circular dichroism spectroscopy in the far-UV spectral region. Circular dichroism is a phenomenon that affects chiral molecules such as DNA and proteins. The difference in absorption of the left (A_l) and right (A_r) circularly polarised light defines circular dichroism. CD spectropolarimeters normally present the results as a spectrum that correlates the wavelength, λ (nm), with the ellipticity, θ (deg). The conversion occurs according the following rule:

$$CD = \Delta A = A_l - A_r = \frac{4\pi\theta}{180 \ln 10} \quad (4.5)$$

Applying the Lambert-Beer law to the CD theory, in order to remove concentration and path length dependence,

$$\Delta A = (\Delta\varepsilon) C l \quad (4.6)$$

where $\Delta\varepsilon$ is the extinction coefficient (M^{-1} cm^{-1} or mol^{-1} dm^3 cm^{-1}), C is the molar concentration (M) and l is the optical path length that crosses the sample (cm) (Rodger, 1997).

The most known arrangement for DNA molecules, discovered in 1953, is a right-handed double helix of the B-form. However DNA can adopt many

other structures, for example right-handed A-type typical from RNA or C-form mostly found in DNA fibers (Figure 4.2) (Baase, 1979; Kypr, 2009; Lu, 2003; Miyahara, 2012; Vorlíčková, 2012).

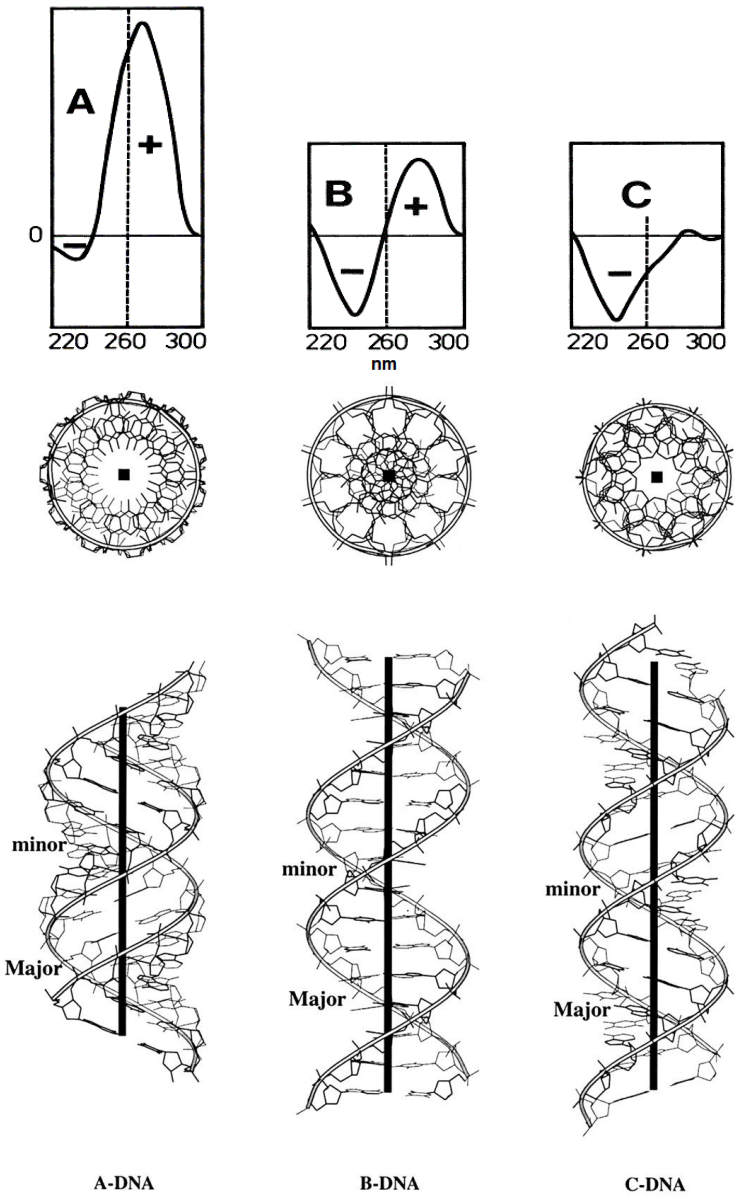

Figure 4.2. Representative scheme of DNA A-, B- and C-form (Lu, 2003).

The circular dichroism spectra were recorded with a Jasco 720 spectrophotometer from 220 to 315 nm using quartz cuvettes with an optical path length of 0.5 cm. The concentration of DNA was kept constant and equal to 0.05 mg/mL for calf thymus DNA (ctDNA) and 0.025 mg/mL for plasmid DNA (pDNA) (pEGFP-N1, BD Biosciences Clontech). The average molecular weight considered for DNA was 348 g/mol (Schindler, 1997; Symietz, 2004). Tris buffer (10 mM) was used as solvent.

4.1.10. *In vitro* transfection studies

The gene transfer and transgene expression after cellular transfection was monitored using green fluorescent protein (GFP) plasmid (pEGFP-N1) encoding for green fluorescent protein, hereafter designed by pDNA, which was amplified and isolated with a PlasmidPrep Midi Flow kit (GE Healthcare). The concentration and purity of pDNA were determined using a NanoDrop 1000 (Thermo Scientific) apparatus. Two cell culture lines were used in this study, SH-SY5Y and HeLa. SH-SY5Y cell line was grown in Minimum Essential Medium (MEM) (Lonza) and Ham's F-12 (Lonza) (1:1), supplemented with 10% (v/v) heat inactivated fetal bovine serum (FBS – Gibco), 2 mM L-Glutamine (Lonza), 100U Penicillin/Streptomycin (Gibco) and 1% MEM non-essential amino acid solution (Sigma). HeLa cell line was grown in Dulbecco's Modified Eagle's Medium (Lonza) supplemented with 10% FBS and 100U Penicillin/Streptomycin. Cells were cultured in a humidified 5% CO_2 atmosphere at 37°C. For transfection studies, cells were seeded at approximately 70% confluence in 6-well tissue culture plates, 24 h before the experiments. Before transfection, growth medium was removed and cells were washed twice with PBS, pH 7.4. Cells were then incubated with 200 µL of lipoplexes prepared with liposomes and pDNA in OPTI-MEM (Gibco). The final

concentration of pDNA was 8 μg/well. The negative control corresponded to cells treated with liposomes without pDNA. After 5 h, the medium was replaced by fresh growth medium and transfection was assessed after 48 h incubation time by flow cytometry (FACS Canto II, BD Biosciences) and CLSM.

4.1.10.1. Pulse cytophotometry

Pulse cytophotometry, usually entitled flow cytometry or FACS (Fluorescence-activated cell sorter) is a biophysical technique used to count cells through detection of a biomarker inside the cell structure. The detection is performed by suspending the cells in a fluid that passes through a laser capable of detecting the biomarkers. This technique is useful because it can analyse multiple parameters of individual cells within heterogeneous populations (Givan, 2001; Shapiro, 2003). Twenty thousand events were measured for each sample. Experimental data were statistically analysed applying one-way analysis of variance (ANOVA) following Tukey test approach.

4.1.10.2. Confocal Laser Scanning Microscopy

Microscopy images of transfected cells were obtained using a confocal laser scanning microscope (CLSM), Leica SP2 AOBS SE (Leica Microsystems). Confocal imaging is an optical microscopy tool that provides a high resolution image in a three dimensional form without destruction. This technique has the ability to acquire in-focus images from selected depths (optical sectioning) and rebuilt a three-dimensional image through computer technology. This process was coupled with fluorescence microscopy, allowing the visualisation of specimens that emit colour from fluorescent markers when exposed to light (Pawley, 2006).

4.2. Results and Discussion

4.2.1. Electric properties and diameter of the complexes

The electric properties of the lipoplexes were firstly studied by evaluating their electrophoretic mobility (μ_e) as a function of the *L/D* ratio. In this way, changes in the electrokinetic behaviour of the systems will be univocally related to the presence of the fluorinated lipid F7-CHOL (heptafluorocholesterol) in one of the systems. The experimental data of μ_e as a function of *L/D* ratio for DOTAP:CHOL/DNA and DOTAP:F7-CHOL/DNA systems fit to a sigmoidal curve that divides the *L*/*D* axis in three different zeta potential regions (Figure 4.3.A and Figure 4.4.A): *i)* a region where lipoplexes show a net negative and almost constant electrophoretic mobility; *ii)* a region where the isoelectric point $(L/D)_0$ is reached and an inversion of the electrophoretic mobility sign takes place and *iii)* a region of net positive electrophoretic mobility that tends to the value of the pure liposomes. This behaviour was previously found in works with other cationic lipoplexes (Barrán-Berdón, 2012; Muñoz-Úbeda, 2010; Muñoz-Úbeda, 2011; Rodriguez-Pulido, 2009). Examples of a sign reversal in the electrophoretic mobility have been also reported for different cationic lipoplexes (Zuzzi, 2007) as well as other colloidal systems such liposomes (Martín-Molina, 2010), latex particles (Martín-Molina, 2003; Martín-Molina, 2008; Martín-Molina, 2009; Popa, 2010; Schneider, 2011) and DNA (Besteman, 2007) in the presence of multivalent counterions. In all these cases, the change of the sign in the electrophoretic mobility is explained in terms of a charge inversion (*or overcharging*) phenomena (Lyklema, 2009).

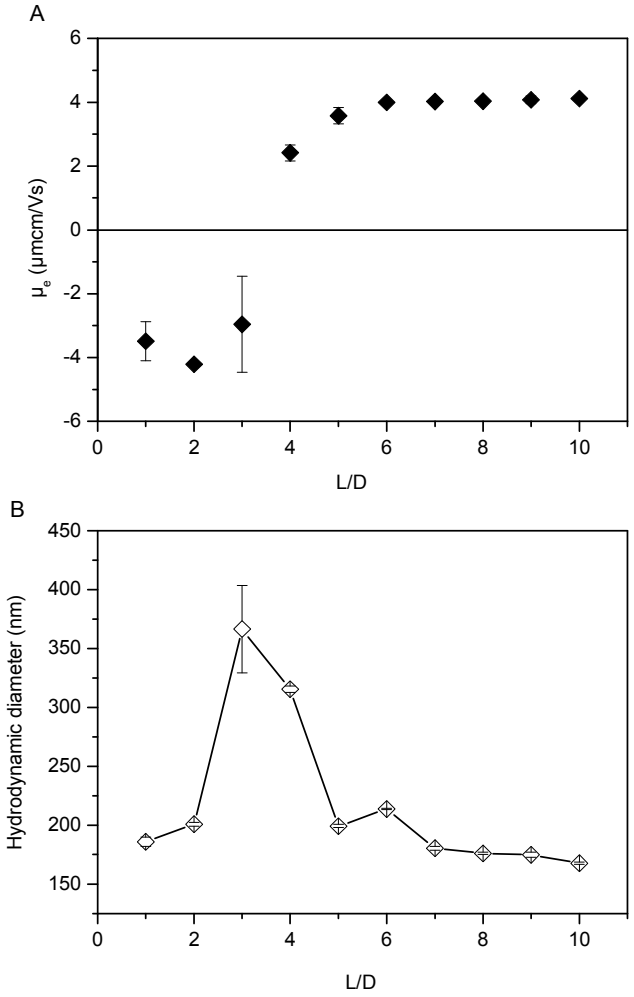

Figure 4.3. Electrophoretic mobility (A) and hydrodynamic diameter (B) of DOTAP:CHOL-DNA lipoplexes at different lipid-DNA (L/D) mass ratios in HEPES buffer (10 mM, pH 7.4). The DOTAP:CHOL molar ratio is 1:1 and DNA concentration is 0.05 mg/mL.

In our case, although the two systems present a similar qualitative behaviour, the curve corresponding to DOTAP:F7-CHOL/DNA lipoplexes appears shifted towards larger *L/D* ratio than that reported for lipoplexes without F7-CHOL. In

particular, the isoelectric point for DOTAP:CHOL/DNA and DOTAP:F7-CHOL/DNA is within the ranges $3 < (L/D)_0 < 4$ and $4 < (L/D)_0 < 5$, respectively.

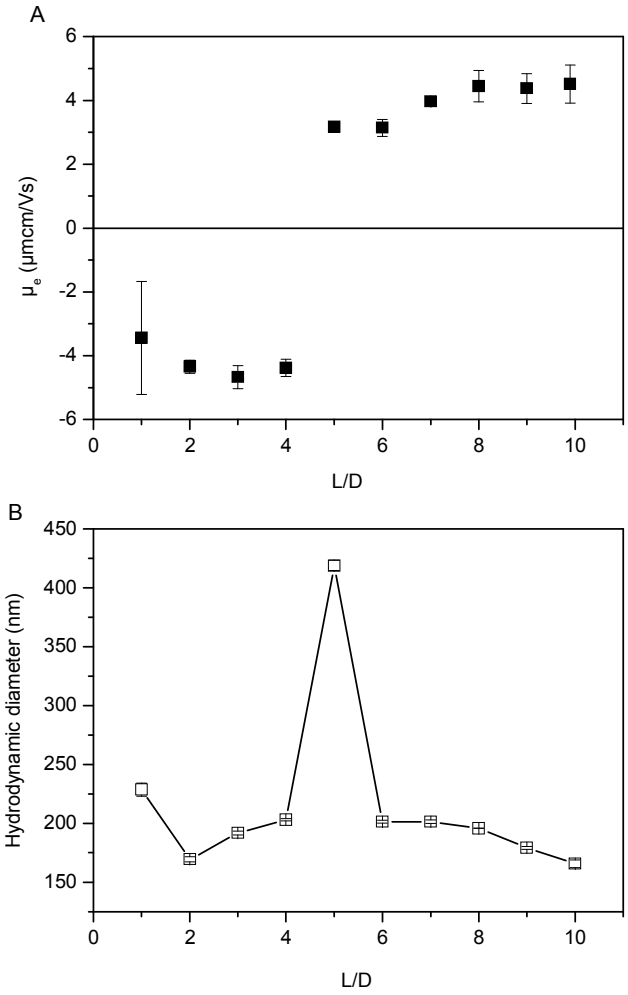

Figure 4.4. Electrophoretic mobility (A) and hydrodynamic diameter (B) of DOTAP:F7-CHOL-DNA lipoplexes at different lipid-DNA (L/D) mass ratios in HEPES buffer (10 mM, pH 7.4). The DOTAP:F7-CHOL molar ratio is 1:1 and DNA concentration is 0.05 mg/mL.

This means that more liposomes are required to neutralise the charge of DNA in the system with F7-CHOL. Although this fluorinated lipid does not provide net charge to the liposomes, its presence in the lipid bilayer seems to reduce the electropositive behaviour of the DOTAP liposomes. This feature could be related to the strong interaction between DOTAP and fluorinated cholesterol. Lipid monolayers studies showed that the area per molecule of DOTAP monolayer is reduced if fluorinated cholesterol lipids are included and that the lipid mixture monolayer is homogeneous at the low surface pressure of 5 mN/m in contrast to DOTAP:CHOL monolayer, which become miscible only when the pressure reaches 20 mN/m (Paiva, 2013). This could explain, at least in part, the differences between the two curves.

The hydrodynamic diameter of complexes that resulted from the interaction of DNA, at a constant concentration, and liposomes increases with liposome concentration and up to the isoelectric point (Figure 4.3.B and Figure 4.4.B). Further increase of the liposome amount leads to a decrease of the diameter of the lipoplexes and at L/D ratios of 9 and 10 the values tend to that of the liposomes. The hydrodynamic diameter of the liposomes was 97 ± 9 nm (PdI = 0.36 ± 0.22) for DOTAP:CHOL and 103 ± 7 nm (PdI = 0.30 ± 0.21) for DOTAP:F7-CHOL. The maximum size value of the complexes is observed at a ratio close to the isoelectric point. Similar behaviour has been reported for other lipoplexes including for complexes of DOTAP liposomes and double strand DNA (Barrán-Berdón, 2012; Besteman, 2007). The aggregation of DNA and liposomes is discussed as a reversible process resulting from a balance of long-range electrostatic repulsion and of short-range attraction (Bordi, 2005; Sennato, 2005). It is also described that the formation of complexes occurs without the rupture of the vesicles and that large clusters result from the aggregation of the liposome-DNA complexes (Sennato, 2005).

The mechanism that is proposed in the literature considering the surface charges agrees with our results: DNA interacts with the liposomes through electrostatic interactions and when the amount of negatively charged DNA nearly counterbalances the liposome positive surface charges, the maximum aggregation is reached (Ciani, 2007; Sennato, 2005).

4.2.2. DNA binding affinity to liposomes

Fluorescence spectroscopy was carried out following the variation on the emission of ethidium bromide (EtBr) in aqueous solutions at constant DNA concentration and increasing liposome amount. EtBr is an aromatic planar cationic probe, which intercalates between base pairs of double-stranded DNA leading to a high fluorescence quantum yield, compared to low fluorescence intensity when dispersed in water. Since liposomes do not quench the fluorescence of EtBr, the decreasing of fluorescence intensity with increasing L/D ratio for DOTAP:F7-CHOL/DNA lipoplexes confirms the exclusion of the EtBr from the DNA base pair microenvironment (Figure 4.5.A). A similar tendency was observed for DOTAP:CHOL/DNA lipoplexes. Since the intercalation of EtBr unwinds the DNA base pairs near the intercalation site by 26°, the conformational flexibility of DNA may decrease after it binds to the liposomes (Jones, 1980). The interaction of DNA with positively charged liposomes is expected to lead to a conformation rearrangement of the DNA macromolecule (Bordi, 2003; Ciani, 2004; Goncalves, 2004; Piedade, 2004). The displacement of EtBr from DNA to bulk might also be a consequence of the strong electrostatic interactions between DNA and cationic liposomes, which will decrease the ionic attractive forces between EtBr and DNA (Chen, 2000).

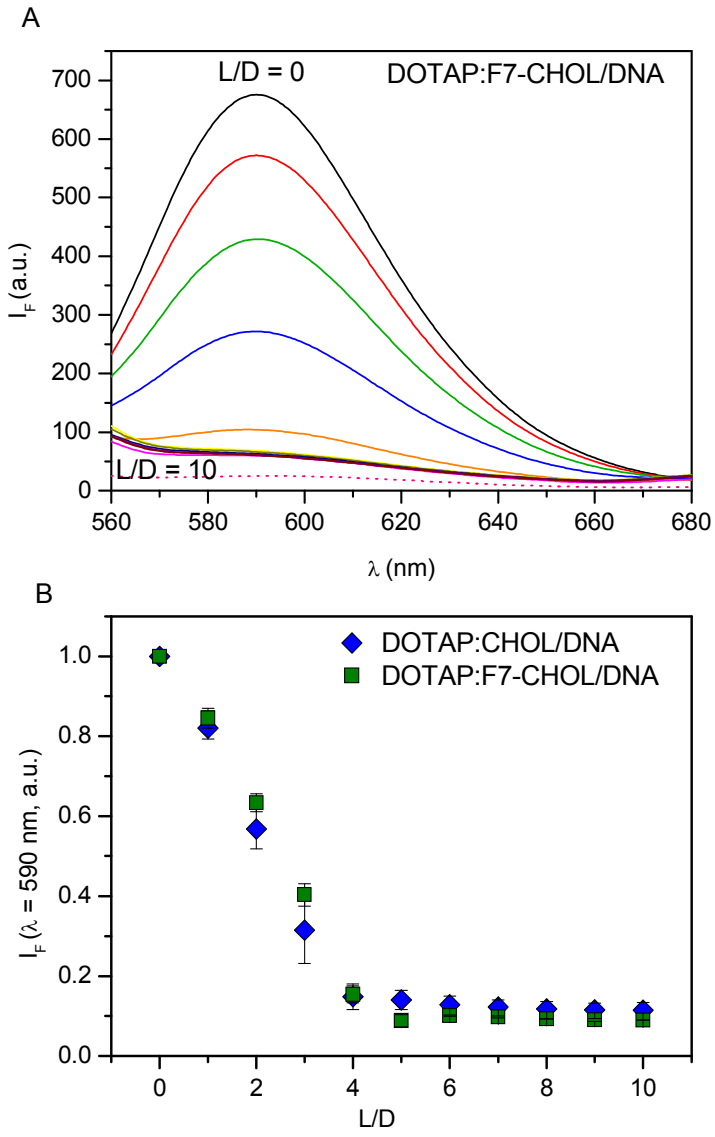

Figure 4.5. (A) Emission fluorescence spectra of DNA:EtBr (6:1) in the presence of DOTAP:F7-CHOL liposomes at the lipid/DNA (L/D) mass ratios from 0 to 10; dotted line shows the emission fluorescence spectrum of EtBr in HEPES buffer solution without liposomes and lipoplexes. (B) Emission fluorescence intensity of DNA:EtBr (6:1) at 590 nm in the presence of DOTAP:CHOL and DOTAP:F7-CHOL liposomes at L/D ratios form 0 to 10. The values were normalised to the maximum fluorescence intensity (DNA:EtBR in the absence of liposomes). DOTAP:sterol ratio is 1:1 and the DNA concentration is 0.025 mg/mL.

The maximum emission intensity, which is at 590 nm, decreases comparably for both DOTAP:CHOL and DOTAP:F7-CHOL liposomes when added at increasing concentrations to DNA:EtBr complex (Figure 4.5.B). The emission intensity at 590 nm is slightly lower for lipoplexes of DOTAP:CHOL and DNA than for DOTAP:F7-CHOL and DNA at L/D ratios of 2 and 3, indicating that more DOTAP:F7-CHOL liposomes are required to compact the same amount of DNA. This result is in accordance with the electrophoretic mobility study.

4.2.3. Morphology of the complexes

The structure, size and morphology of the lipoplexes are known to be key factors in transfection efficiency (Rodriguez-Pulido, 2009). The different nature of the liposomes and consequently the L/D ratios in the lipoplexes were studied by means of TEM imaging. The micrographs were selected to be representative with respect to all observations. Both DOTAP:CHOL and DOTAP:F7-CHOL liposomes are unilamellar and present a spherical shape (Figure 4.6). The size of the vesicles observed by TEM is in agreement with the size distribution obtained by dynamic light scattering. The presence of the fluorinated atoms in the bilayer does not affect the overall size of the liposomes. TEM micrographs were also taken to lipoplex samples at L/D ratios below and above the isoneutrality ratio, $(L/D)_0$. It is expected that liposome structure, size and morphology change in the presence of DNA.

On Figure 4.6 (B-C) and (E-F) is possible to see details of the micrographs taken at a L/D ratio < $(L/D)_0$, for DOTAP:CHOL and DOTAP:F7-CHOL system, respectively. In this case, lipoplexes present an excess of DNA. Not many differences are observed for these lipoplexes when compared to the respective liposome. However is notice a more delimited pattern around the particles in the presence of DNA. This happens because DNA molecules present a negative contrast when exposed to uranyl acetate, evidencing a

darker colour. The presence of a more intense colour around the bilayer indicates an increase on the density on the surface of the vesicles, confirming that DNA is compacted on the surface of the liposomes through strong electrostatic interactions, which is in agreement with potential and fluorescence studies.

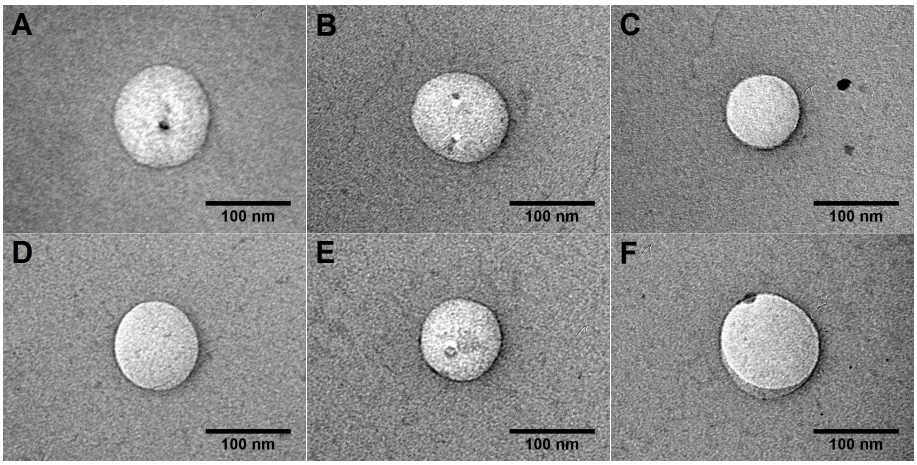

Figure 4.6. TEM micrographs of liposomes in the absence of DNA (A and D) and of lipoplexes at L/D<(L/D)$_0$ (B, C, E, F). (A-C) refers to DOTAP:CHOL system and (D-F) to DOTAP:F7-CHOL. Scale bar: 100 nm.

The strong interaction between the liposome and DNA could have other consequences. One is that it could lead to a disruption on the liposomes, producing smaller complexes, not observed for these systems, meaning that they are very stable with and without DNA. Another consequence is that when L/D is close to $(L/D)_0$ liposomes could fuse due to the action of the condensed DNA (Rodriguez-Pulido, 2008; Rodriguez-Pulido, 2009). From size measurements, for both systems, is observed this fusion or complex aggregation by the increase of the lipoplex diameter with the approximation of the isoneutrality ratio. On Figure 4.7 is presented some micrographs where

L/D ratio is above the isoelectric point, for DOTAP-CHOL (A-C) and DOTAP:F7-CHOL (D-F) systems. In this case, it was not only notice the increase on the density of the liposomes surface, as well as a clear shell covering the entire liposome. The exhibition of ramifications is consistent with the liposome coated by the DNA molecules.

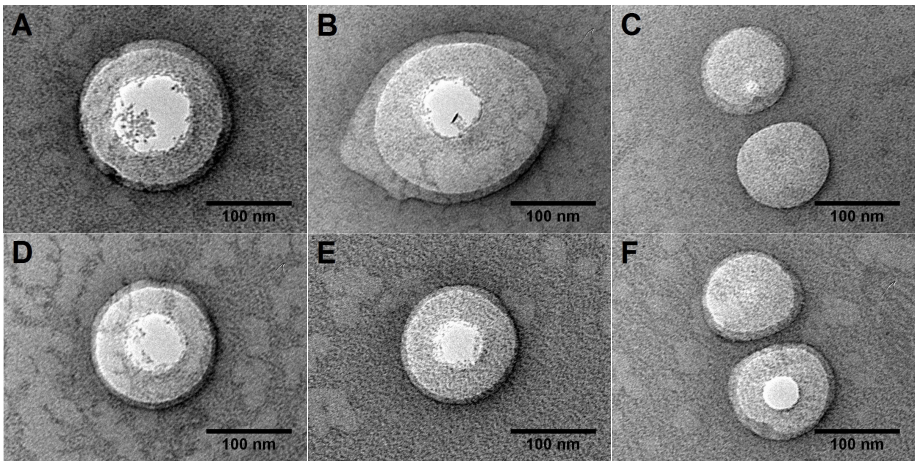

Figure 4.7. Details extrated from the original TEM micrographs of lipoplexes at $L/D>(L/D)_0$. (A-C) refers to DOTAP:CHOL system and (D-F) to DOTAP:F7-CHOL. Scale bar: 100 nm.

4.2.4. Boundary concentrations of the lipoplexes

The different electrokinetic regions found experimentally for the lipoplexes as a function of the *L/D* ratio were also analysed from a theoretical point of view by using the complexation model presented in section 4.1.7. In particular, the model is applied to predict the phase diagrams of the

lipoplexes in this work, *i. e.,* the calculation of the boundary concentrations $S_a(P)$ and $S_d(P)$ as a function of the DNA concentration (P). To this end, the electrophoretic data are used to obtain the experimental values of $S_a(P_{exp})$ and $S_d(P_{exp})$ for the DNA concentration that was used in the experiments (Table 4.1). Then, these inputs are used to solve equations (4.3) and (4.4) in order to determine the characteristic parameters P_0 and E_0 for each system (Table 4.1).

Table 4.1. Phenomenological parameters P_0 and E_0 for each system and the required experimental conditions for their calculation.

Parameter[1]	DOTAP:CHOL/DNA	DOTAP:F7CHOL/DNA
a (nm)	50.0	50.0
κ_D (nm^{-1})	5.33	5.33
C_e ($C^2\ J^{-1}$)	1.17×10^{-13}	1.17×10^{-13}
Q (e)	28500	28500
q (e)	5400	5400
P_{exp} (segments/l)	17.16×10^{15}	17.16×10^{15}
$S_a(P_{exp})$ (part/l)	1.55×10^{15}	1.74×10^{15}
$S_d(P_{exp})$ (part/l)	5.59×10^{15}	3.05×10^{15}
E_0 (J)	5.57×10^{-26}	25.40×10^{-26}
P_0 (segments/l)	5.60×10^{15}	2.91×10^{15}

[1] a, liposome radius; κ_D, reciprocal Debye length; C_e, liposome capacitance; Q, liposome charge; q, charge of DNA segment; P, DNA concentration; $S_a(P)$, liposome concentration at aggregation; $S_d(P)$, liposome concentration at disaggregation; E_0, DNA-liposome interaction energy; P_0, DNA concentration in equilibrium with lipoplexes.

The experimental conditions required for the calculations (Table 4.1) are determined as follows: q is estimated assuming a DNA molecule formed

by 2700 bp fragments on average (obtained from agarose gel electrophoresis experiments (Muñoz-Úbeda, 2010; Rodriguez-Pulido, 2009)); *Q* is calculated from the surface area of the liposome and the estimated area for the headgroup of the lipid. The phenomenological parameter E_0 is much larger for DOTAP:F7-CHOL/DNA than for DOTAP:CHOL/DNA lipoplexes. This feature may be understood as the strength of the liposome-DNA binding being stronger in the case of DOTAP:F7-CHOL/DNA system. On the other hand, $P_0 < P_{exp}$ in both cases, which agrees with the assumption that most of the DNA molecules is forming the complexes. However, the value of P_0 for DOTAP:F7-CHOL/DNA is almost half of that obtained for the lipoplexes without F7-CHOL. Although more DOTAP:F7-CHOL liposomes are required to form the lipoplexes, most of the DNA molecules could be implicated in the complexation once the lipoplexes are formed.

The values of P_0 are similar as those reported for other charged lipoplexes (Barrán-Berdón, 2012; Muñoz-Úbeda, 2010; Rodriguez-Pulido, 2009). The values of E_0, on the other hand, are much lower than those calculated in the present work. This is due to the definition of C_e, which in the previous works was defined in the vacuum instead of in an electrolyte solution. In any case, we must be aware that P_0 and E_0 are two phenomenological parameters and as the authors of the model stated, it is difficult to assign them a real meaning on the basis of a microscopic theory (Nguyen, 2001a).

Once the parameters are calculated, the values of $S_a(P)$ and $S_d(P)$ can be predicted for any DNA concentration by varying *P* in equations (4.3) and (4.4). Figure 4.8 shows the theoretical phase diagram of DOTAP:CHOL/DNA and DOTAP:F7-CHOL/DNA. Given a constant value of *P*, the phase diagram predicts the existence of negatively charged stable lipoplexes for liposome concentrations $S < S_a(P)$, with free anionic polyelectrolyte in excess. If *S*

increases, lipoplexes experience aggregation and the suspension becomes unstable (grey region of the diagrams in Figure 4.8).

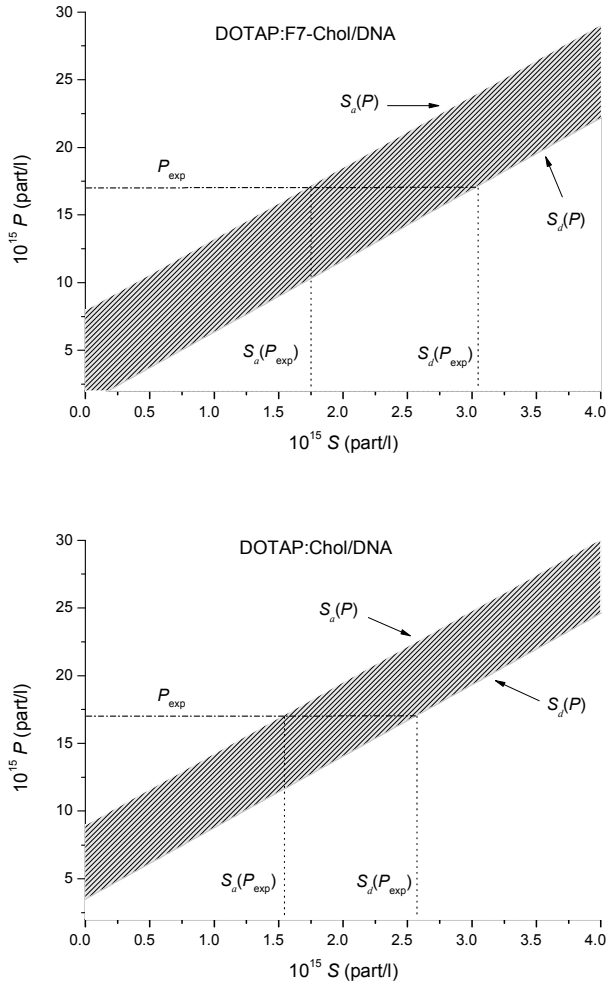

Figure 4.8. Boundary concentration lines, $S_a(P)$ and $S_d(P)$, for DOTAP:CHOL/DNA (up) and DOTAP:F7-CHOL/DNA (down) lipoplexes, according to the aggregation-disaggregation theory.

In this domain of *S* concentration, *i.e.*, for $S_a(P) < S(P) < S_d(P)$, the isoneutrality of the lipoplexes is reached (the electrophoretic mobility is null). However,

the theory predicts that complexes at this point attract more cationic liposomes than those required to neutralise the negative charge (Nguyen, 2001a). As a consequence, a charge inversion process takes place. Finally, for $S > S_d(P)$, clusters start to partially dissolve giving rise to stable and free positively charged lipoplexes in coexistence with the remaining clusters.

4.2.5. Stability ratio

Similar results were obtained for the stability rate of DOTAP:CHOL and DOTAP:F7-CHOL liposomes as a function of DNA concentration (Figure 4.9): the stability of the liposomes decreases as the DNA concentration increases until the systems become unstable. Then if the DNA concentration continues to increase, both systems are stabilised again. This behaviour is in general similar to that found for the electrophoretic mobility measurements in which two asymptotic values of $|\mu_e|$ were reached for low and high values of *L/D* ratio. Consequently, regions in which the systems are stable are attributed to the formation of lipoplexes that are stabilised electrostatically. In contrast, regions where $W \sim 1$ corresponds to a range of DNA concentration at which the isoelectric point of the lipoplexes is expected to be reached. Furthermore, the regions where the systems are stable and unstable agree with those predicted by the complexation model in which a *reentrant condensation* procedure is expected to happen. Concerning the numerical values of CCC and CSC, slight differences are observed: these critical DNA concentrations are, respectively, 0.022 mg/mL and 0.078 mg/m for DOTAP:CHOL. In the case of DOTAP:F7-CHOL, the values of CCC and CSC are, respectively, 0.026 mg/mL and 0.087 mg/mL. The observed small differences agree with those found in the results of electrophoretic mobility, which showed that for the system with F7-CHOL lipids more liposomes are required to neutralise the charge of DNA.

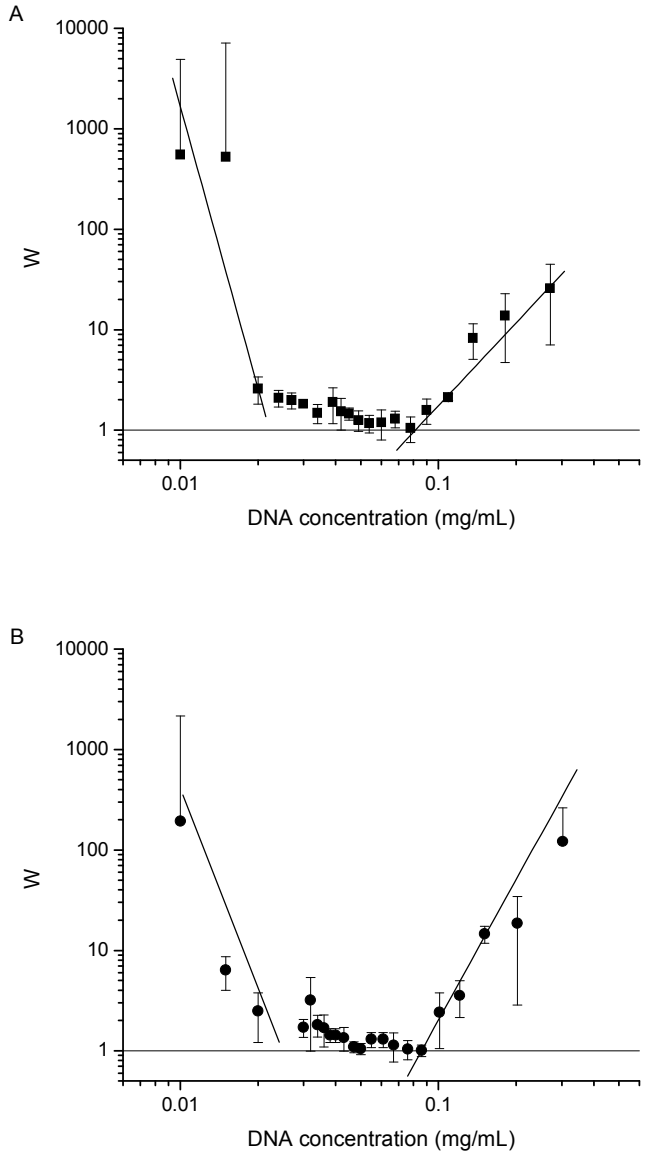

Figure 4.9. Fuchs stability ratio *W* (stability factor) of liposomes DOTAP:CHOL (A) and DOTAP:F7-CHOL (B), as a function of DNA concentration. Data are presented on the logarithmic scale.

Accordingly, the interaction between DOTAP and fluorinated cholesterol can

justify the different electrokinetic and stability behaviour that was found for this system.

The ionic strength of physiological media can affect the process of DNA complexation, shifting the stability ratio, DNA-liposome condensation curve and the isoelectric point of the lipoplexes, which will have a direct implication on the DNA transfection efficiency. In general, salt reduces the electrical surface potential of the liposomes and the increase of the ionic strength shifts the isoelectric point to higher L/D ratios (Eastman, 1997; Kennedy, 2000; Pullmannova, 2012). However, the effect of NaCl on the neutralisation is dependent on the salt concentration and on the type of lipids present in the system (Eastman, 1997; Hirsch-Lerner, 2005). The DOTAP:CHOL system was the least sensitive to increases of NaCl and had better integrity in serum when compared to others such as DOTAP:DOPE liposomes. The percentage of DNA that was associated to the liposomes in 150 mM of NaCl aqueous solution was more than 90% for DOTAP/DNA charge ratios of 1:1 and 1:2 (Hirsch-Lerner, 2005).

4.2.6. DNA conformation

The number of base pairs per turn, the inclination of the base with respect to the helix axis, the distance of the bases from the helix axis, the rise per base pair and the handedness of the helix characterise the polymorphism of the secondary structure of nucleic acids.

Both ctDNA and pDNA samples (Figure 4.10) were analysed by CD spectroscopy. They both show a negative peak at 246 nm, a positive peak around 273 nm with the zero crossing around 260 nm, which is consistent with the CD spectra for a B conformation of a double helical DNA. In this case, the base pairs are perpendicular to the double helix axis, which confers a weak chirality to the molecule, which is characterised by the low peak

intensities. The variation in the amplitude of the CD signal may be due to the different nucleotide sequences (Kypr, 2009; Marty, 2009).

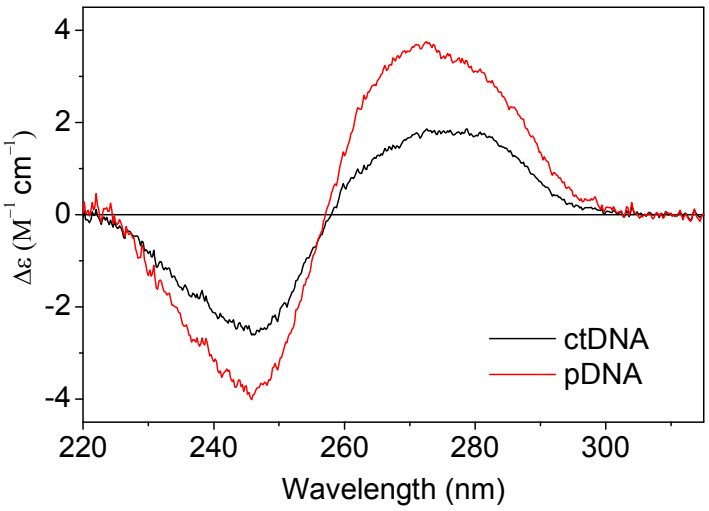

Figure 4.10. CD spectra of ctDNA and pDNA in Tris buffer (pH=7.4).

When DNA is electrostatically bound to the lipid vesicles, a decrease in the Δε (M^{-1} cm^{-1}) signal of the positive peak and an increase in the absolute value of the negative peak of the CD spectra are observed (Figure 4.11). Also both peaks reveal a red wavelength shift. The binding of DNA to the vesicles generates a conformation change or at least a transition on the DNA polymorphism. The differences may suggest a partial B- to C-DNA conformational transition as stated before in the literature for DOTAP complexes (Marty, 2009). The C-form CD spectrum was found for DNA condensed or packaged systems, especially monocationic lipid formulations (Ranjbar, 2009; Simberg, 2001).

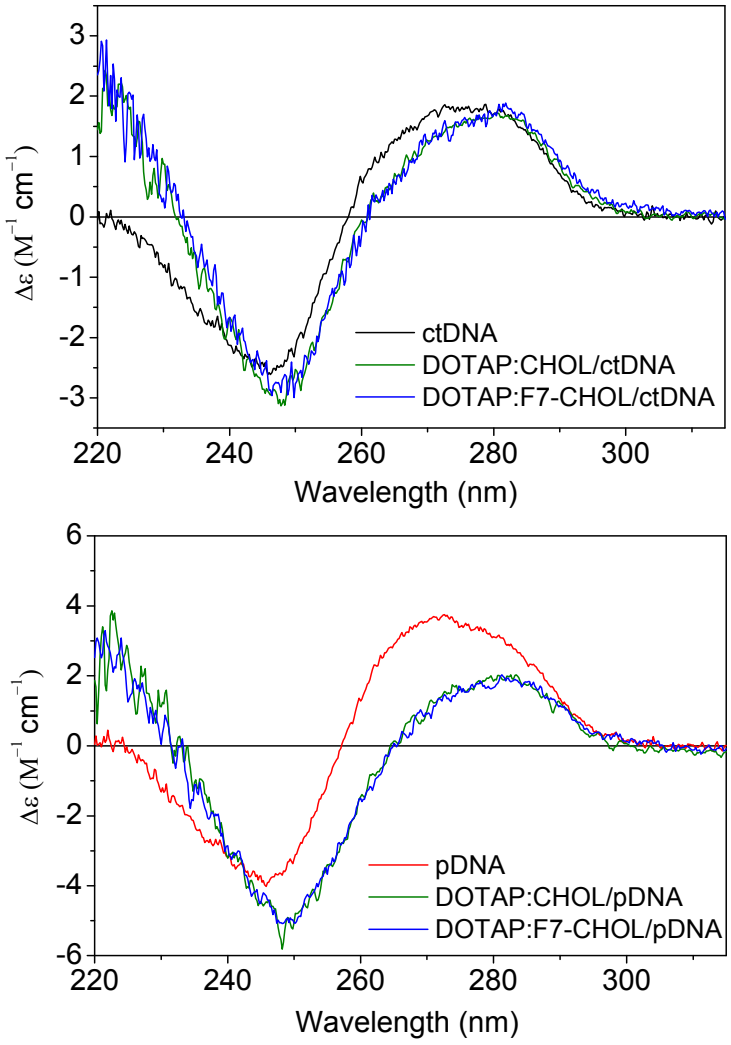

Figure 4.11. CD spectra of ctDNA (up) and pDNA (down) for DNA alone and complexes of DNA with DOTAP:CHOL and DOTAP:F7-CHOL at the L/D ratio of 10:1.

DNA is thus more compacted in the presence of the carrier. The use of the fluorinated helper lipid (F7-CHOL) has no impact on the conformational

structure of the DNA when compared with CHOL lipid, since the spectral curves are overlapped. Different L/D ratios (1, 2, 6 and 20) were also tested, however no significant differences were found between ratios, indicating that the DNA conformation does not change with the increase of the lipid concentration.

4.2.7. Cell transfection studies

The transfection efficiency of lipoplexes was evaluated using two different cell lines: SH-SY5Y, a human neuroblastoma derived cell line, and HeLa, an immortal cell line, derived from cervical cancer. Cell lines were transfected with plasmid DNA (pDNA) encoding green fluorescent protein (GFP). Flow cytometry analysis revealed that GFP expression was induced similarly by DOTAP:F7-CHOL/pDNA and DOTAP:CHOL/pDNA, in both cell lines (Figure 4.12).

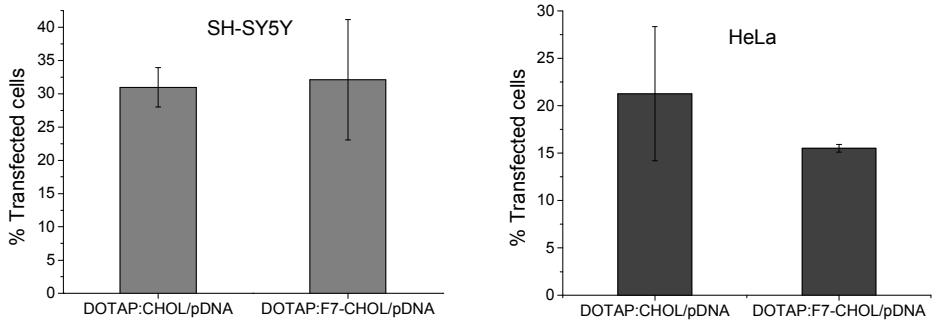

Figure 4.12. Transfection of SH-SY5Y and HeLa cell lines with green fuorescent protein (GFP plasmid (pDNA): cytometry analysis of levels of transfection of cells using DOTAP:CHOL and DOTAP:F7-CHOL systems. The L/D ratio was 10:1. Results are expressed as mean ± S.D. (n = 3).

Comparing the different type of cells, DOTAP:F7-CHOL/pDNA system shows higher transfection efficiency in SH-SY5Y line ($P < 0.01$), whereas for DOTAP:CHOL/pDNA the differences are not significant. Naked pDNA did not transfect the cells (Figure 4.13).

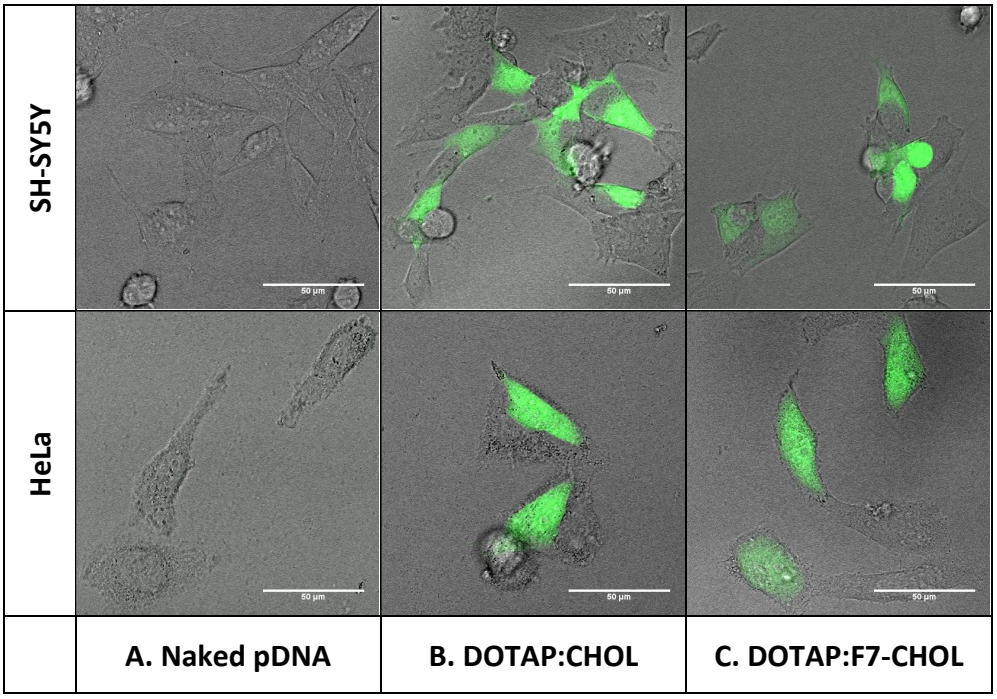

Figure 4.13. Illustrative confocal images of GFP expression for SH-Sy5Y and HeLa cell lines when transfected with naked plasmid DNA (A), DOTAP:CHOL/pDNA (B) and DOTAP:F7-CHOL/pDNA (C). The scale bar is 50 µm.

DOTAP:CHOL was shown to be more efficient than the commercial formulation lipofectamine® (Ramesh, 2001) and to transfect different cell tissues as lung and heart cell tissues (Templeton, 1997). The system has been studied *in vivo* and shown to be efficient also in transporting genetic material to cells (Eliyahu, 2007; Kim, 2007; Ramesh, 2001; Templeton, 1997).

DOTAP:F7-CHOL is thus a good candidate for *in vivo* studies, regarding the similarities of the *in vitro* transfection results with DOTAP:CHOL.

4.3. Conclusions

We propose the use of F7-CHOL (heptafluorocholesterol) as helper lipid in cationic DOTAP liposomes for DNA delivery. This fluorinated derivative of cholesterol was chosen because previous studies highlighted the efficient gene transfer by lipids containing fluorinated hydrophobic chains (Boulanger, 2004; Boussif, 2001; Gaucheron, 2001a; Gaucheron, 2001b; Gaucheron, 2002). The properties of the system with fluorinated cholesterol were compared to that of DOTAP:CHOL liposomes. The results show that more liposomes are required to form the lipoplexes with DOTAP:F7-CHOL system than with DOTAP:CHOL. However, the aggregation-disaggregation model predicts that, even if more DOTAP:F7-CHOL liposomes are needed, most of the DNA is involved in the complexation process when the lipoplexes are formed. Both DOTAP:F7-CHOL and DOTAP:CHOL systems show similar stability in the presence of DNA and have identical transfection efficiency. These results are in agreement with other studies that describe also comparable DNA compaction process, size of lipoplexes and transfection efficiency for the commonly used helper lipid DOPE and its fluorinated analogues when mixed with cationic lipids (Gaucheron, 2001a). Our study verified that fluorine atoms can be included in the cholesterol molecule without dramatically changing the properties of the cationic liposomes.

4.4. References

Aagaard, L.; Rossi, J.J. (**2007**). RNAi therapeutics: Principles, prospects and challenges, *Advanced Drug Delivery Reviews, 59*, 75.

Audouy, S.A.L.; de Leij, L.F.M.H.; Hoekstra, D.; Molema, G. (**2002**). In vivo characteristics of cationic liposomes as delivery vectors for gene therapy, *Pharmaceutical Research, 19*, 1599.

Baase, W.A.; Johnson, W.C., Jr. (**1979**). Circular dichroism and DNA secondary structure, *Nucleic Acids Research, 6*, 797.

Barrán-Berdón, A.L.; Muñoz-Úbeda, M.; Aicart-Ramos, C.; Pérez, L.; Infante, M.R.; Castro-Hartmann, P.; Martín-Molina, A.; Aicart, E.; Junquera, E. (**2012**). Ribbon-type and cluster-type lipoplexes constituted by a chiral lysine based cationic gemini lipid and plasmid DNA, *Soft Matter, 8*, 7368.

Besteman, K.; Van Eijk, K.; Lemay, S.G. (**2007**). Charge inversion accompanies DNA condensation by multivalent ions, *Nature Physics, 3*, 641.

Bohinc, K.; Brezesinski, G.; May, S. (**2012**). Modeling the influence of adsorbed DNA on the lateral pressure and tilt transition of a zwitterionic lipid monolayer, *Physical Chemistry Chemical Physics, 14*, 10613.

Bordi, F.; Cametti, C.; De Luca, F.; Gili, T.; Gaudino, D.; Sennato, S. (**2003**). Charged lipid monolayers at the air-solution interface: coupling to polyelectrolytes, *Colloids and Surfaces B-Biointerfaces, 29*, 149.

Bordi, F.; Cametti, C.; Diociaiuti, M.; Sennato, S. (**2005**). Large equilibrium clusters in low-density aqueous suspensions of polyelectrolyte-liposome complexes: A phenomenological model, *Physical Review E, 71*, 050401.

Boulanger, C.; Di Giorgio, C.; Gaucheron, J.; Vierling, P. (**2004**). Transfection with fluorinated lipoplexes based on new fluorinated cationic lipids and in the presence of a bile salt surfactant, *Bioconjugate Chemistry, 15*, 901.

Boussif, O.; Gaucheron, J.; Boulanger, C.; Santaella, C.; Kolbe, H.V.J.; Vierling, P. (**2001**). Enhanced in vitro and in vivo cationic lipid-mediated gene

delivery with a fluorinated glycerophosphoethanolamine helper lipid, *Journal of Gene Medicine, 3*, 109.

Buschow, K.H.J.C., Robert W.; Flemings, Merton C.; Ilschner, Bernhard; Kramer, Edward J.; Mahajan, Subhash; *Encyclopedia of Materials - Science and Technology,* Volume 1-11, 1st Edition, Elsevier, The Netherlands, **2001**.

Butt, H.-J.; Graf, K.; *Physics and chemistry of interfaces,* Wiley-VCH, Germany, **2006**.

Chen, W.; Turro, N.J.; Tomalia, D.A. (**2000**). Using ethidium bromide to probe the interactions between DNA and dendrimers, *Langmuir, 16*, 15.

Ciani, L.; Ristori, S.; Calamai, L.; Martini, G. (**2004**). DOTAP/DOPE and DC-Chol/DOPE lipoplexes for gene delivery: zeta potential measurements and electron spin resonance spectra, *Biochimica Et Biophysica Acta-Biomembranes, 1664*, 70.

Ciani, L.; Ristori, S.; Bonechi, C.; Rossi, C.; Martini, G. (**2007**). Effect of the preparation procedure on the structural properties of oligonucleotide/cationic liposome complexes (lipoplexes) studied by electron spin resonance and Zeta potential, *Biophysical Chemistry, 131*, 80.

Crook, K.; Stevenson, B.J.; Dubouchet, M.; Porteous, D.J. (**1998**). Inclusion of cholesterol in DOTAP transfection complexes increases the delivery of DNA to cells in vitro in the presence of serum, *Gene Therapy, 5*, 137.

Eastman, S.J.; Siegel, C.; Tousignant, J.; Smith, A.E.; Cheng, S.H.; Scheule, R.K. (**1997**). Biophysical characterization of cationic lipid:DNA complexes, *Biochimica Et Biophysica Acta-Biomembranes, 1325*, 41.

Ebnesajjad, S.; *Surface Treatment of Materials for Adhesion Bonding,* William Andrew, United States of America, **2006**.

Eliyahu, H.; Joseph, A.; Schillemans, J.P.; Azzam, T.; Domb, A.J.; Barenholz, Y. (**2007**). Characterization and in vivo performance of dextran-spermine polyplexes and DOTAP/cholesterol lipoplexes administered locally and systemically, *Biomaterials, 28*, 2339.

Espinosa-Andrews, H.; Báez-González, J.G.; Cruz-Sosa, F.; Vernon-Carter, E.J. (**2007**). Gum Arabic−Chitosan Complex Coacervation, *Biomacromolecules, 8*, 1313.

Farago, O.; Grønbech-Jensen, N.; Pincus, P. (**2006**). Mesoscale Computer Modeling of Lipid-DNA Complexes for Gene Therapy, *Physical Review Letters, 96*, 018102.

Farago, O.; Grønbech-Jensen, N. (**2007**). Computational and Analytical Modeling of Cationic Lipid-DNA Complexes, *Biophysical Journal, 92*, 3228.

Gaucheron, J.; Boulanger, C.; Santaella, C.; Sbirrazzuoli, N.; Boussif, O.; Vierling, P. (**2001a**). In Vitro Cationic Lipid-Mediated Gene Delivery with Fluorinated Glycerophosphoethanolamine Helper Lipids, *Bioconjugate Chemistry, 12*, 949.

Gaucheron, J.; Santaella, C.; Vierling, P. (**2001b**). Improved in vitro gene transfer mediated by fluorinated lipoplexes in the presence of a bile salt surfactant, *The Journal of Gene Medicine, 3*, 338.

Gaucheron, J.; Santaella, C.; Vierling, P. (**2002**). Transfection with fluorinated lipoplexes based on fluorinated analogues of DOTMA, DMRIE and DPPES, *Biochimica et Biophysica Acta (BBA) - Biomembranes, 1564*, 349.

Givan, A.L.; *Flow Cytometry: First Principles,* 2nd Edition, John Wiley & Sons, United States of America, **2001**.

Goncalves, E.; Debs, R.J.; Heath, T.D. (**2004**). The effect of liposome size on the final lipid/DNA ratio of cationic lipoplexes, *Biophysical Journal, 86*, 1554.

Hiemenz, P.C.; Rajagopalan, R.; *Principles of colloid and surface chemistry,* 3rd Edition, Marcel Dekker, United States of America, **1997**.

Hirsch-Lerner, D.; Zhang, M.; Eliyahu, H.; Ferrari, M.E.; Wheeler, C.J.; Barenholz, Y. (**2005**). Effect of "helper lipid" on lipoplex electrostatics, *Biochimica Et Biophysica Acta-Biomembranes, 1714*, 71.

Jones, R.L.; Lanier, A.C.; Keel, R.A.; Wilson, W.D. (**1980**). The effect of ionic strength on DNA-ligand unwinding angles for acridine and quinoline derivatives., *Nucleic Acids Research, 8*, 1613.

Kennedy, M.T.; Pozharski, E.V.; Rakhmanova, V.A.; MacDonald, R.C. (**2000**). Factors governing the assembly of cationic phospholipid-DNA complexes (vol 78, pg 1620, 2000), *Biophysical Journal, 79*, 1168.

Kim, J.Y.; Choung, S.; Lee, E.J.; Kim, Y.J.; Choi, Y.C. (**2007**). Immune activation by siRNA/liposome complexes in mice is sequence- independent: Lack of a role for toll-like receptor 3 signaling, *Molecules and Cells, 24*, 247.

Kypr, J.; Kejnovská, I.; Renčiuk, D.; Vorlíčková, M. (**2009**). Circular dichroism and conformational polymorphism of DNA, *Nucleic Acids Research, 37*, 1713.

Lakowicz, J.R.; *Principles of Fluorescence Spectroscopy,* 3rd Edition, Springer, United States of America, **2006**.

Lu, X.J.; Olson, W.K. (**2003**). 3DNA: a software package for the analysis, rebuilding and visualization of three-dimensional nucleic acid structures, *Nucleic Acids Research, 31*, 5108.

Lv, H.T.; Zhang, S.B.; Wang, B.; Cui, S.H.; Yan, J. (**2006**). Toxicity of cationic lipids and cationic polymers in gene delivery, *Journal of Controlled Release, 114*, 100.

Lyklema, J. (**2009**). Quest for ion-ion correlations in electric double layers and overcharging phenomena, *Advances in Colloid and Interface Science, 147-148*, 205.

Martín-Molina, A.; Quesada-Pérez, M.; Galisteo-González, F.; Hidalgo-Álvarez, R. (**2003**). Primitive models and electrophoresis: An experimental study, *Colloids and Surfaces A: Physicochemical and Engineering Aspects, 222*, 155.

Martín-Molina, A.; Maroto-Centeno, J.A.; Hidalgo-Álvarez, R.; Quesada-Pérez, M. (**2008**). Charge reversal in real colloids: Experiments, theory and simulations, *Colloids and Surfaces A: Physicochemical and Engineering Aspects, 319*, 103.

Martín-Molina, A.; Rodríguez-Beas, C.; Hidalgo-Álvarez, R.; Quesada-Pérez, M. (**2009**). Effect of surface charge on colloidal charge reversal, *Journal of Physical Chemistry B, 113*, 6834.

Martín-Molina, A.; Rodríguez-Beas, C.; Faraudo, J. (**2010**). Charge reversal in anionic liposomes: Experimental demonstration and molecular origin, *Physical Review Letters, 104*,

Martín-Molina, A.; Rodríguez-Beas, C.; Faraudo, J. (**2012**). Effect of Calcium and Magnesium on Phosphatidylserine Membranes: Experiments and All-Atomic Simulations, *Biophysical Journal, 102*, 2095.

Marty, R.; N'soukpoe-Kossi, C.N.; Charbonneau, D.; Weinert, C.M.; Kreplak, L.; Tajmir-Riahi, H.A. (**2009**). Structural analysis of DNA complexation with cationic lipids, *Nucleic Acids Research, 37*, 849.

Mengistu, D.H.; Bohinc, K.; May, S. (**2009**). Binding of DNA to zwitterionic lipid layers mediated by divalent cations, *Journal of Physical Chemistry B, 113*, 12277.

Miyahara, T.; Nakatsuji, H.; Sugiyama, H. (**2012**). Helical Structure and Circular Dichroism Spectra of DNA: A Theoretical Study, *The Journal of Physical Chemistry A, 117*, 42.

Morille, M.; Passirani, C.; Vonarbourg, A.; Clavreul, A.; Benoit, J.P. (**2008**). Progress in developing cationic vectors for non-viral systemic gene therapy against cancer, *Biomaterials, 29*, 3477.

Muñoz-Úbeda, M.; Rodríguez-Pulido, A.; Nogales, A.; Martín-Molina, A.; Aicart, E.; Junquera, E. (**2010**). Effect of lipid composition on the structure and theoretical phase diagrams of DC-Chol/DOPE-DNA lipoplexes, *Biomacromolecules, 11*, 3332.

Muñoz-Úbeda, M.; Rodríguez-Pulido, A.; Nogales, A.; Llorca, O.; Quesada-Pérez, M.; Martín-Molina, A.; Aicart, E.; Junquera, E. (**2011**). Gene vectors based on DOEPC/DOPE mixed cationic liposomes: A physicochemical study, *Soft Matter, 7*, 5991.

Nguyen, T.T.; Shklovskii, B.I. (**2001a**). Complexation of a polyelectrolyte with oppositely charged spherical macroions: Giant inversion of charge, *Journal of Chemical Physics, 114*, 5905.

Nguyen, T.T.; Shklovskii, B.I. (**2001b**). Complexation of DNA with positive spheres: Phase diagram of charge inversion and reentrant condensation, *Journal of Chemical Physics, 115*, 7298.

Paiva, D.; Brezesinski, G.; Pereira, M.d.C.; Rocha, S. (**2013**). Langmuir Monolayers of Monocationic Lipid Mixed with Cholesterol or Fluorocholesterol: DNA Adsorption Studies, *Langmuir, 29*, 1920.

Palmerini, C.A.; Cametti, C.; Sennato, S.; Gaudino, D.; Carlini, E.; Bordi, F.; Arienti, G. (**2006**). Role of cholesterol, DOTAP, and DPPC in

prostasome/spermatozoa interaction and fusion, *Journal of Membrane Biology, 211*, 185.

Pawley, J.B.; *Handbook of Biological Confocal Microscopy,* 3rd Edition, Springer, United States of America, **2006**.

Peula-García, J.M.; Ortega-Vinuesa, J.L.; Bastos-González, D. (**2010**). Inversion of Hofmeister Series by Changing the Surface of Colloidal Particles from Hydrophobic to Hydrophilic, *The Journal of Physical Chemistry C, 114*, 11133.

Piedade, J.A.P.; Mano, M.; de Lima, M.C.P.; Oretskaya, T.S.; Oliveira-Brett, A.M. (**2004**). Electrochemical sensing of the behaviour of oligonucleotide lipoplexes at charged interfaces, *Biosensors & Bioelectronics, 20*, 975.

Popa, I.; Gillies, G.; Papastavrou, G.; Borkovec, M. (**2010**). Attractive and Repulsive Electrostatic Forces between Positively Charged Latex Particles in the Presence of Anionic Linear Polyelectrolytes, *The Journal of Physical Chemistry B, 114*, 3170.

Pullmannova, P.; Bastos, M.; Bai, G.Y.; Funari, S.S.; Lacko, I.; Devinsky, F.; Teixeira, J.; Uhrikova, D. (**2012**). The ionic strength effect on the DNA complexation by DOPC - gemini surfactants liposomes, *Biophysical Chemistry, 160*, 35.

Ramesh, R.; Saeki, T.; Templeton, N.S.; Ji, L.; Stephens, L.C.; Ito, I.; Wilson, D.R.; Wu, Z.; Branch, C.D.; Minna, J.D.; Roth, J.A. (**2001**). Successful treatment of primary and disseminated human lung cancers by systemic delivery of tumor suppressor genes using an improved liposome vector, *Molecular Therapy, 3*, 337.

Ranjbar, B.; Gill, P. (**2009**). Circular Dichroism Techniques: Biomolecular and Nanostructural Analyses- A Review, *Chemical Biology & Drug Design, 74*, 101.

Ravily, V.; Santaella, C.; Vierling, P.; Gulik, A. (**1997**). Phase behavior of fluorocarbon di-O-alkyl-glycerophosphocholines and glycerophosphoethanolamines and long-term shelf stability of fluorinated liposomes, *Biochimica Et Biophysica Acta-Biomembranes, 1324*, 1.

Rodger, A.; Nordén, B.; *Circular Dichroism & Linear Dichroism,* Oxford University Press, United States of America, **1997**.

Rodriguez-Pulido, A.; Aicart, E.; Llorca, O.; Junquera, E. (**2008**). Compaction Process of Calf Thymus DNA by Mixed Cationic−Zwitterionic Liposomes: A Physicochemical Study, *The Journal of Physical Chemistry B, 112*, 2187.

Rodriguez-Pulido, A.; Martin-Molina, A.; Rodriguez-Beas, C.; Llorca, O.; Aicart, E.; Junquera, E. (**2009**). A Theoretical and Experimental Approach to the Compaction Process of DNA by Dioctadecyldimethylammonium Bromide/Zwitterionic Mixed Liposomes, *Journal of Physical Chemistry B, 113*, 15648.

Santaella, C.; Frézard, F.; Vierling, P.; Riess, J.G. (**1993**). Extended in vivo blood circulation time of fluorinated liposomes, *Febs Letters, 336*, 481.

Schindler, T.; Nordmeier, E. (**1997**). The stability of polyelectrolyte complexes of Calf-Thymus DNA and synthetic polycations: Theoretical and experimental investigations, *Macromolecular Chemistry and Physics, 198*, 1943.

Schneider, C.; Hanisch, M.; Wedel, B.; Jusufi, A.; Ballauff, M. (**2011**). Experimental study of electrostatically stabilized colloidal particles: Colloidal stability and charge reversal, *Journal of Colloid and Interface Science, 358*, 62.

Sennato, S.; Bordi, F.; Cametti, C.; Di Biasio, A.; Diociaiuti, M. (**2005**). Polyelectrolyte-liposome complexes: An equilibrium cluster phase

close to the isoelectric condition, *Colloids and Surfaces a-Physicochemical and Engineering Aspects, 270*, 138.

Shapiro, H.M.; *Practical Flow cytometry,* 4th Edition, John Wiley & Sons, United States of America, **2003**.

Sharma, A.; Sharma, U.S. (**1997**). Liposomes in drug delivery: Progress and limitations, *International Journal of Pharmaceutics, 154*, 123.

Simberg, D.; Danino, D.; Talmon, Y.; Minsky, A.; Ferrari, M.E.; Wheeler, C.J.; Barenholz, Y. (**2001**). Phase Behavior, DNA Ordering, and Size Instability of Cationic Lipoplexes, *Journal of Biological Chemistry, 276*, 47453.

Symietz, C.; Schneider, M.; Brezesinski, G.; Möhwald, H. (**2004**). DNA alignment at cationic lipid monolayers at the air/water interface, *Macromolecules, 37*, 3865.

Templeton, N.S.; Lasic, D.D.; Frederik, P.M.; Strey, H.H.; Roberts, D.D.; Pavlakis, G.N. (**1997**). Improved DNA: liposome complexes for increased systemic delivery and gene expression, *Nature Biotechnology, 15*, 647.

Tian, W.-d.; Ma, Y.-q. (**2009**). Molecular Dynamics Simulations of a Charged Dendrimer in Multivalent Salt Solution, *The Journal of Physical Chemistry B, 113*, 13161.

Tian, W.-d.; Ma, Y.-q. (**2010a**). Complexation of a Linear Polyelectrolyte with a Charged Dendrimer: Polyelectrolyte Stiffness Effects, *Macromolecules, 43*, 1575.

Tian, W.-d.; Ma, Y.-q. (**2010b**). Effects of valences of salt ions at various concentrations on charged dendrimers, *Soft Matter, 6*, 1308.

Tian, W.-d.; Ma, Y.-q. (**2011**). Coarse-grained molecular simulation of interacting dendrimers, *Soft Matter, 7*, 500.

Vorlíčková, M.; Kejnovská, I.; Bednářová, K.; Renčiuk, D.; Kypr, J. (**2012**). Circular Dichroism Spectroscopy of DNA: From Duplexes to Quadruplexes, *Chirality, 24*, 691.

Xu, Y.H.; Hui, S.W.; Frederik, P.; Szoka, F.C. (**1999**). Physicochemical characterization and purification of cationic lipoplexes, *Biophysical Journal, 77*, 341.

Zhu, L.; Mahato, R.I. (**2010**). Lipid and polymeric carrier-mediated nucleic acid delivery, *Expert Opinion on Drug Delivery, 7*, 1209.

Zuzzi, S.; Cametti, C.; Onori, G.; Sennato, S. (**2007**). Liposome-induced DNA compaction and reentrant condensation investigated by dielectric relaxation spectroscopy and dynamic light scattering techniques, *Physical Review E, 76*, 011925.

Chapter 5

Bolaamphiphile-based vectors

The prefix “bola” is associated to the shape of an old South American missile weapon that consists of two balls attached together by a cord. It was adopted by the science community to represent visually a molecule with two hydrophilic head groups linked by a hydrophobic carbon chain. There are few molecules in nature with these properties, however, most bolaamphiphiles are chemically synthesized (Baek, 2010; Fuhrhop, 1986). Bolaamphiphile molecules have their physical stability enhanced and they can be assembled into distinct structures that could be used as gene carriers (Jain, 2010). Bolaamphiphile molecules usually have two similar head groups, originating a symmetric monolayer vesicle. However, some bolaamphiphiles are constituted by two different head groups, a positively charged at one end and a neutral one at the other end, assembling into asymmetric monolayers. Both types of bolaamphiphile can be used as vesicles to encapsulate the active principle (Brunelle, 2009; Grinberg, 2010; Kaufman, 2013). There are many applications for these molecules and they can be used not only has components of lipid vesicles but also in nanocapsules that are prepared by the layer-by-layer self-assembly technique.

5.1. Bolaamphiphile particles

Bolaamphiphile molecules can be incorporated on particles through the deposition of layers with different charges by layer-by-layer technique (Figure 5.1). It consists on the use of a core particle, such as silicon oxide (SiO_2), calcium carbonate ($CaCO_3$) or polystyrene (PS). These cores are used to produce multi-layered films by layer-by-layer deposition of oppositely charged polymers (Shchukin, 2004; Zhao, 2006). After deposition of several layers (enough to allow the stability of the capsule) the core can be dissolved.

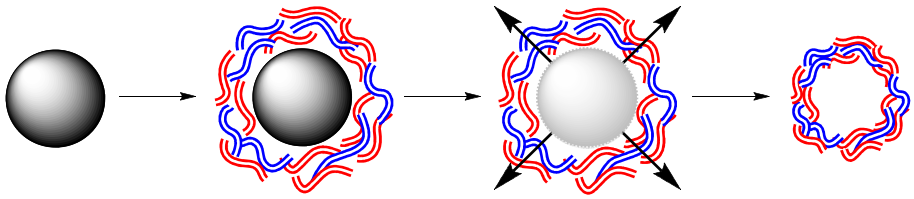

Figure 5.1. Schematic representation of the Layer-by-Layer process (Donath, 1998).

The resulting capsule will be smaller than the microparticle used in the process due to the shrinking of the species in the absence of the core. The active principle can be either entrapped or encapsulated within the carrier.

5.1.1. Materials and methods

5.1.1.1. Chemicals

The bolaamphiphile studied in this work, 22-hydroxy-*N*,*N*,*N*-trimethyldocosan-1-aminium (BA), was synthetized by Prof. Dr. Bodo Dobner's group (Institute of Pharmacy, Biochemical Pharmacy, Martin Luther University of Halle-Wittenberg, Halle an der Saale, Germany) and is shown in Figure 5.2.

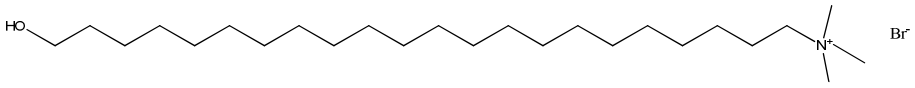

Figure 5.2. Chemical structure of 22-hydroxy-*N*,*N*,*N*-trimethyldocosan-1-aminium (BA).

Monodisperse polystyrene particles (4.1 ± 0.1 μm, negatively charged) in a 10 % w/v aqueous suspension were acquired from Microparticles GmbH and used as cores. DNA (deoxyribonucleic acid sodium salt from calf thymus, type I), sodium chloride (NaCl), PAH (Poly(allylamine hydrochloride), positively charged) and PSS (Poly(sodium 4-styrenesulfonate), negatively charged) were purchased from Sigma-Aldrich and used without further purification. Rhod PE (1,2-dipalmitoyl-sn-glycero-3-phosphoethanolamine-N-(lissamine rhodamine B sulfonyl), ammonium salt, MW 1249.65), was purchased from Avanti Polar Lipids, Inc. The deionized water was purified with Milli-Q apparatus with the specific resistance of 18.2 MΩ·cm. All solutions, except for DNA, were filtered through a 200 nm porous membrane. Chloroform was supplied by Merck.

5.1.1.2. LbL assembly

Solutions of PAH and PSS (5 mg/mL) were prepared in NaCl (0.5 M) aqueous solution. DNA was dissolved in deionized water at a concentration of 0.1 mg/mL and was kept at 4°C under magnetic stirring for at least 2 days to ensure complete dissolution. A volume of 100 µL of PS microparticles was retrieved from the stock solution and used for LbL deposition. The cores were washed with 1 mL of deionized water and centrifuged (Eppendorf centrifuge 5804 R, Eppendorf AG, Germany) at 8000 rpm, during 5 minutes. Then the supernatant was discarded and the particles were re-suspended in 1 mL of water. This procedure was repeated twice. Before the last centrifugation a sample of 20 µL of the re-suspended particles was collected to measure the electrophoretic mobility of the system. The washing process was repeated for each added layers, as standard method. The layers were deposited onto the PS cores in the following order: PAH (1) / PSS (2) / PAH (3) / DNA (4) / BA (5) / DNA (6) / BA (7). After addition of each polymer solution (1 mL) the suspension was kept at room temperature under sporadic manual agitation for 20 minutes following by at least 3 washing steps. Due to the nature of the lipid and its affinity to form vesicles in the presence of water, the addition of the BA layers was performed as follows. BA (0.1 mg) was first dissolved in chloroform, which was evaporated under gaseous N_2 to produce a lipid film (further details on section 4.1.2). The particles re-suspended in water were added to the lipid film. Due to the presence of the charged particles it is expected that the BA organizes itself around the microparticles, forming a new layer. To remove the BA from the glass surface of the vial, some manual agitation was promoted. It is important to avoid the vortex, since it can destroy the previous layers. At least 5 independent assays were performed, to ensure reproducibility.

5.1.1.3. Zeta potential

The electrophoretic mobility (section 4.1.4), converted into zeta potential (ZP, mV), of the microparticles was measured at room temperature with a Malvern Zetasizer Nano series instrument by laser Doppler velocimetry. The results were averaged from three measurements for each sample. The collected 20 µL of each sample was diluted into 1000 µL of deionized water to fill the cuvette volume.

5.1.1.4. Fluorescence spectroscopy

In order to assess the amount of DNA at the particle surface, the supernatant of the microparticles at which DNA layer was added was recovered after centrifugation. The unbound DNA was free to interact with ethidium bromide (EtBr) molecules emitting fluorescence (Cosa, 2001). A calibration curve was established considering the range of possible concentrations and allowed the quantification of the remaining DNA in solution. This way and with the knowledge of the initial concentration, it was possible to determine indirectly the concentration of DNA present at the particle surface. Detailed information about this technique can be found in section 4.1.5.

Steady-state fluorescence measurements were carried out using a Perkin-Elmer LS-50B luminescence spectrometer (REQUIMTE, Department of Chemistry, Faculty of Pharmacy, University of Porto). Ethidium bromide (EtBr, 5 mg/mL, 100 µL) was added to 500 µL of DNA solution, followed by the addition of deionised water up to 1000 µL. Fluorescence emission spectra were recorded between 560-700 nm at an excitation wavelength of 540 nm, emission and excitation band slits of 10 nm and scan rate of 400 nm/min.

5.1.1.5. Confocal Laser Scanning Microscopy (CLSM)

DNA and bolaamphiphile layers were stained for CLSM imaging (Leica TCS SP5 II, Leica Microsystems), detailed in section 4.1.10.2. The bolaamphiphile solution was previously mixed with 0.2% (w/w) of Rhod PE lipid (fluorescent marker) in chloroform, which was evaporated and the film was hydrated, in order to mix properly the two lipids in solution. This was used as marked layer to perform CLSM imaging. After placing a drop of the microparticles on a slide, a drop of DAPI solution was added to stain DNA layers.

5.1.2. Results and Discussion

The layer by layer deposition was assessed by zeta potential (ZP) measurements. PAH and PSS layers were used to provide stability to the shell once the core was removed. The use of NaCl promotes the electrostatic interactions between the charged layers by reducing the repulsion through charge screening (Caruso, 1999; Hall, 2011).

The ZP signal inversion suggests a successful deposition of the layers (Figure 5.3). DNA and BA solutions were prepared without NaCl since it induced sample aggregation.

The DNA concentration per layer was estimated to be 0.035 ± 0.005 mg/mL (the initial DNA concentration was 0.1 mg/mL). These results were reproducible. The last layer must be of BA to protect the DNA layers from degradation.

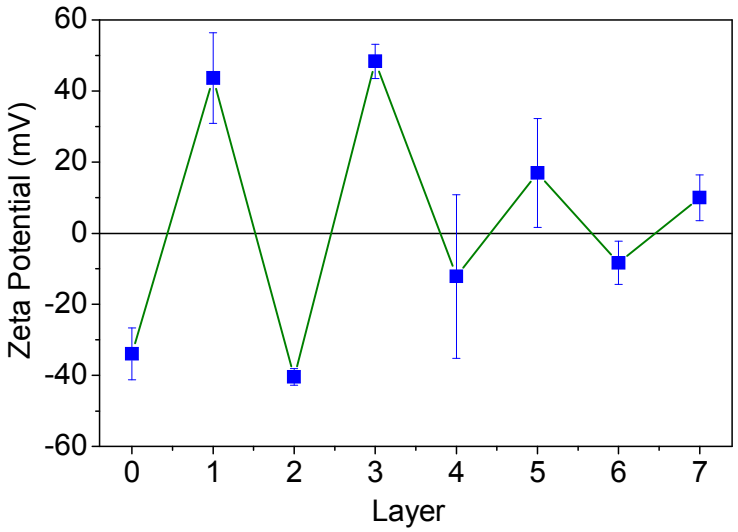

Figure 5.3. Zeta potential of the successive layers added to the PS cores by the LbL technique.

CLSM technique allows to acquiring fluorescence images for the different dyes and separating them to be sure that the colour derives from the specific marker. Images taken from different microparticle samples show the presence of DNA and BA layers (Figure 5.4). The blue staining by DAPI solution confirms the presence of DNA. DAPI binds strongly to A-T rich regions of the DNA molecules and emits light when excited with ultraviolet light (Kapuscinski, 1995). The red colour observed in the images is due to the presence of Rhodamine labelled PE lipid. This lipid mixes with the bolaamphiphile molecules in the bilayer, allowing the visualization through fluorescence spectroscopy. Images in transmission mode were also collected to confirm that all particles were stained.

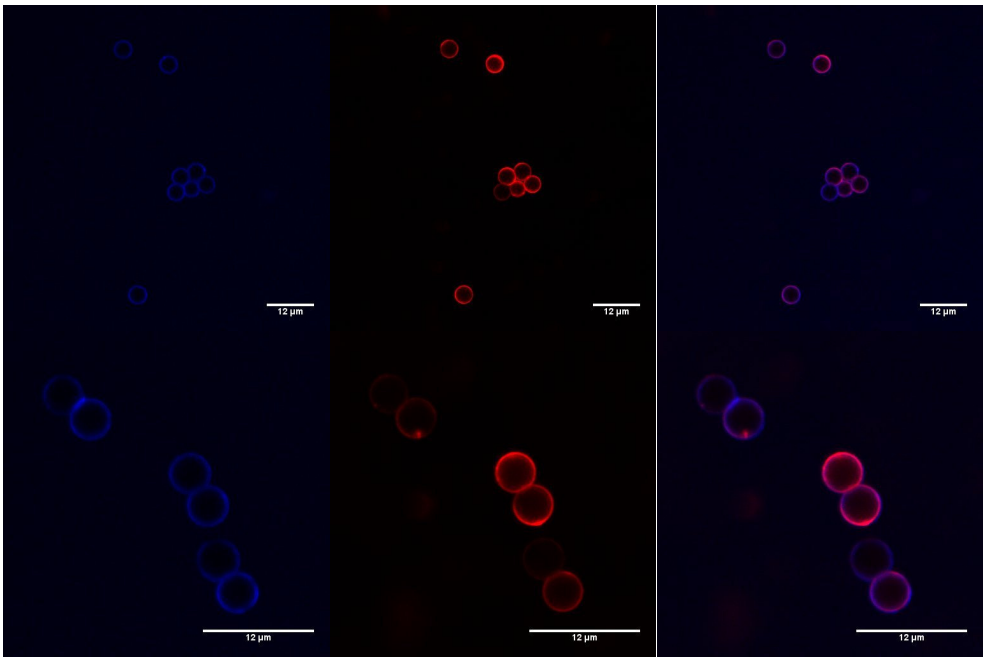

Figure 5.4. CLSM images of multilayered microparticles with PS cores showing the presence of DNA (Blue chanel - left), BA layer (red chanel - center) and the sobreposition of both chanels (right). Scale bar is 12 µm.

5.1.3. Conclusions

The layer-by-layer assembly is one of the many techniques used in the fabrication of particles for gene delivery. Here we described a new system that intercalates layers of DNA molecules and a new bolaamphiphile. The zeta potential variation gives an indication of the layer deposition through the signal change from positive to negative values, according to the charge of the polymer that is deposited at the particle surface. Further tests were carried

out to ensure the presence of DNA within the layers as well the presence of the bolaamphiphile. CLSM images confirm the uniform presence of both compounds at the particle surface. It is possible to remove the cores of these systems in order to obtain a microcapsule. The layers can also be assembled using smaller cores to facilitate the internalisation of the particles by the cells.

5.2. Lipid vesicles

Bolaamphiphile molecules can self-assemble into monolayered or bilayered vesicles, due to their two hydrophilic head groups. These molecules can also be part of a mixture of lipids to improve the properties of the vesicles for DNA transfection.

5.2.1. Materials and methods

5.2.1.1. Chemicals

DOTAP and Rhod PE (1,2-dipalmitoyl-sn-glycero-3-phosphoethanolamine-N-(lissamine rhodamine B sulfonyl), ammonium salt, MW 1249.65) were purchased from Avanti Polar Lipids, Inc. Hepes buffer (4-(2-Hydroxyethyl) piperazine-1-ethanesulfonic acid, ≥ 99.5%) was supplied by Sigma-Aldrich. The green fluorescent protein (GFP) plasmid (pEGFP-N1, BD Biosciences Clontech) encoded for green fluorescent protein, hereafter designed by pDNA, was amplified and isolated with a PlasmidPrep Midi Flow kit (GE Healthcare) and the concentration and purity of pDNA were assessed using a NanoDrop 1000 (Thermo Scientific) apparatus. The deionised water was purified with Milli-Q apparatus with the specific resistance of 18.2 MΩ·cm. Chloroform was from Merck.

5.2.1.2. Preparation of Liposomes

Liposomes were prepared by the thin lipid film hydration method (Palmerini, 2006). Briefly, the appropriate lipid mixture (BA:DOTAP) at different molar ratios was dissolved in chloroform, which was then evaporated under N_2 flow. The lipid film was hydrated with 1 mL of 10 mM Hepes buffer pH 7.4 (ionic strength 0.00325 M). The suspension was vortexed for 15 minutes, sonicated for 15 min at 60°C and extruded through Whatman filters of decreasing pore sizes (up to 100 nm pore size membranes) using a pressure extruder apparatus, at 60°C. The total lipid concentration was 1 mM.

5.2.1.3. DLS and electrophoretic mobility

The hydrodynamic diameter (section 4.1.3) and the electrophoretic mobility (section 4.1.4), μ_e, of liposomes and lipoplexes were measured at room temperature with a Malvern Zetasizer Nano series instrument by, respectively, dynamic light scattering (DLS) and laser doppler velocimetry. The results were averaged from three measurements for each sample and were obtained for at least three independent procedure of sample preparation. The final concentration of liposomes was 0.1 mg/mL and the concentration of pDNA was 0.01 mg/mL.

5.2.1.4. Morphology studies

To characterise the type of structures formed by the bolaamphiphile alone, Transmission Electron Microscopy (TEM) and Confocal Laser Scanning Microscopy (CLSM) were used (described in section 4.1.6 and 4.1.10.2, respectively). For the TEM (Jeol JEM-1400, JEOL) analysis, a drop of the

suspension was placed on copper grids (Formvar/carbon on 400 mesh – Agar) and stained with 2% (w/v) uranyl acetate. For CLSM imaging (Leica TCS SP5 II, Leica Microsystems) the BA was mixed with 0.2% of Rhod PE lipid (fluorescent marker).

5.2.1.5. *In vitro* transfection studies

The gene transfer and transgene expression after cellular transfection was monitored using pDNA encoded with GFP. HEK 293 cell line was used in this study and was grown in Minimum Essential Medium (Lonza), supplemented with 10% (v/v) heat inactivated fetal bovine serum (FBS – Gibco), 2 mM L-Glutamine (Lonza), 100U Penicillin/Streptomycin (Gibco) and 1% MEM non-essential amino acid solution (Sigma). Cells were cultured in a humidified 5% CO_2 atmosphere at 37°C. For transfection studies, cells were seeded at approximately 70% confluence in 12-well tissue culture plates, 24 h before the experiments. Before transfection, growth medium was removed and cells were washed twice with PBS, pH 7.4. Liposome-pDNA complexes were prepared by adding equal volumes of pDNA solution at 0.01 mg/mL to the liposome suspension. The lipid:pDNA ratio was 10:1 (w:w), corresponding to a N:P ratio of 5 for BA:DOTAP liposomes (charge ratio between the cationic groups (amine) of the liposome and the anionic groups (phosphate) of the pDNA) (Crook, 1998; Jain, 2012; Paiva, 2013). DNA solution was added drop wise to the liposomes and the mixture was kept under magnetic stirring for at least 15 minutes. Cells were then incubated with 200 µL of lipoplexes prepared with liposomes and pDNA in OPTI-MEM (Gibco). The final concentration of pDNA was 2 µg/well. The negative control corresponded to cells treated with liposomes without pDNA. After 5 h, the medium was replaced by fresh growth medium and transfection was assessed after 48 h

incubation time by flow cytometry (FACS Canto II, BD Biosciences), detailed in section 4.1.10.1. Twenty thousand events were measured for each sample. Experimental data was statistically analysed applying one-way analysis of variance (ANOVA) following Tukey test approach. Microscopy images of transfected cells were obtained using the CLSM.

5.2.2. Results and Discussion

5.2.2.1. Vesicle characterisation

The properties associated to bolaamphiphiles are very promising with respect to delivery systems (Nuraje, 2012). Attempts of extruding samples containing only BA were not successful, even at high temperatures (~100°C). The size measurements revealed a very poly-dispersed population with mean diameters of 5 ± 2 μm. CLSM and TEM analysis show that BA forms microstructures, some of which present a crystal shape (Figure 5.5). Crystal structures are expected when the size of the two polar groups is not too different. For instance, they could assemble into a bilayer, where the OH- groups will be oriented to the inner space and the N- groups to the outer space (Figure 2.2.a). Also, they may form a mixed orientation where will be a OH- group and a N- group in the inner space, as visible on Figure 2.2.b (Fuhrhop, 2004).

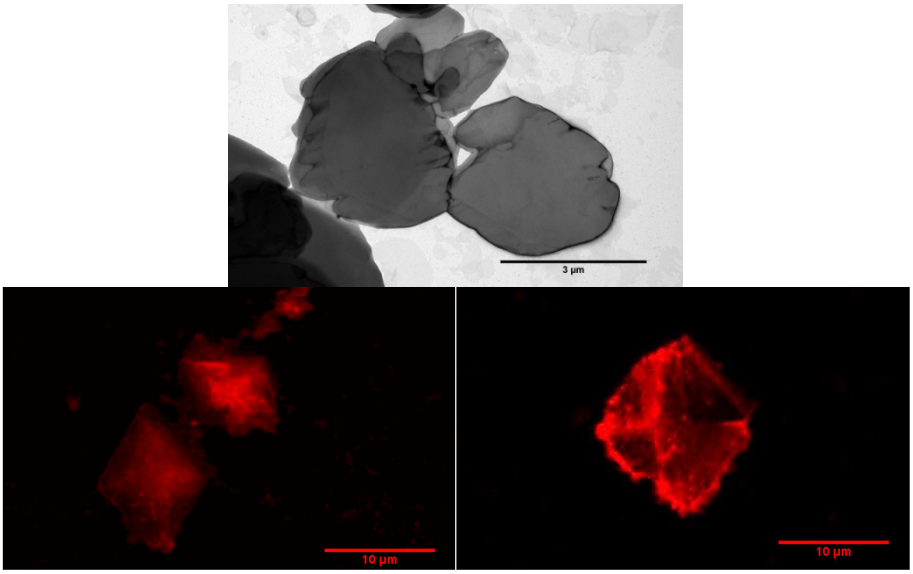

Figure 5.5. Self-assembled bolaamphiphile structure observed by TEM (top) and CLSM (bottom). Scale bar is, respectively, 3 and 10 µm.

Previous works report that these amphiphiles self-assemble into small nanoparticles (50-100 nm) (Jain, 2012; Popov, 2010), suggesting a formation of an asymmetric monolayer, which was confirmed by Langmuir monolayer studies and Grazing incidence X-Ray diffraction (Berchel, 2009; Deleu, 2011; Dolle, 2011; Hutter, 2012). However these structures are influenced by the number of carbons in the hydrophobic part of the molecule as well as the forces present in the hydrophilic part. The hydrophobic tail of the BA has no double bonds, which would allow the formation of vesicles with a monolayer of lipid, where the OH-end group would be directed to the inside of the vesicle and the N group to the outside. Due to its long carbon chain, the BA could also rearrange itself in a U-shape, also reported in the literature for similar molecules (Meister, 2007; Yan, 2009). In this case, a bilayer would be

formed and its structure could be more rigid, generating bigger particles that would not respond so well to the extrusion method due to its assembly. Mixing this BA with other lipids at appropriate ratios could help the formation of large unilamellar vesicles (LUV), where the BA could be intercalated with the other lipids.

The BA was mixed with a well-known and commonly used cationic lipid, DOTAP (Zhu, 2010), at BA:DOTAP molar ratios of 1:1, 1:5 and 1:10. For the ratio 1:1, it was not possible to carry out extrusion of the sample. The size of the structures was smaller than that obtained for the BA alone (Figure 5.6).

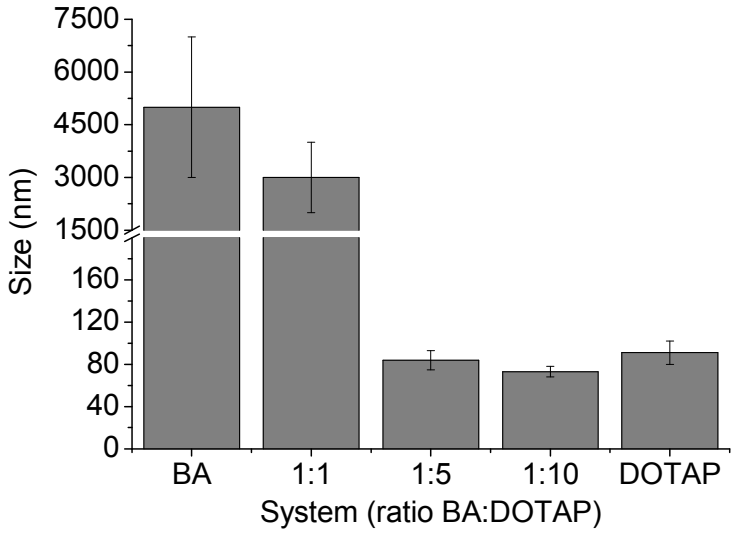

Figure 5.6. Hydrodynamic diameter of vesicles of BA, DOTAP and their mixture at different molar ratios.

At the molar ratios of 1:5 and 1:10, BA:DOTAP vesicles were extruded and it was possible to obtain large unilamellar vesicles using filters of pore size of 100 nm. Due the similarity of the results for the two ratios, vesicles prepared with BA:DOTAP at 1:5 molar ratios were chosen for further studies

using cell cultures. In the literature, mixtures of bolaamphiphiles with other lipids, such as cholesterol (Dakwar, 2012) and DOPE (Jain, 2012) have been reported, mainly to stabilise the liposomes when they are complexed with pDNA. Since the BA does not self-assemble into small vesicles, DOTAP was chosen due its charge, which will help the formation of stable nanoparticles even when they are complexed with pDNA. Zeta potential of the vesicles was measured for the formulations in study (Figure 5.7).

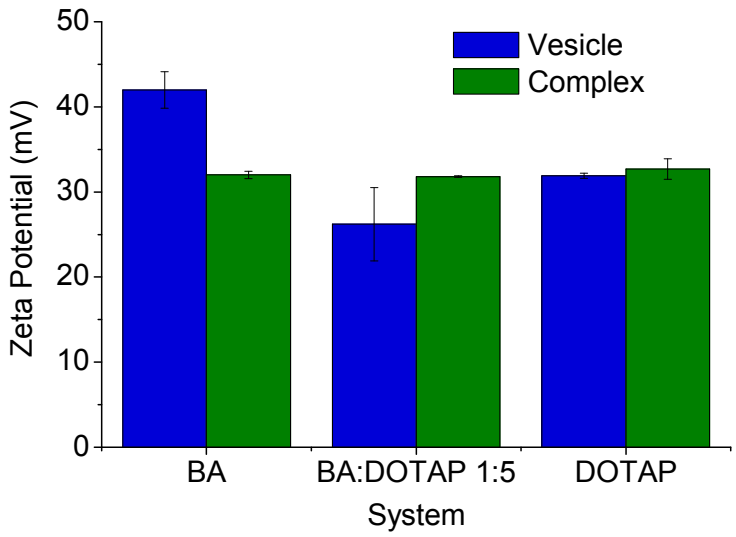

Figure 5.7. Zeta potential values for the studied formulations, before and after complexation.

The complex formation with DNA was observed at the ratio of lipid:pDNA 10:1 (w:w) (Paiva, 2013). To assess the stability of the system, zeta potential measurements were conducted with and without pDNA. Size measurements of the liposomes and the lipoplexes revealed similar values of that obtained for the liposomes alone, however, the pDNA has an effect on the population distribution reduces the polydispersity index (PdI) of the

sample. Zeta potential values were also obtained for the formulations and showed were around 32 mV for all preparations (Figure 5.7). This parameter indicates that all lipoplexes are stable and positively charged, which is a condition desirable for cell transfections studies (Jesorka, 2008; Lonez, 2008).

5.2.2.2. Cell transfection studies

The transfection efficiency of lipoplexes was evaluated using HEK 293 cell line, a human embryonic kidney derived cell line. Cells were transfected with plasmid DNA (pDNA) encoding green fluorescent protein (GFP). Flow cytometry analysis revealed that GFP expression was induced similarly by DOTAP/pDNA and BA:DOTAP/pDNA (Figure 5.8.A). Naked pDNA did not transfect the cells (Figure 5.8.B). DOTAP has been proven to be an efficient and wide used system to complex, deliver and transfect DNA into, for example, human hematopoietic stem cells (Martino, 2009) and cervical cancer cells (Fletcher, 2005). Combined with other lipids, like cholesterol, DOTAP has been studied *in vivo* and shown to be efficient in transporting genetic material to cells (Eliyahu, 2007; Kim, 2007; Ramesh, 2001; Templeton, 1997). These results show that the BA mixed with DOTAP at the molar ratio of 1:5, has potential as vehicle for pDNA delivery, evidencing good results with respect to the DOTAP system. It was observed for all cell trials that BA:DOTAP system achieved higher values than DOTAP system. However and according to the statistical analysis, the transfection values are not significantly different at the 0.05 level, indicating that both systems have a similar ability to transfect cells. The cytometry technique and confocal analysis showed that DOTAP lipoplexes cause more cellular dead than BA:DOTAP lipoplexes, indicating that this system is less cytotoxic.

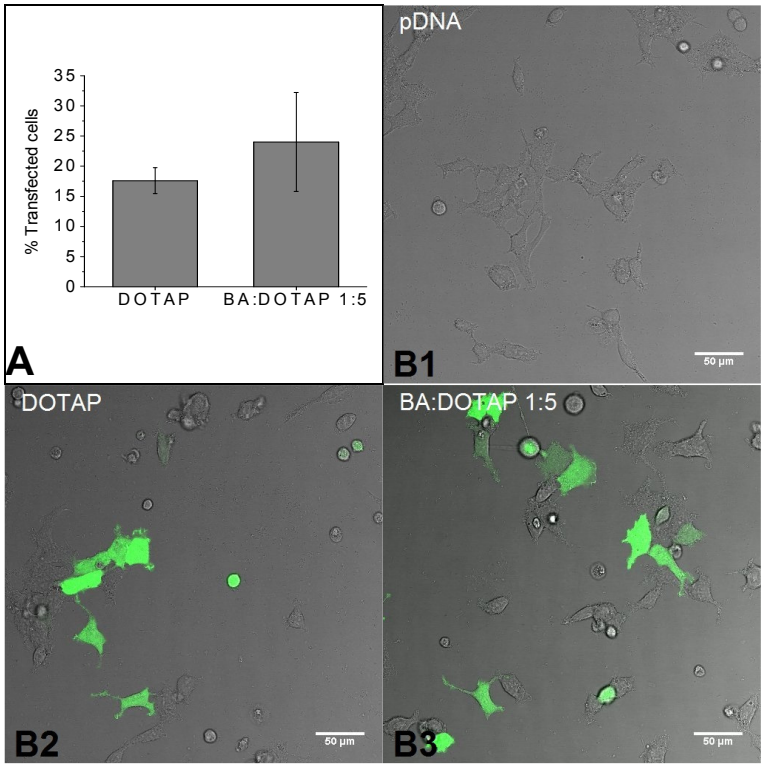

Figure 5.8. Transfection of HEK cell line with green fluorescent protein (GFP) plasmid (pDNA) at 10:1 L/D ratio: (A) cytometry analysis of transfection levels for DOTAP and BA:DOTAP 1:5 systems. Results are expressed as mean ± S.D. (n=3). (B) Illustrative confocal images of GFP expression when transfected with naked pDNA (B1), DOTAP (B2) and BA:DOTAP 1:5 (B3). The scale bar is 50 µm.

5.2.3. Conclusions

We propose vesicles that combine a bolaamphiphile with cationic lipids to form stable and positively charged liposomes capable of compacting efficiently genetic material by electrostatic interactions. Comparing the carrier

made of BA:DOTAP 1:5 with DOTAP vesicles, they present similar properties with respect to size and zeta potential values. The transfection studies show that the bolaamphiphile mixed system has a higher transfection potential when compared to DOTAP vesicles.

5.3. References

Baek, K.; Kim, Y.; Kim, H.; Yoon, M.; Hwang, I.; Ko, Y.H.; Kim, K. (**2010**). Unconventional U-shaped conformation of a bolaamphiphile embedded in a synthetic host, *Chemical Communications, 46*, 4091.

Berchel, M.; Mériadec, C.; Lemiègre, L.; Artzner, F.; Jeftic, J.; Benvegnu, T. (**2009**). Supramolecular structures based on new bolaamphiphile molecules investigated by small angle and wide angle X-ray scattering and polarized optical microscopy, *Journal of Physical Chemistry B, 113*, 15433.

Brunelle, M.; Polidori, A.; Denoyelle, S.; Fabiano, A.S.; Vuillaume, P.Y.; Laurent-Lewandowski, S.; Pucci, B. (**2009**). A structure-activity investigation of hemifluorinated bifunctional bolaamphiphiles designed for gene delivery, *Comptes Rendus Chimie, 12*, 188.

Caruso, F.; Lichtenfeld, H.; Donath, E.; Möhwald, H. (**1999**). Investigation of Electrostatic Interactions in Polyelectrolyte Multilayer Films: Binding of Anionic Fluorescent Probes to Layers Assembled onto Colloids, *Macromolecules, 32*, 2317.

Cosa, G.; Focsaneanu, K.S.; McLean, J.R.N.; McNamee, J.P.; Scaiano, J.C. (**2001**). Photophysical Properties of Fluorescent DNA-dyes Bound to Single- and Double-stranded DNA in Aqueous Buffered Solution, *Photochemistry and Photobiology, 73*, 585.

Crook, K.; Stevenson, B.J.; Dubouchet, M.; Porteous, D.J. (**1998**). Inclusion of cholesterol in DOTAP transfection complexes increases the delivery

of DNA to cells in vitro in the presence of serum, *Gene Therapy, 5*, 137.

Dakwar, G.R.; Hammad, I.A.; Popov, M.; Linder, C.; Grinberg, S.; Heldman, E.; Stepensky, D. (**2012**). Delivery of proteins to the brain by bolaamphiphilic nano-sized vesicles, *Journal of Controlled Release, 160*, 315.

Deleu, M.; Damez, C.; Gatard, S.; Nott, K.; Paquot, M.; Bouquillon, S. (**2011**). Synthesis and physico-chemical characterization of bolaamphiphiles derived from alkenyl d-xylosides, *New Journal of Chemistry, 35*, 2258.

Dolle, C.; Magrone, P.; Riva, S.; Ambrosi, M.; Fratini, E.; Peruzzi, N.; Nostro, P.L. (**2011**). Symmetric and asymmetric bolaamphiphiles from ascorbic acid, *Journal of Physical Chemistry B, 115*, 11638.

Donath, E.; Sukhorukov, G.B.; Caruso, F.; Davis, S.A.; Mohwald, H. (**1998**). Novel hollow polymer shells by colloid-templated assembly of polyelectrolytes, *Angewandte Chemie-International Edition, 37*, 2202.

Eliyahu, H.; Joseph, A.; Schillemans, J.P.; Azzam, T.; Domb, A.J.; Barenholz, Y. (**2007**). Characterization and in vivo performance of dextran-spermine polyplexes and DOTAP/cholesterol lipoplexes administered locally and systemically, *Biomaterials, 28*, 2339.

Fletcher, S.; Ahmad, A.; Perouzel, E.; Heron, A.; Miller, A.D.; Jorgensen, M.R. (**2005**). In Vivo Studies of Dialkynoyl Analogues of DOTAP Demonstrate Improved Gene Transfer Efficiency of Cationic Liposomes in Mouse Lung, *Journal of Medicinal Chemistry, 49*, 349.

Fuhrhop, J.-H.; Wang, T. (**2004**). Bolaamphiphiles, *Chemical Reviews, 104*, 2901.

Fuhrhop, J.H.; Fritsch, D. (**1986**). Bolaamphiphiles form ultrathin, porous and unsymmetric monolayer lipid membranes, *Accounts of Chemical Research, 19*, 130.

Grinberg, S.; Kipnis, N.; Linder, C.; Kolot, V.; Heldman, E. (**2010**). Asymmetric bolaamphiphiles from vernonia oil designed for drug delivery, *European Journal of Lipid Science and Technology, 112*, 137.

Hall, K.; Lee, T.-H.; Aguilar, M.-I. (**2011**). The role of electrostatic interactions in the membrane binding of melittin, *Journal of Molecular Recognition, 24*, 108.

Hutter, T.; Linder, C.; Heldman, E.; Grinberg, S. (**2012**). Interfacial and self-assembly properties of bolaamphiphilic compounds derived from a multifunctional oil, *Journal of Colloid and Interface Science, 365*, 53.

Jain, N.; Arntz, Y.; Goldschmidt, V.r.; Duportail, G.; Mély, Y.; Klymchenko, A.S. (**2010**). New Unsymmetrical Bolaamphiphiles: Synthesis, Assembly with DNA, and Application for Gene Delivery, *Bioconjugate Chemistry, 21*, 2110.

Jain, N.; Goldschmidt, V.; Oncul, S.; Arntz, Y.; Duportail, G.; Mély, Y.; Klymchenko, A.S. (**2012**). Lactose-ornithine bolaamphiphiles for efficient gene delivery in vitro, *International Journal of Pharmaceutics, 423*, 392.

Jesorka, A.; Orwar, O. (**2008**). Liposomes: Technologies and Analytical Applications, *Annual Review of Analytical Chemistry, 1*, 801.

Kapuscinski, J. (**1995**). DAPI: A DNA-specific fluorescent probe, *Biotechnic and Histochemistry, 70*, 220.

Kaufman, Y.; Grinberg, S.; Linder, C.; Heldman, E.; Gilron, J.; Freger, V. (**2013**). Fusion of bolaamphiphile micelles: A method to prepare stable supported biomimetic membranes, *Langmuir, 29*, 1152.

Kim, J.Y.; Choung, S.; Lee, E.J.; Kim, Y.J.; Choi, Y.C. (**2007**). Immune activation by siRNA/liposome complexes in mice is sequence- independent: Lack of a role for toll-like receptor 3 signaling, *Molecules and Cells, 24*, 247.

Lonez, C.; Vandenbranden, M.; Ruysschaert, J.-M. (**2008**). Cationic liposomal lipids: From gene carriers to cell signaling, *Progress in Lipid Research, 47*, 340.

Martino, S.; di Girolamo, I.; Tiribuzi, R.; Angelo, F.; Datti, A.; Orlacchio, A. (**2009**). Efficient siRNA Delivery by the Cationic Liposome DOTAP in Human Hematopoietic Stem Cells Differentiating into Dendritic Cells, *Journal of Biomedicine and Biotechnology,* DOI: 10.1155/2009/410260.

Meister, A.; Weygand, M.J.; Brezesinski, G.; Kerth, A.; Drescher, S.; Dobner, B.; Blume, A. (**2007**). Evidence for a Reverse U-Shaped Conformation of Single-Chain Bolaamphiphiles at the Air−Water Interface, *Langmuir, 23*, 6063.

Nuraje, N.; Bai, H.; Su, K. (**2012**). Bolaamphiphilic molecules: Assembly and applications, *Progress in Polymer Science, 38*, 302.

Paiva, D.; Martin-Molina, A.; Cardoso, I.; Quesada-Perez, M.; Pereira, M.D.; Rocha, S. (**2013**). The effect of a fluorinated cholesterol derivative on the stability and physical properties of cationic DNA vectors, *Soft Matter, 9*, 401.

Palmerini, C.A.; Cametti, C.; Sennato, S.; Gaudino, D.; Carlini, E.; Bordi, F.; Arienti, G. (**2006**). Role of cholesterol, DOTAP, and DPPC in prostasome/spermatozoa interaction and fusion, *Journal of Membrane Biology, 211*, 185.

Popov, M.; Linder, C.; Deckelbaum, R.J.; Grinberg, S.; Hansen, I.H.; Shaubi, E.; Waner, T.; Heldman, E. (**2010**). Cationic vesicles from novel bolaamphiphilic compounds, *Journal of Liposome Research, 20*, 147.

Ramesh, R.; Saeki, T.; Templeton, N.S.; Ji, L.; Stephens, L.C.; Ito, I.; Wilson, D.R.; Wu, Z.; Branch, C.D.; Minna, J.D.; Roth, J.A. (**2001**). Successful treatment of primary and disseminated human lung cancers by

systemic delivery of tumor suppressor genes using an improved liposome vector, *Molecular Therapy, 3*, 337.

Shchukin, D.G.; Patel, A.A.; Sukhorukov, G.B.; Lvov, Y.M. (**2004**). Nanoassembly of Biodegradable Microcapsules for DNA Encasing, *Journal of the American Chemical Society, 126*, 3374.

Templeton, N.S.; Lasic, D.D.; Frederik, P.M.; Strey, H.H.; Roberts, D.D.; Pavlakis, G.N. (**1997**). Improved DNA: liposome complexes for increased systemic delivery and gene expression, *Nature Biotechnology, 15*, 647.

Yan, Y.; Lu, T.; Huang, J. (**2009**). Recent advances in the mixed systems of bolaamphiphiles and oppositely charged conventional surfactants, *Journal of Colloid and Interface Science, 337*, 1.

Zhao, W.; Zheng, B.; Haynie, D.T. (**2006**). A Molecular Dynamics Study of the Physical Basis of Stability of Polypeptide Multilayer Nanofilms, *Langmuir, 22*, 6668.

Zhu, L.; Mahato, R.I. (**2010**). Lipid and polymeric carrier-mediated nucleic acid delivery, *Expert Opinion on Drug Delivery, 7*, 1209.

Chapter 6

Chitosan-*N*-maltodextrin conjugates

Grafting other polymers to chitosan has been used as an alternative technique to improve its properties with respect to cell uptake and release. To further explore this methodology, the synthesis and characterisation of a polymer based on chitosan and maltodextrin (MD) were carried out. Maltodextrin, an oligosaccharide, is a non-ionic excipient of D-glucose units linked by α(1-4) glycosidic bonds that enhances gene expression and has low toxicity (Huang, 2002). Maltodextrins are water soluble compounds and are produced by partial hydrolysis of starch. They are classified in terms of DE (dextrose equivalent), having between 3 and 20 DE. The conjugation of chitosan with maltodextrin (DE 18-20) was achieved by reductive amination and the resultant copolymer was characterised by Fourier-transform infrared spectroscopy (FTIR) and nuclear magnetic resonance spectroscopy (NMR). Nanoparticles of chitosan-graft-maltodextrin copolymer were analysed by dynamic light scattering and electron microscopy techniques.

6.1. Experimental Section

6.1.1. Chemicals

Chitosan (Ch) 20 kDa (degree of deacetylation > 92%) was supplied by Altakitin (Portugal). DNA (deoxyribonucleic acid sodium salt from calf thymus, type I), acetic acid, sodium cyanoborohydride and sodium tripolyphosphate (TPP) were purchased from Sigma and Maltodextrin (DE 18-20) was from Grain Processing Corporation. All reagents were used without further purification. Ultrapure water was obtained using a Milli-Q apparatus with the specific resistance of 18.2 MΩ·cm. Uranyl acetate was purchased from Electron Microscopy Sciences.

6.1.2. Synthesis of chitosan-*graft*-maltodextrin

The synthesis of the graft copolymer is based on reductive amination (Janciauskaite, 2008; Kaneko, 2007; Park, 2001). Chitosan 20 kDa was dissolved in 1% acetic acid, followed by the addition of maltodextrin solution, according to the molar ratio of chitosan glucosamine units and maltodextrin of 1:1 (Ch_n:MD 1:1) and 1:5 (Ch_n:MD 1:5). Sodium cyanoborohydride (molar ratio 10:1 with respect to maltodextrin) was added to the mixture under magnetic stirring. The reaction was carried out for 4 days at 40°C under stirring. The unreacted maltodextrin was removed by dialysis for 4 days using Float-A-Lyzer G2 (Spectrum) dialysis membrane (MWCO 3.5-5 kDa) against ultrapure water. The reaction product (chitosan:maltodextrin 1:1 or 1:5) was lyophilised at -80°C using a Virtis BT6K EL lyophiliser.

6.1.3. Fourier-transform infrared (FTIR) spectroscopy

The infrared spectroscopy measures the frequency of the vibrations of chemical bonds between atoms when occurs excitation, at the medium infrared (4 000 to 200 cm^{-1}) electromagnetic spectrum (Reichenbächer, 2012). The absorption frequencies of radiation depend on the functional groups present and the configuration of the atoms in the molecule. The infrared vibrational spectrum of a molecule consists of a sequence of bands, each of which results from a transition between pairs of vibrational levels related to the ground electronic state (Ramachandran, 2001).

The main goal of an infrared experiment is to determine the intensity ratio between the transmitted radiation by the sample (I) and the incident radiation (I_0) as a function of the frequency of the light:

$$T_r = \frac{I}{I_0} \tag{6.1}$$

where T_r is the transmittance (Ebnesajjad, 2006). The infrared spectrum is usually plotted as a function of transmittance or absorbance. The absorbance (Abs) is related to the transmittance by the Lambert-Beer Law:

$$Abs = -\log T_r = \varepsilon_a lc \tag{6.2}$$

where ε_a is the molar absorptivity at the measured frequency, c is the concentration of chemical bonds responsible for the absorption of infrared radiation and l is the optical path length (Evans, 1992).

FTIR spectroscopy is a multiplexing spectroscopy, where all optical frequencies from the source are observed simultaneously over a period of time. The resulting signal, which is a time domain digital signal, is called an interferogram and contains intensity information about all frequencies present in the infrared beam. This information can be extracted by switching

the signal from a time domain digital signal to a frequency domain digital signal, which is accomplished by applying a Fourier transform over the interferogram (frequency-domain functions) (Griffiths, 2007).

The infrared spectra were recorded using an ALPHA FTIR spectrometer (Bruker) in absorbance mode with a high sensitivity DLATGS detector at room temperature. Pellets of potassium bromide (KBr) with 1% (w:w) were prepared and pressed at a pressure point of 10 000 g.

6.1.4. Nuclear magnetic resonance (NMR) spectroscopy

Nuclear magnetic resonance spectroscopy is based on the magnetic properties of the atomic nucleus and, therefore, is a non-invasive and non-destructive technique. This technique provides information about the molecule structure and bonds through the interaction between the magnetic moments of the sample nuclei and an applied electromagnetic wave (Schnell, 2001).

NMR is a quantum phenomenon based on the magnetic properties of atoms nuclei. Subatomic particles (protons, neutrons and electrons) have the intrinsic quantum property of spin. Atoms with no overall spin (^{12}C, ^{16}O) have electrons pair up in atomic orbitals, meaning that the electron energy cancel each other. However atoms where their electrons cannot pair up (^{1}H, ^{13}C, ^{19}F, ^{31}P) will have magnetic moments (μ) and, consequently, will possess an overall spin (I). The nuclear magnetic moment of the nucleus will line up with the externally applied magnetic field of strength B_0 (Becker, 2000). The NMR method introduces into the system a beam of electromagnetic radiation that will induce in the nucleus a transition from a lower state of energy to a higher one. The nuclei will be distributed throughout the various spin states available

and the number of nuclei (*N*) in each spin state can be determined by the Boltzmann distribution:

$$\frac{N_{upper}}{N_{lower}} = e^{-\gamma_m h B_0 / k_B T} \quad (6.3)$$

where γ_m is the magnetogyric ratio, h is the Planck constant, B_0 is the external magnetic field strength, k_B is the Boltzmann constant and T refers to the temperature (Becker, 2000).

Hydrogen atoms are present in most of the molecules and its nucleus has one of the strongest resonances, thus the applicability of ^{1}H NMR is vast. Two kinds of information are retrieved from the analysis of a NMR spectrum. Identical nuclei have different absorption positions if they have different chemical surroundings, meaning that one atom can be located by studying their position and the closest atoms. The different absorption peaks usually are denominated as chemical shifts. The second information retrieved from the spectra relates with the peak area. For the same type of nuclei (with the same chemical shift) it is possible to predict the number of nuclei since it is proportional to the area of the absorption peak in study (Gerothanassis, 2002). Carbon isotopes (^{12}C and ^{13}C) are also used to retrieve information about the atoms distribution in one molecule, although it is far less sensitive when compared to ^{1}H NMR. ^{13}C spectra have a separate resonance peak for each chemical shift, due to the characteristics of the proton nuclei, that has a precise chemical shift dependent on the attached atoms and their electronegativity. This way, ^{13}C spectra have a very low overlapping of the resonance peaks (Günther, 1994).

The NMR spectra were recorded on a Bruker Avance III 400, operating at 400.15 MHz for protons and 100.62 MHz for carbons, in deuterium oxide (D_2O) solution at a temperature of 25°C and 80°C. To improve the solubility of Ch, few drops of trifluoroacetic acid were added to the solution. The chemical shifts in the spectra were referenced to internal sodium trimethylsilyl-[2,2,3,3-

d_4]-propionate (TSP). Standard 1D ^1H NMR experiments with 30° pulses, acquisition time 2 s, relaxation delay 2 s, 64 transients of a spectral width of 4000 Hz were collected into 32 K time domain points. Two-dimensional (2D) $^1H/^1H$ correlation spectra (COSY), $^1H/^1H$ total correlation spectra (TOCSY), gradient-selected $^1H/^{13}C$ heteronuclear single quantum coherence (HSQC) and $^1H/^{13}C$ heteronuclear multiple bond coherence (HMBC) spectra were acquired using the standard Bruker software. 2D $^1H/^1H$ COSY spectra were acquired with a multiple quantum filter, gradient pulses for selection, a gradient ratio of 16:12:40 and a relaxation delay of 1.5 s. A total of 2048 data points in F2 and 512 data points in F1 over a spectral width of 4000 Hz were collected. The $^1H/^1H$ TOCSY spectra were recorded by use of homo-nuclear Hartman-Hahn transfer and dipsi2 sequence for proton–proton transfer, with a mixing time of 60 ms (Cavanagh, 1990). A total of 4096 data points in F2 and 512 data points in F1 over a spectral width of 4000 Hz were collected. $^1H/^{13}C$ HSQC experiments via double inept transfer, using sensitivity improvement and decoupling during the acquisition were carried out with a spectral width of *ca*. 4000 Hz for ^1H and 10000 Hz for ^{13}C, a relaxation delay of 1.5 s, FT size 2 K × 256 W. $^1H/^{13}C$ HMBC spectra with a spectral width of 12000 Hz in the carbon dimension and 4000 Hz in the proton dimension were recorded and typical acquisition parameters: 90° pulses for protons and carbons, 7 µs and 12.5 µs, respectively, a relaxation delay of 1.5 s, 512 increments and an FT size of 2 K x 1 K.

6.1.5. Preparation of nanoparticles

Chitosan and chitosan-*graft*-maltodextrin nanoparticles were prepared with sodium tripolyphosphate (TPP). All solutions were prepared in 0.3% acetic acid solutions to ensure complete dissolution of chitosan. Nanoparticles

were obtained by adding the TPP solution drop wise to the chitosan or copolymer solutions under magnetic stirring for about 15 minutes at room temperature. Solutions with a desirable volume were mixed to have the final concentrations of 1.00 and 1.25 mg/mL of chitosan or chitosan-*graft*-maltodextrin, and 0.20 and 0.25 mg/mL of TPP; the volume ratio of initial solutions of chitosan/TPP was 2.5.

6.1.6. Preparation of polyplexes

Complexes of chitosan or chitosan-*graft*-maltodextrin nanoparticles and DNA were prepared at different mass ratios of polymer/DNA ranging from 0.25 to 5. The DNA concentration was kept constant for all assays (0.025 mg/mL). Stock solutions of the polymers were prepared according to the mass ratios and to mix equal volumes of both solutions. DNA solution was added drop wise to the nanoparticles and the mixture was kept under magnetic stirring for at least 30 minutes.

6.1.7. DLS and zeta potential measurements

Particle size distribution and zeta potential were determined by dynamic light scattering and laser Doppler velocimetry, respectively, using a Zetasizer Nano ZS (Malvern Instruments Ltd., Malvern, UK), at 25°C. These techniques are described in sections 4.1.3. and 4.1.4. Size measurements were carried out at a scattering angle of 173°. Zeta potential was given by means of electrophoretic mobility and the light is collected at the scattered angle of 17°. Experimental data were statistically analysed applying one-way analysis of variance (ANOVA) following Tukey test approach.

6.1.8. Transmission electron microscopy (TEM)

Each sample (5 µL) was placed on copper grids (Formvar/carbon on 400 mesh – Agar) and let to adsorb for 5 minutes. The staining was performed with 2% (w/v) of filtered aqueous solution of uranyl acetate for 45 seconds. The grids were visualised using a Jeol JEM 1400 electron microscope at 80 kV. A description of this technique can be found in section 4.1.6.

6.1.9. Scanning electron microscopy (SEM)

Scanning electron microscopy (SEM) allows a direct observation and characterisation of the sample either at micrometer or nanometer scale. It produces three-dimensional images of the surface by scanning the sample holder with a focused beam of electrons. The electron interaction emits a signal that is converted into valuable information about the topography, morphology, crystallography and composition of the sample surface. Due to the focused electron beam, SEM micrographs have a large depth of field, generating sample surface images with high resolution, allowing superior magnifications. The visualisation of details can go up to 1 nanometer in size (Goldstein, 1981).

The nanoparticles were characterised by Cryo-SEM (JEOL JSM 6301F/ Oxford INCA Energy 350 / Gatan Alto 2500). Solutions were placed on the support and frozen in liquid nitrogen. A sectional cut was applied to observe the nanoparticles. Polyplexes were observed using SEM (FEI QUANTA 400 FEG / EDAX Pegasus X4M) at a voltage of 15 kV. Liquid state samples were allowed to dry on a mica surface pre-coated with a gold-palladium (Au-Pd) layer,

placed on carbon tape. After drying, samples were coated with a second layer of Au-Pd.

6.2. Results and Discussion

6.2.1. Characterisation of chitosan-*N*-maltodextrin copolymer

Maltodextrin (MD) chains were covalently conjugated to chitosan by reductive amination at molar ratios of chitosan glucosamine units and maltodextrin (Ch_n:MD) of 1:1 and 1:5 (Figure 6.1).

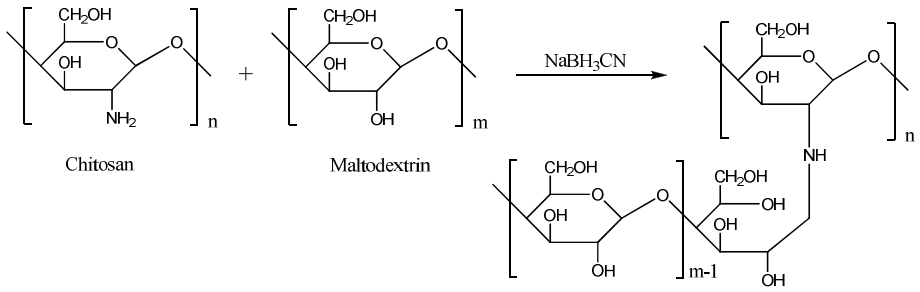

Figure 6.1. Synthesis of chitosan-*N*-maltodextrin graft copolymers.

The initial reaction mixture presented a clear yellow colour, whose intensity decreased during time, indicating the reaction progression. After dialysis and lyophilisation, the resulting compound was soluble in water (at least up to 50 mg/mL). This is a good indication of polymer structural changes and suggests that maltodextrin moieties increase the solubility of chitosan. The analysis of the resultant compound by FTIR spectroscopy indicates that

NH_2 groups of chitosan were substituted (Figure 6.2). Chitosan and maltodextrin show similar bands in the FTIR spectra, except in the region between 1500 and 1700 cm^{-1} (Figure 6.2).

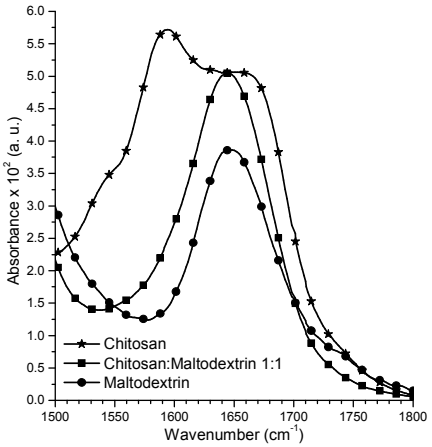

Figure 6.2. Region range between 1500 and 1800 cm^{-1} of the FTIR spectra of chitosan, maltodextrin and chitosan-graft-maltodextrin (chitosan glucosamine:maltodextrin ratio of 1:1).

Chitosan has a broad band between 1550 and 1700 cm^{-1} characteristic of N-H bend of primary amines (Park, 2001). This broad band disappears after reacting with maltodextrin and only the characteristic band at 1650 cm^{-1} from the maltodextrin molecule is visible. The absence of the N-H band from primary amines suggests that the substitution was successful (Park, 2001). Further analyses were carried out by NMR spectroscopy. Typical 400 MHz ^1H NMR spectrum of Ch_n:MD 1:1 is presented in Figure 6.3. The spectra obtained for chitosan and maltodextrin are also included for comparison.

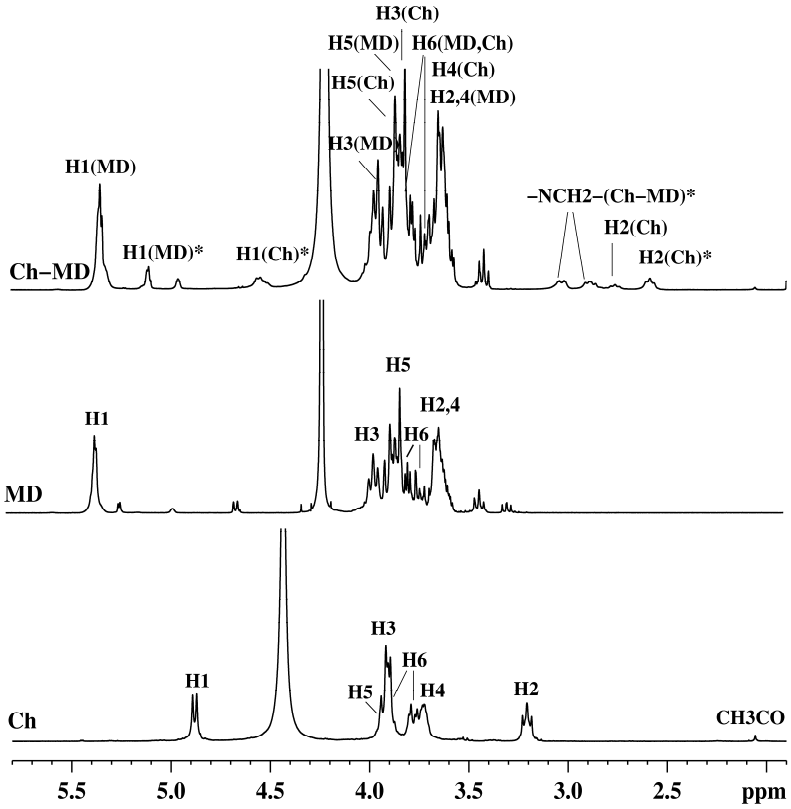

Figure 6.3. 400.15 MHz ^{1}H NMR spectra of chitosan (Ch), maltodextrin (MD) and chitosan-graft-maltodextrin (Ch-MD at ratio Ch_n:MD 1:1) polymers in D_2O, at 80°C. The assignment of 1H resonances is included and the new signals due to the reaction of reductive amination are indicated by asterisk.

The assignment of the resonance signals in the spectra of chitosan-*graft*-maltodextrin (Ch-MD) was based on the analysis of the one- (1D) and two-dimensional (2D: ^{1}H/^{1}H COSY, ^{1}H/^{1}H TOCSY, ^{1}H/^{13}C HSQC), ^{1}H/^{13}C HMBC) NMR spectroscopic data. The results were compared and are consistent with the NMR data published before for chitosan and maltodextrin (Hirai, 1991; Lavertu, 2003; Peres, 2010; Pigman, 1970). However, the appearance of new resonance signals was observed in ^{1}H NMR spectra of Ch-MD, as a result of

the reductive amination process for preparation of chitosan-*graft*-maltodextrin. The assignments of the resonance signals in the spectra of Ch-MD, chitosan and maltodextrin are shown in Figure 6.3. The ^{1}H NMR spectra of Ch-MD are dominated by the intense, broad and overlapped resonance signals of the hydroxymethine and hydroxymethylene protons of the saccharide residues of the polysaccharide structures of chitosan and maltodextrin. Characteristic signals due to the anomeric protons of the chitosan glucosamine and maltodextrin glucose units were detected at *ca.* 4.75 ppm and 5.40 - 4.90 ppm, respectively. The broadening of the anomeric resonance signal of chitosan (4.75 ppm) indicates more restricted mobility of the molecules in Ch-MD and suggests higher molecular mass of the polymer structures. The broad signals at 5.40, 5.23 and 4.97 ppm were attributed to the anomeric protons of α(1→4)- and α(1→6)-linked glucose units of maltodextrin connected in chains of variable length. A doubling of H2 resonance of chitosan and appearance of additional signals with identical intensity at 2.89, 3.03 and 5.11 ppm was observed in the ^{1}H NMR spectra of Ch-MD compared to the spectra of chitosan and maltodextrin. The analysis of 2D ^{1}H/^{1}H COSY, ^{1}H/^{1}H TOCSY, ^{1}H/^{13}C HSQC, ^{1}H/^{13}C HMBC) spectra confirmed a covalent bonding of maltodextrin to the chitosan amino group by reductive amination. The broad signals at 2.89 (d, J= 8.8 Hz) and 3.03 (dd, J=8.8, 11.7 Hz) ppm were assigned to the protons of the new imino-methylene group formed due to coupling the reaction between maltodextrin and amino group of chitosan (Figure 6.1). The signal at 5.11 (d, J= 8.8 Hz) ppm was attributed to the anomeric proton of the second glucose units in the maltodextrin chain included in the reductive amination process of chitosan. The two resonance signals for H2 ($HCNH_2$) of chitosan observed in ^{1}H NMR spectra of Ch-MD were assigned to H2 of N-substituted (2.59 ppm, dd, J=7.8, 8.5 Hz) and N-non-substituted (2.76 ppm, dd, J=7.8, 8.5 Hz) glucosamine residues of Ch. The

mole fraction of the substituted and non-substituted chitosan glucosamine residues in Ch-MD was found to be 3:1, as it was determined from the relative peak intensities of the corresponding proton resonances. The results indicate that the Ch-MD samples are composed of chitosan-*N*-maltodextrin graft copolymers. The content of 2-acetamido-2-deoxy-β-D-glucopyranose units (2.5%) in Ch-MD was calculated from the ratio of the integral intensity of the signal at 2 ppm due to acetyl protons in residual chitin and those of chitosan anomeric protons (4.75 ppm). From here, the actual content of 2-amino-2-deoxy-β-D-glucopyranose units available to participate in the reaction of reductive amination was estimated. The degree of substitution of maltodextrin to chitosan was defined from the integral intensity of the resonance signal at 4.75 ppm (H1 of Ch, corrected for the content of 2-acetamido-2-deoxy-β-D-glucopyranose) and the signal at 2.59 ppm due to H2 of N-substituted chitosan glucosamine residues. An alternative possibility is the ratio of the integral intensity of the signals of H2 of N-substituted (2.59 ppm) and N-non-substituted (2.76 ppm) glucosamine residues. The degree of substitution of 74% and 81% was calculated for Ch_n:MD 1:1 and Ch_n:MD 1:5, respectively. The molar ratio of saccharide residues of the polysaccharide structures of maltodextrin and chitosan (MD:Ch) for these samples was found to be 6:1 and 11:1, as it was determined from the integral intensity of the resonance signal of the corresponding anomeric protons in their ^{1}H NMR spectra. Janciauskaite *et al.* synthetised chitosan-*graft*-dextran polymers and achieved similar degrees of substitution for dextrans with different molecular weight for the same molar ratio of chitosan glucosamine units and dextran, discarding the molecular weight of the graft copolymer as a property to take into consideration. For the tested ratio 1:1, they obtained a degree of substitution of 47% by NMR. In our case, a maltodextrin substitution of 74% was obtained for the same ratio. This difference may be related to the

different degrees of deacetylation of chitosan, because a low content of deacetylated groups leads to more amine groups available for reaction. The molecular weight of chitosan might also play a role because larger molecules could present problems derived from stereo chemical conformations (Janciauskaite, 2008). An increase of maltodextrin molar concentration did not significantly increase the degree of substitution. Above Ch_n:MD 1:1 ratio, it is difficult to attach more maltodextrin molecules to chitosan chains, probably due stereo chemical constrains of the NH_2 groups. Ch_n:MD 1:5 sample was not considered for further studies because its high substitution degree (81%) leads to fewer free NH_2 groups available for interacting with charged molecules.

6.2.2. Chitosan-*N*-maltodextrin nanoparticles

Ch-MD self-assembles into nanoparticles with mean diameters of 310 ± 90 nm and a zeta potential of 29 ± 3 mV (Table 6.1). These nanoparticles present a high polydispersity index (PdI = 0.71) probably due to the polydispersity of the copolymer. The size of nanoparticles prepared with Ch-MD copolymer (Ch_n:MD 1:1 ratio) and TPP as cross-linking agent (normally used to prepare chitosan nanoparticles) was not significantly different from that of Ch-MD nanoparticles (P>0.05) (Table 6.1 and Figure 6.4). Both Ch-MD and Ch-MD:TPP nanoparticles show similar morphology to that of chitosan:TPP nanoparticles (Figure 6.4). Calvo *et al.* observed a strong influence of both chitosan and TPP concentrations on the size of chitosan nanoparticles (Calvo, 1997). Chen *et al.* observed as well this phenomenon for chitosan/dextran nanoparticles prepared by complex coacervation (Chen, 2007).

Table 6.1. Mean particle diameter (z-average diameter), polydispersity index (PdI) and zeta potential of chitosan-*graft*-maltodextrin nanoparticles.

	Chitosan-*graft*-maltodextrin Polymer concentration [a] (mg/mL)	
TPP concentration [a] (mg/mL)	1.00	1.25
0.00	310 ± 90 nm PdI = 0.71 29 ± 3 mV	
0.20	400 ± 200 nm PdI = 0.64 15 ± 1 mV	240 ± 40 nm PdI = 0.57 18 ± 1 mV
0.25	300 ± 100 nm PdI = 0.69 14 ± 1 mV	200 ± 40 nm PdI = 0.77 15 ± 1 mV

[a] Final concentration in nanoparticle suspension

The concentration effect of both species used in nanoparticle formation should be considered carefully because of the generated forces between the oppositely charged species. High concentrations of one of the species might lead to aggregation since it interferes with their stability as individual colloids (Gaspar, 2011; Richardi, 2009). Csaba *et al.* studied the impact of TPP on the properties and DNA transfection efficiency of the nanoparticles. Nanoparticles of chitosan cross-linked with TPP and then complexed with DNA show higher transfection efficiency than the system obtained by direct complexion of DNA to chitosan (Csaba, 2009).

Nanoparticles of chitosan and cyclodextrin, prepared by ionotropic gelification using TPP, resulted in vectors with high DNA association capacity and low cytotoxicity (Teijeiro-Osorio, 2009). Using complex coacervation

method, Chen *et al.* prepared small nanoparticles based on chitosan and dextran that were used to encapsulate positively charged drugs (Chen, 2007). The zeta-potential values of Ch-MD decrease with the addition of TPP, indicating less positive charges available, which can be an advantage when considering the compatibility with cellular membranes (Table 6.1) (Gao, 2008). The high polydispersity of Ch-MD-TPP particles might be explained by maltodextrin chains located at the surface of the nanoparticles (Csaba, 2009). It can also result from the inhomogeneity of intermolecular cross-linking by TPP.

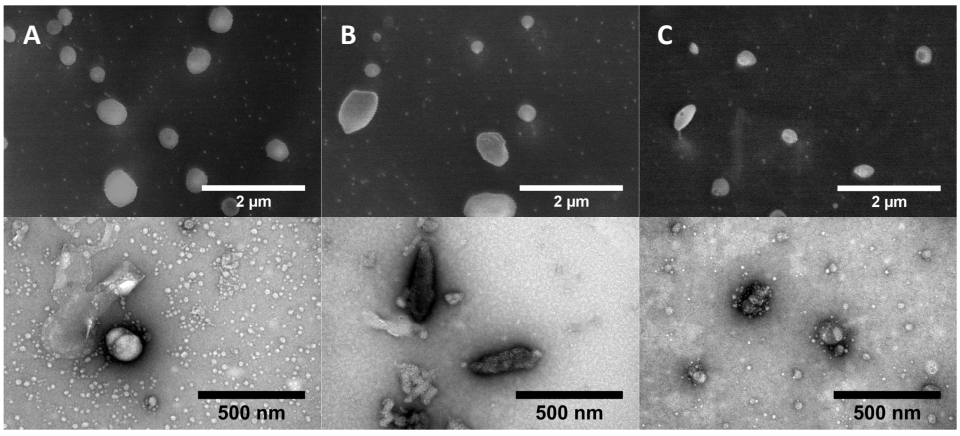

Figure 6.4. Morphological characterisation of chitosan-*graft*-maltodextrin (A), chitosan-TPP (B) and chitosan-*graft*-maltodextrin-TPP (C) nanoparticles at the final concentrations of 1.25 mg/mL of polymers and 0.25 mg/mL of TPP by Cryo-SEM (up, scale bar 2 µm) and TEM (down, scale bar 500 nm).

6.2.3. Chitosan-*N*-maltodextrin/DNA complexes

Alatorre-Meda *et al.* suggested that DNA compaction is completely achieved when polyplexes reach a positive zeta potential (above the isoneutrality point) (Alatorre-Meda, 2011; De Smedt, 2000; Tang, 1997). The transition of the zeta potential signal of a DNA solution to which chitosan was added occurs at a ratio of polymer:DNA between 0.5 and 1 (Figure 6.5). The positive values in the case of titration of DNA solution with Ch-TPP nanoparticles appear at polymer:DNA ratios between 0.25 and 0.5. The isoelectric point of Ch-MD nanoparticles:DNA appears at ratio of 3.5 and Ch-MD-TPP particles:DNA at 2. The results indicate that more Ch-MD and Ch-MD-TPP are required to neutralize the same amount of DNA when compared to, respectively, chitosan and Ch-TPP, which might be explained by the lower number of free positive charges in Ch-MD copolymer. The primary amine groups become unavailable when chitosan reacts with maltodextrin, thus DNA might complex with Ch-MD copolymer not only through electrostatic interactions but also through hydrogen bonding and hydrophobic interactions (Mao, 2010).

SEM images show that Ch-TPP and Ch-MD particles (with TPP or not) have a rough surface (Figure 6.6**,** bigger particles were considered for visualisation purposes). The complexes of nanoparticles and DNA exhibit a smooth surface, evidencing that a layer may be coating the particles, which is consistent with the presence of DNA around the nanoparticles (Gaspar, 2011). EDS (Energy dispersive X-ray spectroscopy) analysis confirmed the presence of both DNA and chitosan macromolecules.

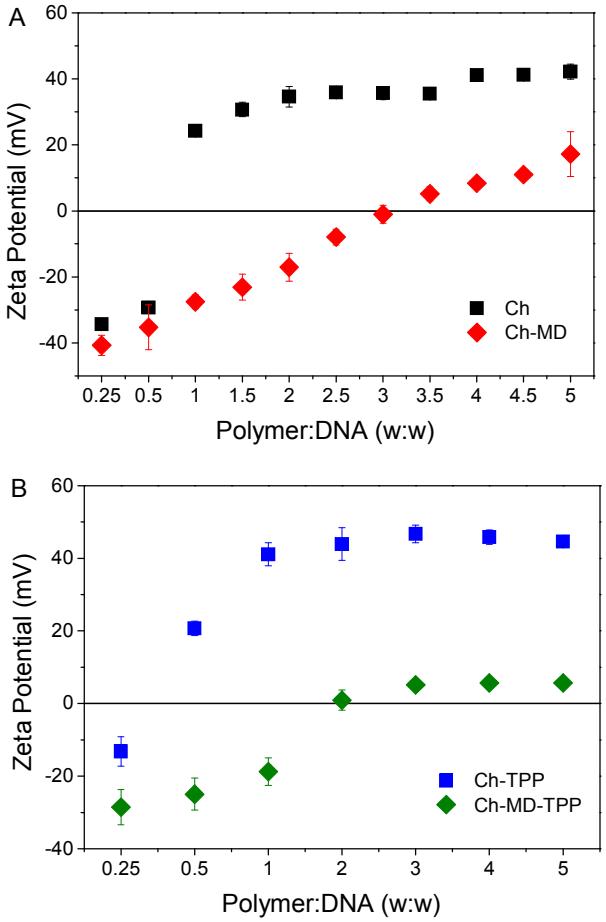

Figure 6.5. Zeta potential of chitosan:DNA and chitosan-maltodextrin:DNA polyplexes at different polymer:DNA mass ratios. DNA concentration is 0.025 mg/mL.

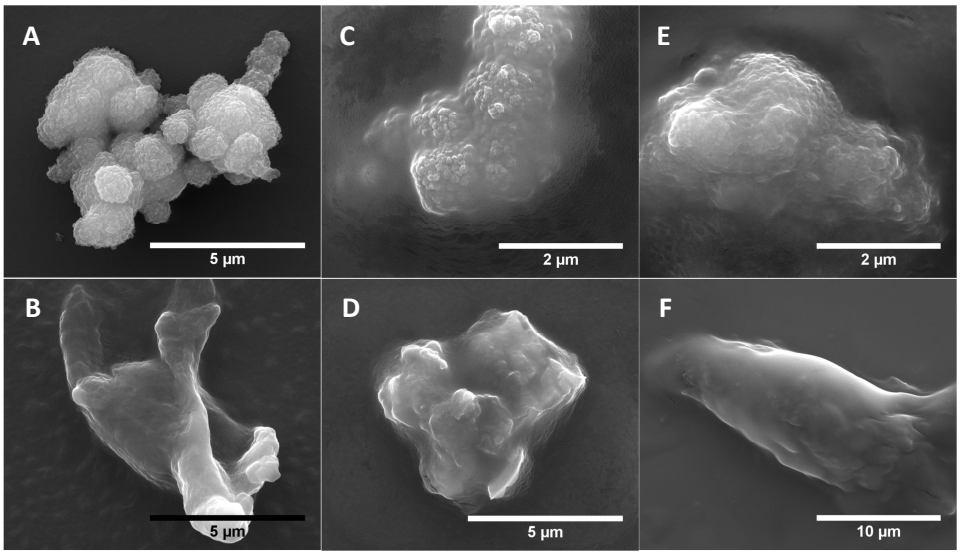

Figure 6.6. Morphology of chitosan and chitosan:maltodextrin nanoparticles complexed with DNA, characterised by SEM: (A) Ch-TPP, (B) Ch-TPP:DNA 2:1, (C) Ch-MD, (D) Ch-MD:DNA 2:1 (E) Ch-MD-TPP, (F) Ch-MD-TPP:DNA 2:1.

6.3. Conclusions

A copolymer based on chitosan and maltodextrin molecules for the preparation of DNA vectors is proposed. This compound shows improved properties as water solubility and self-assembly into spherical nanoparticles when compared to chitosan. Nanoparticles with diameters of about 200 nm can be obtained by cross linking chitosan-*graft*-maltodextrin with TPP. Their spherical shape and lower zeta-potential values (about 15 mV) when compared with chitosan particles (55 mV) may favour their uptake by cells. In

addition, the maltodextrin chains, which are expected to be at the particle surface, will contribute to the stabilisation of the system.

6.4. References

Alatorre-Meda, M.; Taboada, P.; Hartl, F.; Wagner, T.; Freis, M.; Rodríguez, J.R. (**2011**). The influence of chitosan valence on the complexation and transfection of DNA: The weaker the DNA–chitosan binding the higher the transfection efficiency, *Colloids and Surfaces B: Biointerfaces, 82*, 54.

Becker, E.; *High Resolution NMR: Theory and Chemical Applications,* 3rd Edition, Academic Press, United States of America, **2000**.

Calvo, P.; Remuñán-López, C.; Vila-Jato, J.L.; Alonso, M.J. (**1997**). Novel hydrophilic chitosan-polyethylene oxide nanoparticles as protein carriers, *Journal of Applied Polymer Science, 63*, 125.

Cavanagh, J.; Rance, M. (**1990**). Sensitivity improvement in isotropic mixing (TOCSY) experiments, *Journal of Magnetic Resonance (1969), 88*, 72.

Chen, Y.; Mohanraj, V.J.; Wang, F.; Benson, H.A. (**2007**). Designing chitosan-dextran sulfate nanoparticles using charge ratios, *AAPS PharmSciTech, 8*, E98.

Csaba, N.; Köping-Höggård, M.; Alonso, M.J. (**2009**). Ionically crosslinked chitosan/tripolyphosphate nanoparticles for oligonucleotide and plasmid DNA delivery, *International Journal of Pharmaceutics, 382*, 205.

De Smedt, S.C.; Demeester, J.; Hennink, W.E. (**2000**). Cationic Polymer Based Gene Delivery Systems, *Pharmaceutical Research, 17*, 113.

Ebnesajjad, S.; *Surface Treatment of Materials for Adhesion Bonding,* William Andrew, United States of America, **2006**.

Evans, C.; Brundle, R.; Wilson, S.; *Encyclopedia of Materials Characterization,* Butterworth-Heinemann, United States of America, **1992**.

Gao, Y.; Xu, Z.; Chen, S.; Gu, W.; Chen, L.; Li, Y. (**2008**). Arginine-chitosan/DNA self-assemble nanoparticles for gene delivery: In vitro characteristics and transfection efficiency, *International Journal of Pharmaceutics, 359*, 241.

Gaspar, V.M.; Sousa, F.; Queiroz, J.A.; Correia, I.J. (**2011**). Formulation of chitosan–TPP–pDNA nanocapsules for gene therapy applications, *Nanotechnology, 22*, 015101.

Gerothanassis, I.P.; Troganis, A.; Exarchou, V.; Barbarossou, K. (**2002**). NUCLEAR MAGNETIC RESONANCE (NMR) SPECTROSCOPY: BASIC PRINCIPLES AND PHENOMENA, AND THEIR APPLICATIONS TO CHEMISTRY, BIOLOGY AND MEDICINE, *Chemistry Education Research and Practice, 3*, 229.

Goldstein, J.; Newbury, D.; Joy, D.; Echlin, P.; Lifshin, E.; Fiori, C.; *Scanning Electron Microscopy and x-Ray Microanalysis,* Plenum Press, Unites States of America, **1981**.

Griffiths, P.R.; Haseth, J.A.; *Fourier Transform Infrared Spectrometry,* 2nd, John Wiley & Sons, Inc., New Jersey, USA, **2007**.

Günther, H.; *NMR spectroscopy : basic principles, concepts, and applications in chemistry,* 2nd Edition, Wiley, United Satates of America, **1994**.

Hirai, A.; Odani, H.; Nakajima, A. (**1991**). Determination of degree of deacetylation of chitosan by 1H NMR spectroscopy, *Polymer Bulletin, 26*, 87.

Huang, C.-Y.; Ma, S.S.; Lee, S.; Radhakrishnan, R.; Braun, C.S.; Choosakoonkriang, S.; Wiethoff, C.M.; Lobo, B.A.; Middaugh, C.R. (**2002**). Enhancements in gene expression by the choice of plasmid

DNA formulations containing neutral polymeric excipients, *Journal of Pharmaceutical Sciences, 91*, 1371.

Janciauskaite, U.; Rakutyte, V.; Miskinis, J.; Makuska, R. (**2008**). Synthesis and properties of chitosan-N-dextran graft copolymers, *Reactive and Functional Polymers, 68*, 787.

Kaneko, Y.; Matsuda, S.I.; Kadokawa, J.I. (**2007**). Chemoenzymatic synthesis of amylose-grafted chitin and chitosan, *Biomacromolecules, 8*, 3959.

Lavertu, M.; Xia, Z.; Serreqi, A.N.; Berrada, M.; Rodrigues, A.; Wang, D.; Buschmann, M.D.; Gupta, A. (**2003**). A validated 1H NMR method for the determination of the degree of deacetylation of chitosan, *Journal of Pharmaceutical and Biomedical Analysis, 32*, 1149.

Mao, S.; Sun, W.; Kissel, T. (**2010**). Chitosan-based formulations for delivery of DNA and siRNA, *Advanced Drug Delivery Reviews, 62*, 12.

Park, I.K.; Park, Y.H.; Shin, B.A.; Choi, E.S.; Kim, Y.R.; Akaike, T.; Cho, C.S. (**2001**). Galactosylated chitosan-graft-dextran as hepatocyte-targeting DNA carrier, *Journal of Controlled Release, 75*, 433.

Peres, I.; Rocha, S.; Pereira, M.d.C.; Coelho, M.; Rangel, M.; Ivanova, G. (**2010**). NMR structural analysis of epigallocatechin gallate loaded polysaccharide nanoparticles, *Carbohydrate Polymers, 82*, 861.

Pigman, W.W.; Horton, D.; Herp, A.; *The carbohydrates : chemistry and biochemistry,* Volume 1, 2nd Edition, Academic Press, United States of America, **1970**.

Ramachandran, V.S.; Beaudoin, J.J.; *Handbook of Analytical Techniques in Concrete Science and Technology,* William Andrew, United States of America, **2001**.

Reichenbächer, M.; Popp, J.; *Challenges in molecular Structure Determination,* Springer, Germany, **2012**.

Richardi, J. (**2009**). One-dimensional assemblies of charged nanoparticles in water: A simulation study, *Journal of Chemical Physics, 130*, 044701.

Schnell, I.; Spiess, H.W. (**2001**). High-Resolution 1H NMR Spectroscopy in the Solid State: Very Fast Sample Rotation and Multiple-Quantum Coherences, *Journal of Magnetic Resonance, 151*, 153.

Tang, M.X.; Szoka, F.C. (**1997**). The influence of polymer structure on the interactions of cationic polymers with DNA and morphology of the resulting complexes, *Gene Therapy, 4*, 823.

Teijeiro-Osorio, D.; Remuñán-López, C.; Alonso, M.J. (**2009**). Chitosan/cyclodextrin nanoparticles can efficiently transfect the airway epithelium in vitro, *European Journal of Pharmaceutics and Biopharmaceutics, 71*, 257.

Chapter 7

Concluding remarks

In this thesis three different systems are proposed with impact on gene therapy. The study of physical, chemical and biological properties of these systems allowed a better understanding of the process involved on the transport and release of DNA. They have shown potential as gene carriers and, therefore, further studies either *in vitro* or *in vivo* can be performed.

The use of F7-cholesterol as helper lipid in cationic (DOTAP) non-viral gene vectors is proposed. This fluorinated derivative of cholesterol was chosen because previous studies highlighted the efficient gene transfer by lipids containing fluorinated hydrophobic chains. Studying the physical forces between two lipids in a monolayer is of great importance to understand their behaviour when they are part of a bilayer structure like a liposome. Monolayer studies showed that the mixture of DOTAP with F7-cholesterol is completely miscible. Regarding the interaction of the lipid monolayer with DNA molecules, the monolayer system adsorbs DNA even at ionic strength close to the physiological values, thus F7-cholesterol is a promising candidate for the preparation of gene delivery vectors.

Liposomes of DOTAP and fluorinated cholesterol were prepared and compared to the DOTAP/cholesterol system in terms of biophysical properties when complexed with DNA. The results showed that a higher lipid amount is required to form complexes with DNA in the case of DOTAP/F7-cholesterol system. However, the aggregation-disaggregation model predicts that, even if more DOTAP:F7-CHOL liposomes are needed, most of the DNA is involved in the complexation process when the lipoplexes are formed. Also, both systems showed similar stability in the presence of DNA and have identical transfection efficiency. This study confirmed that fluorinated cholesterol molecule could be included in cationic liposomes without dramatically changing their properties.

A new synthesised bolaamphiphile was used to prepare two different systems for DNA delivery. The layer-by-layer assembly was used to deposit layers of DNA and bolaamphiphile at the surface of the particles. The zeta potential variation gives an indication of the layer deposition through the signal reversal, according to the charge of the molecule used. Further assays were done to ensure the presence of DNA within the layers as well as the presence of the bolaamphiphile. CLSM images confirm the uniform presence of both compounds on the particles.

A type of vesicles that combine bolaamphiphile with cationic lipids is also proposed to form stable and positively charged liposomes capable of condensing efficiently genetic material by electrostatic interactions. Comparing the carrier made of BA:DOTAP 1:5 with DOTAP vesicles, they present similar properties with respect to size and zeta potential values. The transfection studies show that the bolaamphiphile mixed system has a higher transfection potential when compared to DOTAP vesicles.

Chitosan-*N*-maltodextrin was synthesised via reductive amination by covalently conjugating chitosan molecules to maltodextrin chains. This copolymer is proposed for the preparation of DNA polymer-based vectors. This compound shows improved properties as water solubility and self-assembly into spherical nanoparticles when compared to chitosan. Nanoparticles with diameters of about 200 nm can be obtained by cross linking chitosan-*graft*-maltodextrin with TPP. Their spherical shape and lower zeta-potential values (about 15 mV) when compared with chitosan particles (55 mV) may favour their uptake by cells. In addition the maltodextrin chains, which are expected to be at the particle surface, will contribute to the stabilisation of the system.

List of Abbreviations

Abbreviations

AIDS	Acquired immunodeficiency syndrome
ANOVA	One-way analysis of variance
AuNPs	Gold nanoparticles
BA	22-hydroxy-*N*,*N*,*N*-trimethyldocosan-1-aminium (Bolaamphiphile)
BAM	Brewster angle microscopy
Ca.	Approximately
CCC	Critical coagulation concentration
CCD	Charge-coupled device
CD	Circular dichroism
β-CD	β-cyclodextrin
Ch	Chitosan
Ch-MD	Chitosan-*N*-maltodextrin
CHOL	Cholesterol
CLSM	Confocal laser scanning microscopy
COSY	Two-dimensional (2D) $^{1}H/^{1}H$ correlation spectroscopy
CSC	Critical stabilisation concentration
ctDNA	Calt thymus DNA
d	Doublet
dd	Double of doublets
DAPI	4',6-diamidino-2-phenylindole

DC-Chol	3β-[N-(N',N'-dimethylaminoethane)-carbamoyl]cholesterol hydrochloride
DDAB	Didodecyldimethylammonium bromide
DE	Dextrose equivalent
DLATGS	Deuterated l-alanine-doped triglycine sulfate
DLS	Dynamic light scattering
DMPC	1,2-dimyristoyl-*sn*-glycero-3-phosphocholine
DMPG	1,2-dimyristoyl-sn-glycero-3-[phospho-rac-(1-glycerol)]
DNA	Deoxyribonucleic acid
DOGS	Dioctadecylaminoglycylspermine
DOPE	1,2-dioleoyl-sn-glycero-3-phosphoethanolamine
DOPG	1,2-dioleoyl-sn-glycero-3-[phospho-rac-(1-glycerol)]
DOSPA	2,3 Dioleyloxy-N-[2(sperminecarboxaminino)ethyl]-N,N-dimethyl-1-propanaminium trifluroacetate
DOTAP	1,2-dioleoyl-3-trimethylammonium-propane (chloride salt)
DOTMA	1,2-di-O-octadecenyl-3-trimethylammonium propane
EDL	Electrical double layer
EDS	Energy dispersive X-ray spectroscopy
Et al.	and co-workers
EtBr	3,8-Diamino-5-ethyl-6-phenylphenanthridinium bromide (Ethidium Bromide)
F7-CHOL	25,26,26,26,27,27,27-heptafluorocholesterol (F7-cholesterol)
FACS	Fluorescence-activated cell sorter
FBS	Heat inactivated fetal bovine serum
FTIR	Fourier transform infrared spectroscopy
G	Gaseous
GC	Classical Gouy-Chapman model
GFP	Green fluorescent protein
HEK 293	Human embryonic kidney 293 cells
HeLa	Human cervical cancer immortal cell line
HEPES	4-(2-Hydroxyethyl) piperazine-1-ethanesulfonic acid

HIV	Human immunodeficiency virus infection
HMQC	$^{1}H/^{13}C$ heteronuclear multiple bond coherence spectroscopy
HSQC	$^{1}H/^{13}C$ heteronuclear single quantum coherence spectroscopy
i. e.	That is
iep	Isoelectric point
IR	Infrared
IRRAS	Infrared reflection absorption spectroscopy
J	Coupling constant
JL1	Antigen of human cortical thymocyte
KRS-5	Thallium bromide and iodide mixed crystal
LbL	Layer-by-layer
LC	Liquid-condensed
L/D	Liposome/DNA mass ratio
$(L/D)_0$	Liposome/DNA mass ratio at isoelectric point
LDV	Laser Doppler velocimetry
LE	Liquid-expanded
LUV	Large unilamellar vesicles
MC	Monte Carlo simulations
MCT	Mercury cadmium telluride
MD	Maltodextrin
MEM	Minimum essential medium
miRNA	Mediated gene regulation circuits of ribonucleic acid
MLV	Multilamellar vesicles
MNPs	Magnetic nanoparticles
Mw	Molecular weight
MWCO	Molecular weight cut off
NMR	Nuclear magnetic resonance
N/P	Nitrogen/phosphate
NPs	Nanoparticles
PAH	Poly(allylamine hydrochloride)
PAMAM	Polyamidoamine

PBS	Phosphate buffered saline
PdI	Polydispersity index
pDNA	Plasmid DNA (pEGFP-N1)
PEG	Polyethylene glycol
PEI	Polyethylenimine
pH	Potential hydrogen
PhD	Doctor of philosophy
PLGA	Poly(lactic-*co*-glycolic acid)
PLL	Poly(L-lysine)
PS	Polystyrene
PSS	Poly(sodium 4-styrenesulfonate)
PTFE	Polytetrafluoroethylene
pzc	point of zero charge
QDs	Quantum dots
Rhod PE	1,2-dipalmitoyl-sn-glycero-3-phosphoethanolamine-N-(lissamine rhodamine B sulfonyl) (ammonium salt)
RNA	Ribonucleic acid
S	Solid
S.D.	Standard deviation
SEM	Scanning electron microscopy
SH-SY5Y	Human neuroblastoma cell line
siRNA	Small interfering ribonucleic acid
SPIONs	Super paramagnetic iron oxide nanoparticles
SUV	Small unilamellar vesicles
T-cells	T lymphocites cells
TEM	Transmission electron microscopy
TOCSY	$^{1}H/^{1}H$ total correlation spectroscopy
TPP	Sodium tripolyphosphate
Tris	2-amino-2-(hydroxymethyl)-1,3-propanediol
TSP	Sodium trimethylsilyl-[2,2,3,3-d_4]-propionate
UV-VIS	Ultraviolet-visible spectroscopy

ZP	Zeta potential

Symbols

A	Area
Abs	Absorbance
A_m	Average molecular area
a.u.	Arbitrary units
a	Liposome radius
B_0	External magnetic field strength
C	Molar concentration
C_e	Liposome electrical capacitance
D	Diffusion coefficient
e	Dielectric constant
E_0	DNA-liposome interaction energy
f	Stokes coefficient
$f(ka)$	Henry's function
h	Planck's constant
I	Transmitted radiation
I_0	Incident radiation
I_F	Fluorescence intensity
k_B	Boltzmann's constant
k_r	Rate constant for rapid coagulation regime
k_s	Rate constant for slow coagulation regime
l	Optical path length
N	Number of nuclei
P	DNA concentration
P_0	DNA concentration in equilibrium with lipoplexes
Q	Liposome charge
q	Charge of DNA segment
R_H	Hydrodynamic radius

$S_a(P)$	Liposome concentration at aggregation
$S_d(P)$	Liposome concentration at disaggregation
T	Absolute temperature
T_r	Transmittance
W	Fuchs stability ratio
X	Molar fraction

Greek lyrics

α	Brewster angle
γ	Surface tension
γ_m	Magnetogyric ratio
ε	Relative permittivity
ε_0	Absolute permittivity of vacuum
ε_a	Molar absorptivity
$\Delta\varepsilon$	Extinction coefficient
ΔV	Surface potential
ζ	Zeta potential
η	Viscosity
θ	Ellipticity
κ_D	Reciprocal Debye length
λ	Wavelength
μ	Magnetic moment
μ_e	Electrophoretic mobility
$\mu_{\perp,m}$	Vertical component of the molecular dipole moment
ν	Wavenumber
π	Lateral surface pressure
π_c	Critical lateral surface pressure
Ψ	Diffuse double layer contribution

Units

% (v/v)	Volume percent
% (w/v)	Weight-volume percent
% (w/w)	Weight percent
m	Length (meter)
Å	Length (10^{-10} m)
g	Mass (gram)
mol	Mole
M (mol/m^3)	Molar concentration
kg/m^3	Mass concentration
$m^3 = 10^3$ L	Volume (cubic meter or liter)
Da= g/mol	Unified atomic mass unit
ppm	parts per million
s	Time (seconds)
min	Time (minutes)
h	Time (hours)
°	degree
°C	Temperature (Celsius)
K	Temperature (Kelvin)
V	Voltage (Volts)
Hz = s^{-1}	Frequency (Hertz)
W	Power (watt)
N	Force (newton)
Ω·m	Electrical resistivity (ohm·meter)

Units prefix

G	giga	10^9
M	mega	10^6

k	kilo	10^{3}
	unit	10^{0}
d	deci	10^{-1}
c	centi	10^{-2}
m	mili	10^{-3}
μ	micro	10^{-6}
n	nano	10^{-9}
p	pico	10^{-12}

List of Figures

List of Tables